JSCSEN 75(6)733–873(2010)

Journal of the Serbian Chemical Society

Electronic version

VOLUME 75

No 6

BELGRADE 2010

Available on line at

www.shd.org.rs/JSCS/

The full search of JSCS is available through

DOAJ DIRECTORY OF OPEN ACCESS JOURNALS

www.doaj.org

Journal of the Serbian Chemical Society
JSCS@tmf.bg.ac.rs • www.shd.org.rs/JSCS

J. Serb. Chem. Soc. Vol. 75, No. 6 (2010)

CONTENTS

Published by the Serbian Chemical Society
Karnegijeva 4/III, 11000 Belgrade, Serbia
Printed by the Faculty of Technology and Metallurgy
Karnegijeva 4, P.O. Box 35-03, 11120 Belgrade, Serbia

Journal of the Serbian Chemical Society
JSCS@tmf.bg.ac.rs • www.shd.org.rs/JSCS
J. Serb. Chem. Soc. 75 (6) 733–738 (2010)
JSCS–4002
UDC 582.635.38+543.422.25:547.918:547.814.5
Original scientific paper

Rhamnopyranosylvitexin derivatives from *Celtis australis*

MARGARETHE KALTENHAUSER[1], ERNST P. ELLMERER[2] and CHRISTIAN ZIDORN[1]*

[1]*Institut für Pharmazie der Universität Innsbruck, Abteilung Pharmakognosie, Josef-Moeller-Haus, Innrain 52, A-6020 Innsbruck and* [2]*Institut für Organische Chemie der Universität Innsbruck, Innrain 52a, A-6020 Innsbruck, Austria*

(Received 17 August 2009, revised 8 January 2010)

Abstract: A methanolic extract of *Celtis australis* leaves yielded 2''-*α*-rhamnopyranosylvitexin and 2''-*α*-rhamnopyranosyl-7-*O*-methylvitexin. Both compounds are known from other sources from earlier investigations but the full NMR data for the latter compound are reported for the first time.

Keywords: Cannabaceae; *Celtis australis*; *C*-glycosides; flavonoids; NMR.

INTRODUCTION

Celtis australis L. is a southern European and western Asian species of the Cannabaceae family.[1] Formerly the genus *Celtis* was either placed in the Ulmaceae or in a distinct family, Celtidaceae.[1,2] New data including molecular, morphological, and phytochemical data support the inclusion of the genus *Celtis* in the family Cannabaceae.[3] Fruits and young twigs of *C. australis* were formerly used against dysentery and as expectorants, respectively.[4] Recently, three flavonoids, *i.e.*, acacetin 7-*O*-glucoside, isovitexin and cytisoside, were reported from *C. australis*.[5]

The present communication deals with two known flavonoids isolated for the first time from *C. australis* collected near Auer/Ora in South Tyrol/northern Italy and encompasses the first complete set of NMR data of 2''-*α*-rhamnopyranosyl-7-*O*-methylvitexin.

RESULTS AND DISCUSSION

Compounds **1** and **2** were isolated from the *n*-butanol layer of the methanolic extract of *C. australis* leaves employing repeated Sephadex LH-20 column chromatography (CC) and semi-preparative RP-18 HPLC.

The mass spectrum of compound **1** indicated a molecular mass of 578 based on the $[M–H]^-$ signal at *m/z* 577 in the negative mode. Taking into account the

* Corresponding author. E-mail: Christian.H.Zidorn@uibk.ac.at
doi: 10.2298/JSC090817049K

NMR data (Table I), which indicated the presence of a flavonoid moiety (C_{15}), a glucose moiety (C_6), and a rhamnose moiety (C_6), the molecular formula of $C_{27}H_{30}O_{14}$ was established for compound **1** (Fig. 1). The ^{1}H-NMR coupling patterns of the aromatic protons of compound **1** indicated the presence of an AA'XX' system (at 8.04 and 6.91 ppm) and two additional singlets at 6.79 and 6.26 ppm, respectively. Thus, compound **1** was identified as an apigenin derivative with an additional substitution in ring A (position 6 or 8). The HMBC signals of the anomeric proton of the glucose moiety to three aromatic carbons at 104.5 (C-8), 155.9 (C-9), and 162.5 ppm (C-7), respectively, revealed that the glucose moiety was attached as a *C*-glycoside in position 8. This was verified by cross peaks from the one remaining free proton in ring A (H-6) to four aromatic carbons at 104.3 (C-10), 104.5 (C-8), 160.8 (C-5), and 162.5 ppm (C-7). A downfield shift of the proton in position H-2'' of the glucose moiety and an HMBC cross peak from the anomeric proton of the rhamnose moiety (H-1''') to the respective carbon signal (C-2'') revealed that the rhamnose moiety was attached in this position. Thus, compound **1** was identified as 2''-*α*-rhamnopyranosylvitexin. This compound has already been reported from a number of sources including the genus *Crataegus* (Rosaceae),[6] *Onobrychis montana* DC. subsp. *scardica* (Griseb.) P. Ball (Fabaceae),[7] *Passiflora alata* Curtis (Passifloraceae),[8] *Piper umbellatum* L. (Piperaceae)[9] and *Turnera diffusa* Willd. ex Schult. (Turneraceae).[10]

NMR data of **1** measured in methanol-d_4 were reported by Kumamoto *et al.*[11] However, full NMR data measured in DMSO-d_6 have not hitherto been published. Therefore, to enable comparisons with the NMR data of compound **2** which have not hitherto been published at all, the NMR data of **1** measured in DMSO-d_6 are included in Table I.

Mass spectrum of compound **2** indicated a molecular mass of 592 based on the $[M–H]^–$ signal at *m/z* 591 in the negative mode. Taking into account the NMR data (Table I), which indicated the presence of a flavonoid moiety (C_{15}), a glucose moiety (C_6), a rhamnose moiety (C_6) and an *O*-methyl group (C_1), a molecular formula of $C_{28}H_{32}O_{14}$ was established for compound **2**. The NMR data in most parts of the spectra were almost superimposable on the spectra of compound **1**. The position of the additional methyl group was established by an HMBC experiment which proved that this group was connected *via* O-7 with rest of the molecule. This fact was corroborated by the shift differences between **1** and **2** in the ^{1}H-NMR and ^{13}C-NMR spectra for signals assignable to carbons C-6 and C-8 and to proton H-6. Conclusively, compound **2** was identified as 2''-*α*-rhamnopyranosyl-7-*O*-methylvitexin, a rare natural product. *β*-Linkages of the glucose and *α*-linkages of the rhamnose moieties of both compounds were deduced by the coupling pattern of H-1'' and H-1''', respectively. In contrast, the assignment to the D- and L-series of glucose and rhamnose, respectively, was not proven using

the available methodologies (*i.e.*, optical rotation of the isolated sugar moiety or chiral GC after silylation) but implied from the prevailing pattern in plant secondary metabolites. However, to the best of our knowledge, no D-rhamnopyranosides are currently known as natural products from higher plants, although abstracts of some papers erroneously imply the opposite.[12] Compound **2** has hitherto only been reported from *Avena sativa* L. (Poaceae),[13] *Gnetum africanum* Welw. (Gnetaceae)[14] and *Mollugo disticha* Ser. (Molluginaceae).[15] The NMR data of this substance have not been reported before and are therefore given in Table I.

TABLE I. NMR data from 2''-α-rhamnopyranosylvitexin (**1**) and 2''-α-rhamnopyranosyl-7--*O*-methylvitexin (**2**) isolated from *C. australis*; measured in DMSO-d_6 at 300 MHz and 75 MHz, respectively; referenced to solvent residual signals and solvent signals of DMSO-d_6 (^{1}H-NMR: 2.50 ppm and ^{13}C-NMR: 39.50 ppm), respectively

Position	**1**		**2**	
	^{13}C	^{1}H	^{13}C	^{1}H
		Flavonoid moiety		
2	164.1	–	164.6	–
3	102.0	6.79, 1H, *s*	102.1	6.84, 1H, *s*
4	182.2	–	182.1	–
5	160.8	–	161.7	–
6	98.0	6.26, 1H, *s*	95.0	6.51, 1H, *s*
7	162.5	–	163.0	–
8	104.5	–	105.7	–
9	155.9	–	155.0	–
10	104.3	–	104.6	–
1'	121.7	–	121.2	–
2'/6'	128.6	8.04, AA'XX'	128.9	8.07, AA'XX'
3'/5'	115.5	6.91, AA'XX'	115.7	6.91, AA'XX'
4'	161.3	–	161.7	–
		Glucose moiety		
1''	71.3	4.77, 1H, *d* (9.0)	71.2	4.81, 1H, *d* (9.0)
2''	74.7	4.05, 1H, *t* (9.0)	75.0	4.02, 1H, *t* (9.0)
3''	79.6	3.42, 1H, *m*[a]	79.6	3.43, 1H, *m*[a]
4''	70.3	3.41, 1H, *m*[a]	70.3	3.42, 1H, *m*[a]
5''	81.6	3.25, 1H, *m*[a]	81.7	3.25, 1H, *m*[a]
6''	60.7	3.76, 1H, br *d* (12.0), 3.54, 1H, *dd* (12.0, 5.5)	60.7	3.77, 1H, br *d* (12.0), 3.54, 1H, *dd* (12.0, 5.5)
		Rhamnose moiety		
1''	99.8	4.98, 1H , br *s*	100.0	4.96, 1H, br *s*
2''	70.1	3.57, 1H, *m*[a]	70.1	3.57, 1H, *m*[a]
3''	70.3	3.08, 1H, *m*[a]	70.0	3.03, 1H, *m*[a]
4''	71.1	2.91, 1H, *t* (9.0)	71.1	2.90, 1H, *t* (9.0)
5''	67.9	2.12, 1H, *m*[a]	68.0	1.96, 1H, *m*[a]
6''	17.3	0.47, 3H, *d* (6.0)	17.4	0.45, 3H, *d* (6.0)
		O-methyl moiety		
7-*O*-CH_3	–	–	56.3	3.89, 3H, *s*

[a]Overlapping signals

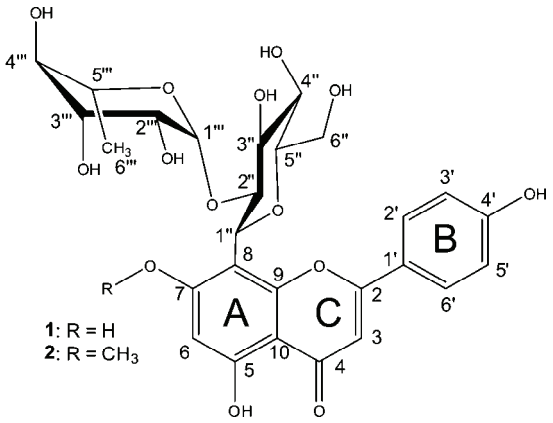

Fig. 1. The structure of compounds **1** and **2**.

C-Glycosides reported here from the leaves of *C. australis* and related compounds are also found in *Crataegus* and are supposed to contribute to the bioactivity of this well-known genus of medicinal plants.[6] Future investigations on the bioactivity of *C. australis* extracts are therefore of interest, in particular in areas where hawthorn (*Crataegus*) is medicinally used and where its content in flavonoids is believed to be responsible for its bioactivity.[16] Extracts rich in *Crataegus* flavonoids are mainly used against cardiovascular conditions and cardiovascular effects are believed to be the result of positive inotropic activity, ability to increase the integrity of the blood vessel wall and improve coronary blood flow, and positive effects on oxygen utilization.[16]

EXPERIMENTAL

Plant material

Leaves of *Celtis australis* L. were collected in May 2008 near Klughammer S of Bozen/Bolzano/TN/Italy at 230 m above mean sea level (coordinates (WGS84): N 46°21'; E 11°16'). Voucher specimens were deposited in the herbarium of the Institut für Botanik (IB #26883) and the private herbarium of CZ (code: CZ-20070506A-1).

Extraction and isolation

Air-dried, ground leaves (547 g) of *C. australis* were exhaustively macerated with MeOH to yield 91.0 g of crude extract after evaporation of the solvent *in vacuo*. The crude extract was re-dissolved in a mixture of MeOH and H_2O (1/2, v/v) and successively partitioned with petroleum ether, CH_2Cl_2 and *n*-BuOH. Finally, the aqueous layer was acidified with acetic acid and again partitioned with *n*-BuOH. The first *n*-BuOH layer was brought to dryness *in vacuo* to yield 10.7 g of residue. This was successively partitioned on Sephadex LH-20 using a mixture of methanol, acetone, and water (3/1/1, v/v/v) as the mobile phase. In the first separation step, a fraction of 5.72 g was obtained which contained compounds **1** and **2**. This was again fractionated by Sephadex LH-20 CC to yield a fraction of 4.03 g containing **1** and **2** and a fraction of 700 mg containing acacetin 7-*O*-glucoside, isovitexin, and cytisoside.[5] The fraction containing **1** and **2** was further fractionated by Sephadex LH-20 CC using the same system. Fractions enriched in **1** and **2** were united to yield 607 mg of dry material. 562 mg of this fraction were soluble in pure MeOH and fractionated by Sephadex LH-20 CC

using MeOH as the mobile phase. The fraction enriched in compounds **1** and **2** (total weight: 52.8 mg) was dissolved in 1.5 ml DMSO and compounds **1** and **2** were separated by semi-preparative RP-18 HPLC using a gradient of H_2O acidified with acetic and formic acid (0.9 and 0.1 %, respectively) and pure MeOH to yield 9.9 mg of **1** and 4.0 mg of **2**.

Acknowledgements. The authors wish to thank R. Spitaler (Innsbruck/Austria) and M. Sgarbossa (Auer/Italy) for helping collect the plant material and S. Gurschler (Meran/Italy) for extracting the leaves and for partitioning the crude extract.

ИЗВОД

РАМНОПИРАНОЗИЛВИТЕКСИНСКИ ДЕРИВАТИ ИЗОЛОВАНИ ИЗ *Celtis australis*

MARGARETHE KALTENHAUSER[1], ERNST P. ELLMERER[2] и CHRISTIAN ZIDORN[1]

[1]*Institut für Pharmazie der Universität Innsbruck, Abteilung Pharmakognosie, Josef-Moeller-Haus, Innrain 52, A-6020 Innsbruck и* [2]*Institut für Organische Chemie der Universität Innsbruck, Innrain 52a, A-6020 Innsbruck, Austria*

Из метанолног екстракта лишћа биљке *Celtis australis* изоловани су 2”-*α*-рамнопиранозилвитексин и 2”-*α*-рамнопиранозил-7-*O*-метилвитексин. Оба једињења су позната, али у овом раду су по први пут дати потпуни NMR подаци за друго једињење.

(Примљено 17. августа 2009, ревидирано 8. јануара 2010)

REFERENCES

1. T. G. Tutin, *Celtis*, in *Flora Europaea*, Vol. I, T. G. Tutin, V. H. Heywood, N. A. Burges, D. H. Valentine, S. M. Walters, D. A. Webb, Eds., Cambridge University Press, Cambridge, 1972, pp. 65–66
2. K. Ueda, K. Kosuge, H. Tobe, *J. Plant Res.* **110** (1997) 171
3. K. J. Sytsma, G. Morawetz, J. C. Pires, M. Nepokroeff, E. Conti, M. Zjhra, J. C. Hall, M. W. Chase, *Am. J. Bot.* **89** (2002) 1531
4. F. Siegmund, *Gemeinnütziges Kräuterbuch*, Hartleben’s Verlag, Wien, 1874
5. R. Spitaler, S. Gurschler, E. Ellmerer, B. Schubert, M. Sgarbossa, C. Zidorn, *Biochem. Syst. Ecol.* **37** (2009) 120
6. S. Prinz, A. Ringl, A. Hüfner, E. Pemp, B. Kopp, *Chem. Biodiv.* **4** (2007) 2920
7. D. Gođevac, B. Pejin, G. Zdunić, K. Šavikin, D. Stešević, V Vajs, S. Milosavljević, *J. Serb. Chem. Soc.* **73** (2008) 525
8. J. T. Doyama, H. G. Rodrigues, E. L. B. Novelli, E. Cereda, W. Vilegas, *J. Ethnopharm.* **96** (2005) 371
9. T. K. Tabopda, J. Ngoupayo, J. Liu, A.-C. Mitaine-Offer, S. A. K. Tanoli, S. N. Khan, N. Shamsun, M. S. Ali, B. T. Ngadjui, E. Tsamo, M.-A. Lacaille-Dubois, B. Luu, *Phytochemistry* **69** (2008) 1726
10. J. Zhao, R. S. Pawar, Z. Ali, I. A. Khan, *J. Nat. Prod.* **70** (2007) 289
11. H. Kumamoto, Y. Matsubara, Y. Iizuka, K. Okamoto, K. Yokoi, *Agric. Biol. Chem.* **49** (1985) 2613
12. T. Řezanka, P. Řezanka, K. Sigler. *Phytochemistry* **70** (2009) 1049
13. J. Chopin, G. Dellamonica, M. L. Bouillant, A. Besset, G. Popovici, G. Weissenböck, *Phytochemistry* **16** (1977) 2041
14. A. Ouabonzi, M. L. Bouillant, J. Chopin. *Phytochemistry* **22** (1983) 2632

15. J. Chopin, M. L. Bouillant, A. G. Ramachandran Nair, P. Ramesh, T. J. Mabry. *Phytochemistry* **17** (1978) 299
16. J. M. Rigelsky, B. V. Sweet. Am. J. Health-Syst. Pharm. **59** (2002) 417.

J. Serb. Chem. Soc. 75 (6) 739–747 (2010)
JSCS–4003

Journal of the Serbian Chemical Society
JSCS@tmf.bg.ac.rs • www.shd.org.rs/JSCS

UDC *NEPETA:665.52/54:615.28–188(540)(1–925.36)
Original scientific paper

Constituents and antimicrobial activity of the essential oils of six Himalayan *Nepeta* species

DINESH S. BISHT[1], RAJENDRA C. PADALIA[1,2], LALIT SINGH[3], VEENA PANDE[3], PRIYANKA LAL[4] and CHANDRA S. MATHELA[1]*

[1]*Department of Chemistry, Kumaun University, Nainital-263 002, Uttarakhand,* [2]*Central Institute of Medicinal and Aromatic Plants (CIMAP), Pantnagar-263 149, Uttarakhand,* [3]*Department of Biotechnology, Kumaun University, Nainital-263 002, Uttarakhand and* [4]*Department of Biotechnology, IIT, Roorkee-247 667, Uttarakhand, India*

(Received 6 November 2009, revised 11 January 2010)

Abstract: The essential oils from six Himalayan *Nepeta* species, *viz. Nepeta leucophylla* Benth., *Nepeta discolor* Royle ex Benth., *Nepeta govaniana* Benth., *Nepeta clarkei* Hook. f., *Nepeta elliptica* Royle ex Benth. and *Nepeta erecta* Benth., were tested for their *in vitro* antimicrobial activity against six pathogenic bacterial and two fungal strains. The results showed that *Pseudomonas aeruginosa* was the most sensitive strain tested to the essential oils of *Nepeta* species. The essential oils of *N. elliptica* and *N. erecta* exhibited the highest activity against *P. aeruginosa*, followed by the essential oils of *N. leucophylla* and *N. clarkei*. The essential oils from *N. elliptica* and *N. erecta* were also found to be very effective against *Serratia marcescens*; while the essential oil from *N. leucophylla* displayed significant activity against *Proteus vulgaris* and *Staphylococcus aureus*. Other bacterial strains displayed variable degree of susceptibility against one or more of the tested essential oils. The essential oil from *N. leucophylla* also showed the highest antifungal activity against both tested fungal strains, *viz. Candida albicans* and *Trichophyton rubrum*, followed by the essential oils from *N. clarkei*, *N. govaniana* and *N. erecta*. Iridodial derivatives, *viz.* iridodial *β*-monoenol acetate (25.4 %), dihydroiridodial diacetate (18.2 %) and iridodial dienol diacetate (7.8 %) were identified as the major constituents of *N. leucophylla*, while the essential oils from *N. elliptica* and *N. erecta* were dominated by (7*R*)-*trans*,*trans* nepetalactone (83.4 %) and isoiridomyrmecin (66.7 %), respectively. The essential oil of *N. discolor* was characterized by 1,8-cineole (25.5 %) and *β*-caryophyllene (18.6 %), while *N. clarkei* was dominated by *β*-sesquiphellandrene (22.0 %) and germacrene D (13.0 %). Isoiridomyrmecin (35.2 %) and pregeijerene (20.7 %) were identified as the major constituents of *N. govaniana*. In general the *Nepeta* species containing constituents with an iridoid or lactone skeleton were found to have the

* Corresponding author. E-mail: mathelacs@rediffmail.com
doi: 10.2298/JSC091106052B

greater antagonistic activity against most of the microbial strains as compared to those containing regular terpene constituents.

Keywords: *Nepeta*; essential oils; antimicrobial activity; iridoids; isoiridomyrmecin; nepetalactone.

INTRODUCTION

Nepeta genus (Lamiaceae) is comprised of about 250 species, widely distributed in temperate Europe, Asia, North America, North Africa and in the Mediterranean region.[1,2] Besides being used as antispasmodic, diuretic, febrifuge, diaphoretic, antimicrobial and antiseptic agents, *Nepeta* species are used as laxatives in the treatment of dysentery, for tooth troubles and for kidney and liver diseases.[3,4] Various biologically active iridoids/monoterpene nepetalactones were reported in *Nepeta* species possessing diverse biological activities, *viz*. feline attractant, canine attractant, insect repellant and arthropod defense.[5–8] Some of them act as pheromones and catnip response factors and are also known as ginseng of the cat.[9] The essential oil composition and antimicrobial activity of various *Nepeta* species were previously reported.[10–23] In earlier communications, some Himalayan *Nepeta* species were screened for their terpenoid constituents.[18–23] Iridodial β-monoenol acetate isolated from essential oil of *N. leucophylla* Benth. and actinidine isolated from essential oil of *N. clarkei* Hook. f. were shown to have significant antibacterial and antifungal activities.[24,25] The present communication reports the antibacterial and antifungal activities of the essential oils from six *Nepeta* species from Himalayan region of Uttarakhand, India.

EXPERIMENTAL

Plant materials

The fresh flowering aerial parts of *Nepeta leucophylla*, *N. discolor*, *N. govaniana*, *N. clarkei*, *N. elliptica* and *N. erecta* were collected from different locations of the Himalayan region of Uttarakhand, India (Table I). The plant herbaria were identified by the Botanical Survey of India, Dehradun and voucher specimens have been deposited in the Phytochemistry Laboratory, Chemistry Department, Kumaun University, Nainital.

TABLE I. Sites for collection of the *Nepeta* species and the essential oil yields

Plants	Collection site[a]	Oil yield[b], % (v/w)
Nepeta leucophylla	Nainital, 2400 m	0.68
Nepeta discolor	Malari, Chamoli, 2800 m	0.90
Nepeta govaniana	Bhundiar, Chamoli, 2600 m	0.85
Nepeta clarkei	Malari, Chamoli, 2800 m	0.70
Nepeta elliptica	Clips, Nainital 2700 m	0.92
Nepeta erecta	Hemkund, 3250 m	0.76

[a]Locations in Uttarakhand (Himalayan region, India); [b]oil yields were determined on fresh weight basis, average of three extraction (*SD* = 0.04)

Isolation of essential oil and major isolates

The fresh flowering aerial parts (2 kg) of each plant were subjected to steam distillation using an electric copper still, fitted with spiral glass condensers. The distillates were saturated with NaCl and extracted with *n*-hexane and dichloromethane. The organic phase was dried over anhydrous Na_2SO_4 and the solvent was distilled off in a rotary vacuum evaporator at 30 °C. The essential oils were fractionated by column chromatography (CC) on silica gel (230––400 mesh, Merck, 600×25 cm column) packed with hexane, and eluted with hexane followed by a gradient elution with Et_2O/hexane (5–20 %). The isolated compounds (**1**–**12**) were further purified using a Waters HPLC fitted with a μ-Porosil column (250 mm×7.8 mm) and an RI detector at an attenuation of 32X, using 5–15 % Et_2O in hexane at a flow rate of 2.0 mL/min and a pressure of 3000 psi.

GC and GC–MS analysis

The oils were analyzed using a Nucon 5765 gas chromatograph equipped with an Rtx-5 non-polar fused silica capillary column (30 m×0.32 mm, film thickness: 0.25 μm). The oven temperature (60–210 °C) was programmed at 3 °C/min and N_2 was used as the carrier gas at 4 kg/cm^2. The injector temperature was 210 °C, detector temperature 210 °C and the injection volume 0.5 μL, using a 10 % solution of the oil in *n*-hexane. GC–MS was conducted on a ThermoQuest Trace GC 2000 fitted with an Rtx-5 non-polar fused silica capillary column (30 m×0.25 mm, film thickness: 0.25 μm) and interfaced with a Finnigan MAT Polaris Q ion trap mass spectrometer. The oven temperature (60–210 °C) was programmed at 3 °C/min and helium was used as the carrier gas at 1.0 mL/min. The injection, ion source and MS transfer line temperatures were 210, 200 and 275 °C, respectively; the injection volume was 0.10 μL and the split ratio was 1:40. The MS were taken at 70 eV with a mass range of 40–450 amu.

Identification of constituents

The identification was realized based on their linear retention index (LRI) and the retention times determined with reference to homologous series of *n*-alkanes (C_9–C_{24}, Polyscience Corp., Niles IL) and standards (Sigma) under identical experimental conditions. The identification was further supported by MS Library searches (NIST and WILEY) and by comparing MS literature data,[26,27] as well as by IR, NMR (^{1}H-and ^{13}C-NMR) data of the major isolates. The relative amounts of individual components were calculated based on the GC peak area (FID response) without using a correction factor.

Test microorganisms

The *in vitro* antibacterial activities of the essential oils were evaluated against a total of six bacteria, which includes five gram negative bacteria *viz*. *Pseudomonas aeruginosa* (MTCC 424), *Escherichia coli* (MTCC 443), *Pasteurella multocida* (MTCC 1148), *Proteus vulgaris* (MTCC 1771) and *Serratia marcescens* (MTCC 8708) with one gram positive bacterium *Staphylococcus aureus* (MTCC 737). The antifungal activity of the oils was performed against *Candida albicans* (MTCC 183) and *Trichophyton rubrum* (MTCC 296). The test strains were purchased from the Institute of Microbial Technology (IMTECH), Chandigarh, India. Microbial technology culture collection (MTCC) numbers represent the standard strain numbers assigned to these microorganisms. The cultures of bacteria and fungi were maintained on their appropriate agar slants at 4 °C throughout and used as stock cultures.

Determination of zone of inhibition

The antimicrobial activity of the essential oils was investigated by the disc diffusion method using 24–48 h grown strains reseeded on nutrient broth (bacterial strains) and potato

dextrose agar (PDA, fungal strains).[28] The cultures were adjusted to 5×10^6 CFU/mL with sterile water. 100 μL of the suspensions were spread over nutrient agar and PDA plates to obtain uniform microbial growth. Filter paper discs (6.0 mm in diameter) were impregnated with 20 μL of the oils and then placed onto the agar plates which had previously been inoculated with the test microorganism. The petri dishes were kept at 4 °C for 2 h. The plates were incubated at 37 (24 h) and at 30 °C (48 h) for bacterial and fungal strains, respectively. The diameter of the inhibition zones (mean values) were measured in millimeter and considered as the zone of inhibition (ZOI). All experiments were performed in triplicate.

Determination of the minimum inhibitory concentration (MIC)

The minimum inhibitory concentration (MIC) values were determined using a modified agar-well diffusion method.[28] In the agar-well diffusion technique, two-fold serial dilutions of the essential oils were prepared by diluting oil with hexane to achieve a decreasing concentration range from 50 to 0.19 μL/mL (for the fungi) and 50 to 0.15 μL/mL (for the bacteria), using 100 μl of a suspension containing 5×10^6 CFU/ml of bacteria spread on nutrient agar plates, whereas the fungal strains were reseeded on PDA. The wells were filled with 20 μl of essential oil solutions in the inoculated nutrient/PDA agar plates. The bacterial cultures were incubated at 37 °C for 24 h, while fungal cultures were incubated at 30 °C for 48 h. The least concentration of each essential oil showing a clear zone of inhibition was taken as the *MIC*. Hexane was used as the negative control. Streptomycin and clotrimazole were used as positive controls for bacteria and fungi, respectively.

RESULTS AND DISCUSSION

The oil yield from different *Nepeta* species varied from 0.70 to 0.92 % calculated on the basis of the fresh weight of the plant material (Table I). The marker constituents identified in the essential oils of *Nepeta* species are listed in Table II. Iridodial derivatives, *viz*. iridodial *β*-monoenol acetate (**1**), dihydroiridodial diacetate (**2**) and iridodial dienol diacetate (**3**) were the major constituents of the essential oil of *N. leucophylla*. The essential oil of *N. discolor* was characterized by 1,8-cineole (**4**), *β*-caryophyllene (**5**) and *p*-cymene (**6**). Isoiridomyrmecin (**7**) and pregeijerene (**8**) were identified as the major constituents of *N. govaniana*. The essential oil from *N. clarkei* was dominated by *β*-sesquiphellandrene (**9**), germacrene D (**10**), *α*-guaiene (**11**) and diastereomeric iridodial esters. On the contrary, the essential oil from *N. elliptica* and *N. erecta* were dominated by a single major constituent, *viz*. (7*R*)-*trans*,*trans*-nepetalactone (**12**) and isoiridomyrmecin (**7**), respectively. The structures of marker compounds/ /major constituents are given in Fig. 1.

The essential oils were screened for possible antagonistic activity against six bacterial and two fungal strains. The results of *in vitro* test (Table III) showed that almost all the tested essential oils showed moderate to high activities against one or more of the tested pathogens in the petri plate assay, based on the zone of inhibition and *MIC* values. Some of the essential oils showed significant antibacterial and antifungal activities when the zone of inhibition values were compared to those of the standards, *viz*. streptomycin and clotrimazole. The mean zones of inhibition for the bacterial strains were in the range 6.0 to 28.4 mm, with the *MIC*

values ranging from 0.15 to 30.34 μL/mL. The inhibition zones for the fungal strains varied from 9.3 to 20.0 mm, with the *MIC* values ranging from 0.19 to 12.50 μL/mL. The positive control streptomycin (for bacteria) showed 18.6 to 27.6 mm mean inhibition zones and clotrimazole (for fungi) showed 18.2 and 19.1 mm inhibition zones. The negative control did not show an inhibitory effect on any of the tested strains.

TABLE II. Marker constituents of the essential oils from Himalayan *Nepeta* species

Plant	Marker constituents[a]	Content, % (based on FID response)
Nepeta leucophylla	Iridodial *β*-monoenol acetate (**1**)	25.4
	Dihydroiridodial diacetate (**2**)	18.2
	Iridodial dienol diacetate (**3**)	7.8
Nepeta discolor	1,8-Cineole (**4**)	25.5
	β-Caryophyllene (**5**)	18.6
	p-Cymene (**6**)	9.8
Nepeta govaniana	Isoiridomyrmecin (**7**)	35.2
	Pregeijerene (**8**)	20.7
Nepeta clarkei	Iridodial *β*-monoenol acetate diastereomers	25.3
	β-Sesquiphellandrene (**9**)	22.0
	Germacrene D (**10**)	13.0
	α-Guaiene (**11**)	10.0
Nepeta elliptica	(7*R*)-*trans*,*trans*-Nepetalactone (**12**)	83.4
Nepeta erecta	Isoiridomyrmecin (**7**)	66.7

[a]Mode of identification: linear retention index (LRI, based on a homologous series of *n*-alkanes; C_9–C_{24}), co-injection with standards (Sigma), MS (GC–MS)

The data indicated that *P. aeruginosa* was the tested strain most sensitive to the essential oils of the *Nepeta* species, with the strongest inhibition zones varying from 18.2 to 28.4 mm. The essential oils of *N. elliptica* and *N. erecta* were found to exhibit the largest zones of inhibition (28.4 mm, *MIC* = 0.31 μL/mL; 28.0 mm, *MIC* = 0.62 μL/mL) against *P. aeruginosa* followed by *N. leucophylla* (27.4 mm, *MIC* = 0.42 μL/mL) and *N. clarkei* (22.0 mm, *MIC* = 0.15 μL/mL).

P. aeruginosa is known to have a high level of intrinsic resistance to virtually all known antimicrobials and antibiotics due to a very restrictive outer membrane barrier, which is highly resistant even to synthetic drugs. Furthermore, earlier reports on the antimicrobial activity of essential oils of *Nepeta* species stated they possessed very little or no activity against *P. aeruginosa*.[11–13,29] Thus, the results of the antibacterial activity of all the tested oils against *P. aeruginosa* evidenced in the present study are very promising. The essential oils from *N. elliptica* and *N. erecta* were also found to be very effective against *S. marcescens* (20.2 mm, *MIC* = 0.43 μL/mL; 18.3 mm, *MIC* = 1.59 μL/mL). The essential oil from *N. leucophylla* also displayed significant activity against *P. vulgaris* and *S. aureus* (21.2 mm, *MIC* = 3.21 μL/mL; 16.4 mm; *MIC* = 1.78 μL/mL). Other bac-

terial strains displayed variable degrees of susceptibility against one or more of the tested essential oils. Furthermore, most gram negative bacteria are more resistant to various antimicrobials,[30] but in the present study, the tested essential oils showed promising antimicrobial activities against most of the gram negative bacteria.

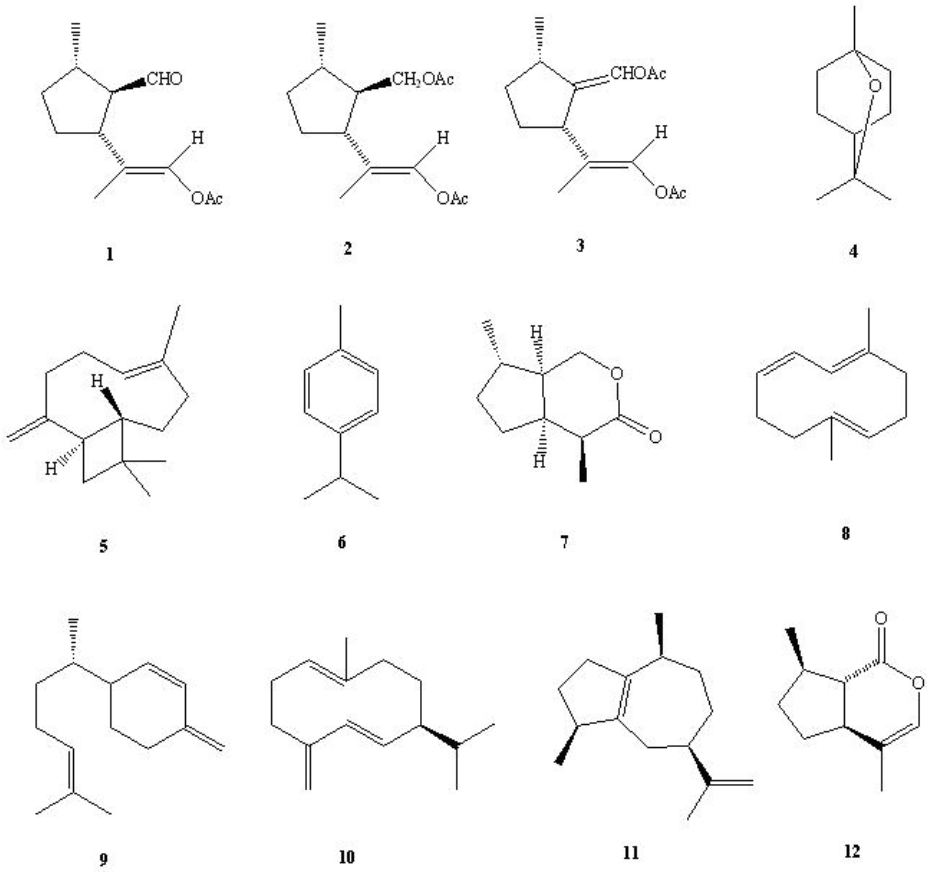

Fig. 1. Structures of major/marker constituets of Himalayan *Nepta* species.

The essential oil from *N. leucophylla* showed maximum antifungal activity against both *C. ablicans* (20.0 mm, *MIC* = 0.78 μL/mL) and *T. rubrum* (19.2 mm, *MIC* = 0.19 μL/mL). The essential oils from *N. elliptica*, *N. erecta* and *N. govaniana* also showed significant activity against both the fungal strains, whereas, *N. clarkei* and *N. discolor* showed poor activity against both the fungal strains.

The essential oils possessing chemical constituents with an iridoid or lactone skeleton were noticed to be more active antibacterial/antifungal as compared to those containing regular terpene constituents. This might be due to their higher

water solubility and diffusion coefficient through the medium and also due to their higher hydrogen bonding potential. By inhibiting the growth of almost all human and plant pathogenic and/or food spoilage bacteria and fungi tested, the essential oil from Himalayan *Nepeta* species exerted a broad antimicrobial spectrum, the iridoid/ lactone containing oils showed higher activity. Furthermore, the obtained results showing a wide spectrum of antibacterial and antifungal activities may provide support to the traditional applications of these plants.

TABLE III. Antibacterial and antifungal activities of essential oils of six Himalayan *Nepeta* species

Plant	Zone of inhibition[a], mm (*MIC* / μL mL^{-1})							
	Bacteria						Fungi	
	E. coli	*P. aeruginosa*	*S. aureus*	*P. multocida*	*P. vulgaris*	*S. marcescens*	*C. albicans*	*T. rubrum*
N. leucophylla	9.0 (15.62)	27.4 (0.42)	20.0 (6.24)	na[b]	21.2 (3.21)	16.4 (1.78)	20.0 (0.78)	19.2 (0.19)
N. discolor	10.4 (7.54)	18.2 (1.42)	na	na	9.4 (7.2)	na	12.0 (3.21)	9.3 (7.30)
N. govaniana	13.0 (10.24)	20.1 (0.37)	7.3 (3.90)	16.0 (11.34)	na	na	16.1 (1.56)	18.1 (1.58)
N. clarkei	11.1 (9.24)	22.0 (0.15)	16.2 (11.03)	6.9 (30.34)	14.2 (1.54)	7.5 (16.52)	13.7 (3.50)	12.5 (12.50)
N. elliptica	20.8 (2.58)	28.4 (0.31)	19.4 (2.05)	10.4 (2.60)	na	20.2 (0.43)	18.0 (0.19)	19.1 (0.39)
N. erecta	22.2 (3.25)	28.0 (0.62)	18.5 (2.36)	na	18.2 (1.56)	18.8 (1.59)	18.2 (1.50)	15.4 (1.41)
Standard[c]	27.1	27.6	23.5	18.6	23.0	19.5	19.1	18.2

[a]Diameter of inhibition zones (mm) including the diameter of the disc (6.0 mm); values are the mean of three replicates; oil concentration 20 μL/disc; [b]not active; [c]standard: streptomycin (10 μg/disc for bacterial strains) and clotrimazole (20 μg/disc for fungal strains)

Acknowledgements. The authors are grateful to the authorities of BSI, Dehradun for the identification of the plants. DSB is grateful to GBPIHE&D-IERP, Kosi-Katarmal, Uttarakhand for a fellowship.

И З В О Д

САСТАВ И АНТИМИКРОБНА АКТИВНОСТ ЕТАРСКИХ УЉА ИЗОЛОВАНИХ ИЗ ШЕСТ ВРСТА БИЉКЕ *Nepeta* СА ХИМАЛАЈА

DINESH S. BISHT[1], RAJENDRA C. PADALIA[1,2], LALIT SINGH[3], VEENA PANDE[3], PRIYANKA LAL[4] и CHANDRA S. MATHELA[1]

[1]Department of Chemistry, Kumaun University, Nainital-263 002, Uttarakhand, [2]Central Institute of Medicinal and Aromatic Plants (CIMAP), Pantnagar-263 149, Uttarakhand, [3]Department of Biotechnology, Kumaun University, Nainital-263 002, Uttarakhand и [4]Department of Biotechnology, IIT, Roorkee-247 667, Uttarakhand, India

Испитана је антимикробна активност спрам шест врста патогених бактерија и две врсте гљива етарских уља изолованих из шест врста биљке *Nepeta*, која расте на Хималајима: *Ne-*

peta leucophylla Benth., *Nepeta discolor* Royle ex Benth., *Nepeta govaniana* Benth., *Nepeta clarkei* Hook. f., *Nepeta elliptica* Royle ex Benth. и *Nepeta erecta* Benth. Резултати су показали да је *Pseudomonas aeruginosa* најосетљивији сој на етарска уља врста *Nepeta*. Етарска уља *N. elliptica* и *N. erecta* су имала највећу активност спрам *P. aeruginosa*, а затим етарска уља *N. leucophylla* и *N. clarkei*. Етарска уља *N. elliptica* и *N. erecta* су била веома активна спрам *Serratia marcescens*, док је уље *N. leucophylla* испољило значајну активност спрам *Proteus vulgaris* и *Staphylococcus aureus*. Остали бактеријски сојеви су испољили различит степен осетљивости на тестирана етарска уља. Етарско уље *N. leucophylla* је имало највећу антифунгалну активност, спрам обе врсте тестираних гљива: *Candida albicans* и *Trichophyton rubrum*, док су уља *N. clarkei*, *N. govaniana* и *N. erecta* испољила мању активност. Деривати иридодиала, иридодиал-β-моноенол-ацетат (25,4 %), дихидроиридодиал диацетат (18,2 %) и иридодиал-диенол-диацетат (7,8 %) су главни састојци уља *N. leucophylla*, док су у уљима *N. elliptica* и *N. erecta* доминантни (7R)-*trans*,*trans*-непеталактон (83,4 %) и изоиридомирмецин (66,7 %). У етарском уљу *N. discolor* је највише 1,8-цинеола (25,5 %) и β-кариофилена (18,6 %), док је у уљу *N. clarkei* највише β-сесквифеландрена (22,0 %) и гермакрена Д (13,0 %). Изоиридомирмецин (35,2 %) и прегеијерен (20,7 %) су главни састојци *N. govaniana*. Уопштено, *Nepeta* врсте које садрже једињења са иридоидним или лактонским скелетом имају већу антагонистичку активност спрам микробних сојева у поређењу са врстама која садрже стандардне терпенске састојке.

(Примљено 6. новембра 2009, ревидирано 11. јануара 2010)

REFERENCES

1. D. J. Mabberly, *The Plant Book*, Cambridge University Press, Cambridge, 1997
2. C. Turner, *Nepeta L.*, in *Flora Europaea*, Cambridge University Press, Cambridge, U.K., 1972
3. G. Usher, *A Dictionary of Plants Used by Man*, C.B.S Publishers, New Delhi, 1984
4. J. Hussain, N. Jamila, S. A. Gilani, G. Abbas, S. Ahmed, *African J. Biotech.* **8** (2009) 935
5. T. Eisner, *Science* **148** (1965) 966
6. G. Gkinis, O. Tzakou, D. Ilipoulou, V. Roussis, *Z. Naturforsch. C.* **58** (2003) 681
7. A. O. Tucker, S. S. Tucker, *Econ. Bot.* **42** (2009) 214
8. H. Wagner, P. Wolf, *New Natural Products and Plant Drugs with Pharmacological, Biological and Therapeutical Activity*, Springer Verlag, New York, 1977
9. Y. Zhao, X. Wang, Z. Wang, Y. Lu, C. Fu, S. Chen, *J. Zhejiang Uni. Sci. B* **7** (2006) 708
10. A. Alim, I. Goze, A. Cetin, A. D. Atlas, S. A. Cetinus, N. Vural, *African J. Microbiol. Res*. **3** (2009) 463
11. L. Zenasni, H. Bouidida, A. Hancali, A. Boudhane, H. Amjal, A. Il Idrissi, R. El Aouad, Y. Bakri, A. Benjouad, *J. Med. Plant Res.* **2** (2008) 111
12. A. Celik, N. Mercan, I. Arslan, H. Davran, *Chem. Nat. Com*. **44** (2008) 119
13. G. Stojanovic, N. Radulovic, J. Lazarevic, D. Miladinovic, D. Dokovic, *J. Essent. Oil Res.* **17** (2005) 587
14. A. Ozturk, *Asian J. Chem*. **21** (2009) 6440
15. A. Sonboli, A. Gholipour, M. Yousefzadi, M. Mojarrad, *Nat. Prod. Commun*. **4** (2009) 283
16. U. Suschke, F. Sporer, J. Schneele, H. K. Geiss, J. Reichling, *Nat. Prod. Commun*. **2** (2007) 1277
17. M. L. Gribić, M. Stupar, J. Vukojević, M. Soković, D. Mišić, D. Grubišić, M. Ristić, *J. Serb. Chem. Soc*. **73** (2008) 961

18. A. T. Bottini, V. Dev, D. J. Garfagnoli, H. Lohani, A. K. Pant, C. S. Mathela, *Phytochemistry* **26** (1987) 1200
19. A. T. Bottini, V. Dev, G. C. Shah, C. S. Mathela, A. B. Melkani, A. T. Nerio, N. S. Strum, *Phytochemistry* **35** (1992) 1653
20. C. S. Mathela, H. Kharkwal, R. Laurent, *J. Essent. Oil Res*. **6** (1994) 425
21. a) C. S. Mathela, H. Kharkwal, R. Laurent, *J. Essent. Oil Res*. **6** (1994) 519; b) R. Bhandari, C. S. Mathela, P. Beauchamp, A. T. Bottini, V. Dev, *Phytochemistry* **34** (1993) 1438
22. M. Bisht, S, Sharma, C. S. Mathela, *Asian J. Chem*. **9** (1997) 612
23. T. K. Kashyap, A. B. Melkani, C. S. Mathela, V. Dev, M. M. Olmstead, H. Hope, A. T. Bottini, *J. Essent. Oil Res.* **15** (2003) 28
24. J. Saxena, C. S. Mathela, *Appl. Environ. Microbiol*. **62** (1996) 702
25. C. S. Mathela, N. Joshi, *Nat. Prod. Commun*. **3** (2008) 945
26. R. P. Adams, *Identification of Essential Oil Components by Gas Chromatography/Mass Spectroscopy*, *Allured Publishing Corporation*, Carol Stream, IL, 1995
27. R. P. Adams, *Identification of Essential Oil Components by Gas Chromatography/ Quadrupole Mass Spectrometry*, Allured Publishing Corporation, Carol Stream, IL, 2001
28. J. L. Rios, M. C. Recio, A. Vilar, *J. Ethnopharm*. **23** (1988) 127
29. P. Salehi, A. Sonboli, L. Allahyari, *J. Essent. Oil Bear. Plants* **10** (2007) 324
30. H. J. D. Darman, S. G. Deans, *J. Appl. Microbiol*. **88** (2000) 308.

Journal of the Serbian Chemical Society
JSCS@tmf.bg.ac.rs • www.shd.org.rs/JSCS

J. Serb. Chem. Soc. 75 (6) 749–761 (2010)
JSCS–4004

UDC 546.795.4+547.72'828'288.3:
543.57:615.277–188
Original scientific paper

Synthesis, thermal and antitumour studies of Th(IV) complexes with furan-2-carboxaldehyde4-phenyl-3-thiosemicarbazone

GANGADHARAN RAJENDRAN[1]*, CHIRAKUZHI S. AMRITHA[1], RUBY JOHN ANTO[2] and VINO T. CHERIYAN[2]

[1]*Department of Chemistry, University College, Thiruvananthapuram-695034, Kerala and* [2]*Division of Cancer Research, Rajiv Gandhi Centre for Biotechnology, Thiruvananthapuram-695014, Kerala, India*

(Received 29 July 2009, revised 2 February 2010)

Abstract: Thorium(IV) complexes with the Schiff base furan-2-carboxaldehyde4-phenyl-3-thiosemicarbazone (L) were synthesised and characterized. The composition and structure of the metal complexes were proposed based on elemental analysis, molar conductivity measurements, FTIR and ^{1}H-NMR spectroscopy. The Schiff base behaves as a neutral bidentate ligand coordinating through the azomethine N and the thioketo S atoms. From various studies, complexes were ascertained the general formula $[ThL_2X_4]$ and $[ThL_2Y_2]$, where X represents NO_3^-, NCS^-, CH_3COO^-, $CH_3CHOHCOO^-$, ClO_4^- and Y $SO_4^{2-}$and $C_2O_4^{2-}$. The thermal behaviour of the nitrato and oxalato complexes was studied and kinetic and thermodynamic parameters were calculated using the Coats-Redfern Equation. The ligand and a representative complex $[ThL_2(NO_3)_4]$ were screened *in vitro* for their antitumour activity against the human cervical cancer cell line (HeLa).

Keywords: thorium(IV) complexes; furan-2-carboxaldehyde4-phenyl-3-thiosemicarbazone; antitumour activity; thermal analysis.

INTRODUCTION

Complexes of thiosemicarbazones have been explored for a variety of reasons, such as variable bonding properties, presence of several donor sites, structural diversity and pharmacological aspects.[1] They present a variety of biological activities, including anticancer and anti-inflammatory activities.[2–4] Metal thiosemicarbazonate complexes are emerging as a new class of experimental anticancer and chemotherapeutic agents which exhibit inhibitory activities against most cancer through inhibition of a crucial enzyme obligatory for DNA biosynthesis and cell division, *viz*. ribonucleotide diphosphate reductase (RDR).[5] Some thiosemi-

* Corresponding author. E-mail: drrajendranetal@gmail.com
doi: 10.2298/JSC090729048R

carbazones even increase their antitumour activity by their ability to form chelates with specific metal ions.[6] It was reported that the anticancer activities of thiosemicarbazones were closely related to the parent aldehyde or ketone group, metal chelation ability and terminal amino substitution. Among them, the parent aldehyde or ketone group was considered critical for the anticancer activity of thiosemicarbazones. Heterocyclic thiosemicarbazone showed higher activity compared with aromatic thiosemicarbazones.[7] Heterocyclic thiosemicarbazones and their metal complexes are among the most widely studied compounds for their potential therapeutic uses, such as antitumoural, fungicidal, bactericidal or antiviral activity.[8] The activity of these compounds is dependent on the nature of the hetroaromatic ring and the position of attachment of the ring as well as on the form of the thiosemicarbazone moiety.[9] There were several studies involving thiosemicarbazones with different metal ions.[10–13] However, only a few reports described studies on thorium thiosemicarbazone complexes. Hence as part of ongoing research regarding thiosemicarbazone complexes of thorium[14,15], the synthesis, characterization and antitumour activity of Th(IV) complexes with furan--2-carboxaldehyde4-phenyl-3-thiosemicarbazone (Fig. 1) are reported herein.

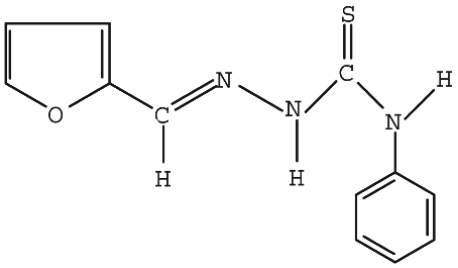

Fig. 1. Schematic view of the ligand.

EXPERIMENTAL

Materials and analytical methods

All employed chemicals were of analytical grade purchased from Merck, Sisco (India), *etc*. Commercial solvents were distilled and used for synthesis, but for the physicochemical studies, they were purified by standard methods.

The IR spectral studies were performed using KBr discs on a Schimadzu 8201 PC FT infrared spectrophotometer. The ^{1}H-NMR spectra were recorded on a Bruker DRX-300 FT NMR spectrophotometer employing TMS as the internal reference and DMSO-d_6 as the solvent. X-Ray diffraction studies were realized using a Philips X-ray PW 1710 diffractometer using K-α1 radiation of wavelength 1.54056 Å. Molar conductance measurements of 10^{-3} M solutions in CH_3CN and $C_6H_5NO_2$ were performed at room temperature using a direct reading Elico conductivity bridge. TG and DTG curves were recorded on a Mettler Toledo 850 C simultaneous TG/DTA thermal analyzer system in dynamic air at a heating rate of 10 °C/min. The TG data was analyzed using the Coats-Redfern Equation for calculating the kinetic and thermodynamic parameters. Elemental analyses were realized using an Elementar Vario EL III Carlo Erba 1108 elemental analyzer at the Central Drug Research Institute, Lucknow, India.

The metal content was estimated gravimetrically by the oxalate–oxide method.[16] Standard gravimetric procedures were adopted for the estimation of the anions in the prepared complexes.[17] The sulphate and thiocyanate present in the complexes were estimated gravimetrically as $BaSO_4$ and AgNCS, respectively, while the perchlorate content was determined by the Kurz method.[18] The nitrate, oxalate, acetate and lactate contents were indirectly fixed by performing elemental analysis for carbon, hydrogen and nitrogen by micro analytical methods.

Synthesis of ligand

The ligand, furan-2-carboxaldehyde4-phenyl-3-thiosemicarbazone, was prepared by the following method. Furan-2-carboxaldehyde (0.010 mol) in methanol (10 ml) was added dropwise to a hot solution of 4-phenyl-3-thiosemicarbazide (0.010 mol) in methanol (30 ml) under constant stirring. The resulting mixture was heated on a water bath for 3 h, concentrated and allowed to cool. The formed dark brown crystals of the ligand were washed, dried and recrystallized from ethanol. Yield: 84 %; m.p. 120 °C ; Anal. Calcd. for $C_{12}H_{11}N_3OS$: C, 58.77; H, 4.49; N, 17.14; S, 13.06 %. Found: C, 58.56; H, 4.54; N, 17.63; S, 13.21 %. IR (KBr, cm^{-1}): 3256, (*m*, –NH), 1623 (*vs*, C=N), 1526 (*m*, C–O furan ring), 1060 (*m*, (N–N), 868 (*s*, C=S).

Synthesis of metal complex

The metal complexes were prepared by refluxing a methanolic solution of the metal salt and the ligand in the stoichiometric ratio 1:2. For the preparation of the nitrato complex, the appropriate amount of the metal salt (0.0020 mol) dissolved in a minimum quantity of methanol (10 ml) was added to a solution of the ligand (0.0040 mol, 0.10 g) dissolved in methanol (25 ml). The pH of the solution was raised to 7 and refluxed on a water bath for about 5 h. It was then concentrated and left standing over night. The separated complex was filtered, washed with a methanol–water mixture (50 % v/v) and then with ether and dried over P_4O_{10} *in vacuo*. The other anionic complexes were prepared from the nitrato complex by the substitution method[19] by refluxing stoichiometric amounts of the nitrato complex with the respective anionic salts of lithium.

Antitumour screening

The *in vitro* antitumour activities of the ligand and a representative complex were examined by the MTT assay method[20,21] against human cervical cancer cell line (HeLa).

The human cervical cancer cell line (HeLa) was obtained from the National Centre for Cell Science Pune, India. The cells were grown in Dulbecco's modified eagles medium (DMEM) containing 10 % foetal bovine serum (FBS), streptomycin (100 μg/ml), penicillin (100 units/ml) and amphotericin B (2.5 μg/ml). The cells were incubated at 37 °C in a 5 % CO_2 incubator in a humid condition and harvested using trypsin–ethylene diamine tetraacetic acid.

The test samples were dissolved in DMSO and diluted to the required concentration for the biological experiments. Studies were undertaken with the test compounds in the concentration range from 10 to 100 μg/ml.

For the determination of the cytotoxic effects, cells harvested from the exponential phase were seeded equivalently (5000 cells/well) in a 96-well plate and incubated for 24 h. Test solutions of different concentrations were added in triplicate to the well plates. Six well plates were maintained in a drug free medium to determine the control, cell survival and the percentage of live cells after culture. Cells with various concentrations of the test samples were incubated at 37 °C for 72 h.

To determine the numbers of live cells, the dye 3-(4,5-dimethylthiazol-2yl)-2,5-diphenyltetrazolium bromide (MTT) was added to the cells, which were then incubated for 2 h

at 37 °C. MTT is metabolized in the presence of the pyridine cofactors NADH and NADPH, to give blue insoluble crystals. The cells were solubilised with 0.1 ml of extraction buffer (20 % sodium dodecyl sulphate in 50 % dimethylformamide) and then incubated for 4 h at 37 °C. Following the solubilisation of the cells, the colour intensity was read at 570 nm using an Elisa plate reader (Bio-Rad). The percentage viability of the cells or cell survival (*CS*) was expressed as mean optical density (drug exposed cell) divided by mean optical intensity (control).

RESULTS AND DISCUSSION

All the prepared complexes were brown coloured, non-hygroscopic solids stable at room temperature. They were soluble in DMSO and DMF but insoluble in water and common organic solvents. The room temperature molar conductivities of 10^{-3} M solutions of the complexes in CH_3CN and $C_6H_5NO_2$ corresponded to those of non-electrolytes.[22] The analytical data revealed that all complexes possessed 1:2 metal to ligand stoichiometry. Based on elemental analysis, the complexes were assigned the composition shown in Table I.

TABLE I. Molar conductance at room temperature and elemental analyses data of the complexes (L = $C_{12}H_{11}N_3OS$)

Complex	Found (Calcd.), %					Molar conductance S cm^2 mol^{-1}	
	Metal	C	H	N	S	$C_6H_5NO_2$	CH_3CN
$[ThL_2(NO_3)_4]$ (**1**)	23.85 (23.92)	29.63 (29.69)	2.16 (2.26)	14.53 (14.43)	6.79 (6.59)	5.7	13.8
$[ThL_2(SO_4)_2]$ (**2**)	25.25 (25.38)	31.45 (31.51)	2.30 (2.41)	9.09 (9.19)	14.15 (14)	7.5	12.1
$[ThL_2(NCS)_4]$ (**3**)	24.21 (24.32)	35.12 (35.22)	2.51 (2.31)	14.47 (14.67)	20.21 (20.13)	8.8	10.8
$[ThL_2(C_2O_4)_2]$ (**4**)	25.64 (25.84)	37.22 (37.42)	2.15 (2.45)	9.55 (9.35)	7.03 (7.13)	6.9	9.6
$[ThL_2(CH_3COO)_4]$ (**5**)	24.30 (24.22)	40.02 (40.08)	3.25 (3.55)	8.17 (8.77)	6.28 (6.68)	7.1	11.1
$[ThL_2(C_3H_5O_3)_4]$ (**6**)	21.27 (21.52)	40.26 (40.07)	3.87 (3.89)	7.81 (7.79)	5.73 (5.93)	7.9	13.6
$[ThL_2(ClO_4)_4]$ (**7**)	20.67 (20.71)	25.76 (25.71)	1.50 (1.96)	7.63 (7.5)	5.49 (5.71)	12.9	17.1

Spectral studies

The IR spectrum of the ligand showed a strong absorption band at 1623 cm^{-1} which was assigned to the azomethine group, ν(C=N).[23] In principle, the ligand can exhibit thione–thiol tautomerism owing to the presence of a thioamide –NH–C=S functionality (Fig. 2). The possibility of thione–thiol tautomerism in the ligand was ruled out as no band around 2700–2500 cm^{-1}, characteristic of the thiol group, was observed in the IR spectrum[24] (Fig. 3). The strong band observed at 868 cm^{-1} in the spectrum was due to the stretching vibrations of

C=S.[7,25] The bands observed at 3256 and 3423 cm^{-1} were assigned to N–H vibrations. This further indicates that the ligand remained in the thione form.

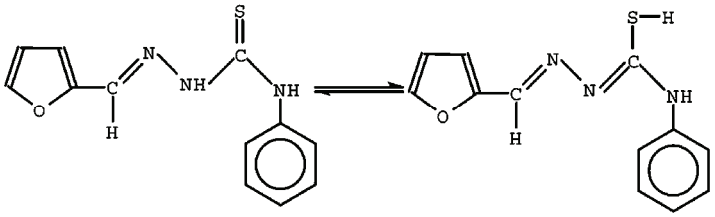

Fig. 2. Tautomeric forms of the ligand.

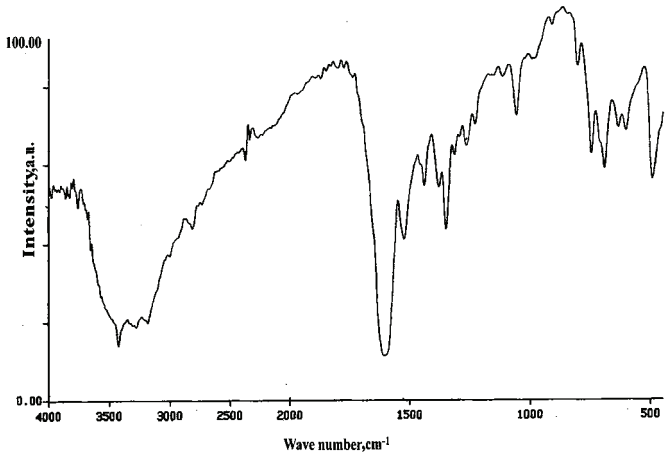

Fig. 3. IR spectrum of furan-2-aldehyde-*N*-phenylthiosemicarbazone.

The diagnostic IR spectral bands of the complexes are presented in Table II, together with their tentative assignments. In the spectra of all the complexes, the band due to the azomethine moiety (C=N) was shifted to a lower frequency by ≈ 20–30 cm^{-1}, indicating its involvement in coordination with metal ion. The ν(C=S) stretching frequency was lowered by ≈20–40 cm^{-1} in the spectra of the complexes, indicating the involvement of the thioketo sulphur in the coordination. These findings are further supported by the appearance of new bands in the far IR region at 495–505 and 359–370 cm^{-1}, which are assignable to ν(Th–N) and ν(Th–S) vibrations, respectively.

The IR spectra of the complexes differed among themselves due to the various coordinating anions and possessed additional non-ligand bands characteristic of the anion present. The spectrum of the complex **1** showed three bands at 1495, 1373 and 1033 cm^{-1}, assignable to the ν_4, ν_1 and ν_2 modes of the coordinated nitrate ions. The magnitude of the separation between the split bands (ν_4 and ν_1) was 120 cm^{-1}, indicating monodentate coordination[26] of the nitrate ion to the metal. In the spectra of complexes **5** and **6**, $\nu_a(COO^-)$ was observed at

1598 and 1596 cm^{-1}, respectively, and $\nu_s(COO^-)$ at 1362 and 1352 cm^{-1}, respectively, apart from the skeletal vibrations of the ligand. The separation between the two frequencies adequately supports the monodentate coordination of the acetate and lactate group.[27] The spectrum of complex **4** showed additional bands at 1665 and 1361 cm^{-1}, which were assigned to $\nu_a(COO)$ and $\nu_s(COO)$ modes of the bidentately coordinated dicarboxylate ion.[28] The IR spectrum of complex **3** had additional non-ligand bands at 2072, 777 and 493 cm^{-1}, assignable to ν(C–N), ν(C–S) and δ(NCS) of thiocyanate.[29] The presence of these bands revealed the N-coordinated nature of the thiocyanate ion.[29] The spectrum of complex **2** exhibited additional non-ligand bands at 1248, 1177 and 1085 cm^{-1}, and the values showed the bridging bidentate coordination of the sulphate group.[30] For complex **7**, the spectral bands at 1110, 1071 and 627 cm^{-1} indicated the monodentate coordination of the perchlorate group.[31] The nature of the bonding of the various anions is further supported by the non-electrolytic nature of all the complexes.

TABLE II. IR spectral data of the complexes (cm^{-1})

Compound	ν(N–H)	ν(C=N)	ν(C–O) Furan ring	ν(N–N)	ν(C=S)	ν(Th–N)	ν(Th–S)
$[ThL_2(NO_3)_4]$ **(1)**	3255 *m*	1598 *vs*	1520 *m*	1064 *m*	827 *s*	503 *m*	364 *m*
$[ThL_2(SO_4)_2]$ **(2)**	3256 *m*	1601 *vs*	1522 *m*	1066 *m*	823 *s*	506 *m*	368 *m*
$[ThL_2(NCS)_4]$ **(3)**	3252 *m*	1590 *vs*	1521 *m*	1062 *m*	834 *s*	507 *m*	363 *m*
$[ThL_2(C_2O_4)_2]$ **(4)**	3524 *m*	1597 *vs*	1522 *m*	1066 *m*	846 *s*	504 *s*	369 *m*
$[ThL_2(CH_3COO)_4]$ **(5)**	3253 *m*	1593 *vs*	1524 *m*	1068 *m*	848 *s*	508 *m*	362 *m*
$[ThL_2(C_3H_5O_3)_4]$ **(6)**	3256 *m*	1596 *vs*	1527 *m*	1067 *m*	848 *s*	506 *m*	360 *m*
$[ThL_2(ClO_4)_4]$ **(7)**	3257 *m*	1591 *vs*	1523 *m*	1061 *m*	846 *s*	498 *s*	359 *m*

The ^{1}H-NMR spectrum of the ligand recorded in DMSO-d_6 showed no peak at 4 ppm attributable to SH protons[8] but showed a peak at 9.87 ppm, which was attributed to the N–H group, indicating that the ligand was in the thione form, which is in conformity with the IR spectrum. A significant azomethine proton signal due to CH=N was observed at 8.98 ppm, while that due to aromatic protons were observed in the region 7.21–7.36 ppm. Signals for the furan ring protons were observed at 6.57, 7.38 and 7.41 ppm.

The ^{1}H-NMR spectrum of the complex $[ThL_2(NO_3)_4]$ recorded in DMSO-d_6 showed proton signals in the expected regions but showed slight shifts compared to the ligand spectrum. In the spectrum of the complex, an azomethine proton signal was observed at 9.12 ppm; the N–H proton signal was observed at 9.98 ppm, the aromatic and furan ring proton signals were observed as multiplets in the region 6.5 to 7.52 ppm. These data are consistent with the IR spectral data. Based on spectral evidence, the proposed geometry for the complex is given in Fig. 4.

X-Ray diffraction study

The structure of $[ThL_2(NO_3)_4]$ evaluated using powder X-ray diffraction indicated the amorphous nature of the complex. The X-ray diffraction pattern is given in Fig. 5.

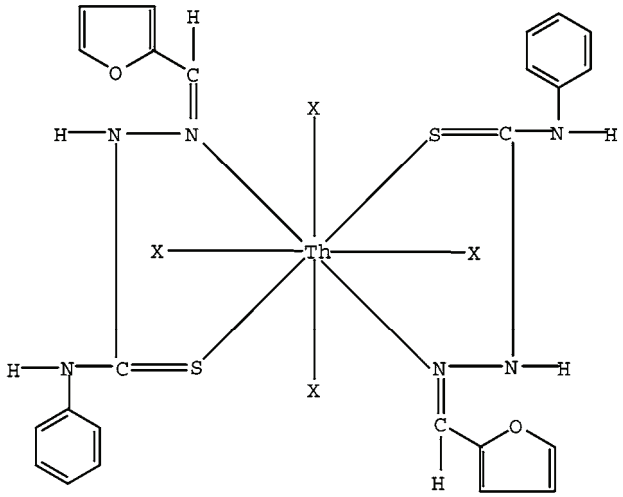

Fig. 4. Proposed geometry of the complexes.

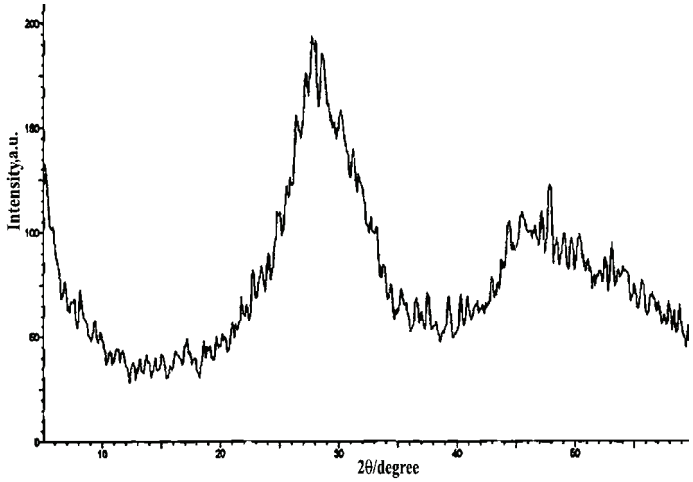

Fig. 5. XRD Pattern of the $[ThL_2(NO_3)_4]$ complex.

Thermal studies

The thermal behaviour of $[ThL_2(NO_3)_4]$ and $[ThL_2(C_2O_4)_2]$ were investigated by the TG and DTG techniques under non-isothermal conditions.

The $[ThL_2(NO_3)_4]$ complex showed a single stage decomposition, as shown by the DTG curve. The TG curve showed the absence of water or any other solvent molecules, as the complex was stable up to 190 °C (Fig. 6). Decomposition started at 190 °C and ended at 270 °C with a peak temperature of 247 °C, indicating the loss of the ligand and nitrate group. The residue 27.57 % (calcd. 27.82 %) showed that the final product formed was ThO_2, which is in agreement with the analytical result for the metal content.

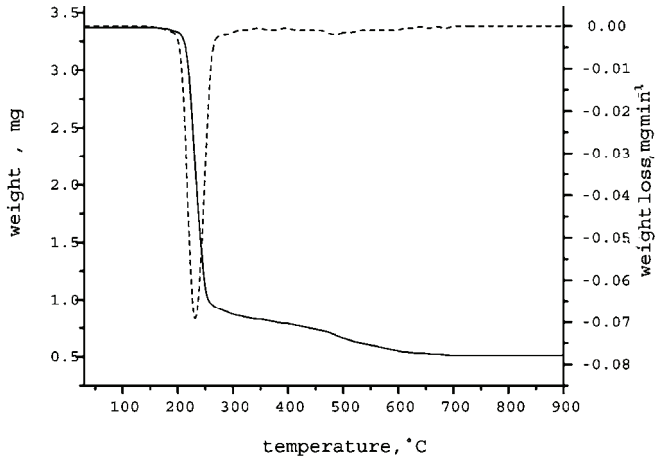

Fig. 6. TG and DTG curves of $[ThL_2(NO_3)_4]$.

For the complex $[ThL_2(C_2O_4)_2]$, the TG plateau up to 220 °C showed the absence of coordinated water or any other solvent molecules and the stability of complex (Fig. 7). Decomposition began at 220 °C and ended at 310 °C. The peak temperature for the decomposition was 265 °C. The complex showed a single stage decomposition, as evident from the DTG curve, and the decomposition occurred with the loss of both ligand and oxalate molecules. The final product formed was ThO_2 and the residue obtained 29.55 % (calcd. 29.40 %) agreed well with the analytical result obtained by an independent pyrolysis experiment.

Kinetic aspects

A kinetic evaluation of the thermal decomposition data of complexes was carried out. The kinetic parameters, *viz*., the activation energy, *E*, and the pre-exponential factor, *A*, were calculated using the Coats-Redfern Equation.[32] Computational data for the evaluation of kinetic parameters are given in Tables III and IV. Here the $\ln g(\alpha)/T^2$ *vs*. $1000/T$ plots (Figs. 8 and 9) gave straight lines, from the slope and intercept of which were calculated the kinetic parameters by the least square method. The goodness of fit was tested by evaluating the correlation coefficient. The entropy of activation ΔS was calculated using the equation:

$$\Delta S = R \ln (Ah/kT_S) \quad (1)$$

where R is the gas constant, A is the pre-exponential factor, k is the Boltzmann constant, T_S is the DTG peak temperature and h is the Planck constant.

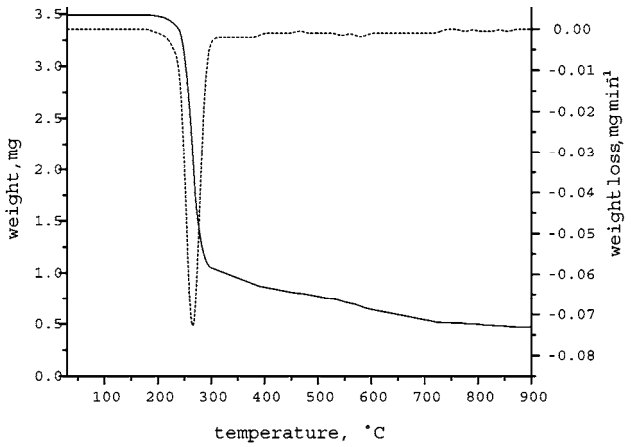

Fig. 7. TG and DTG curves of $[ThL_2(C_2O_4)_2]$.

TABLE III. Computational data for the thermal decomposition of $[ThL_2(NO_3)_4]$ (n = 2; r = 0.99295)

t / °C	m / mg	T/ K	T / 10^{-3} K^{-1}	Weight loss, %	α	$g(\alpha)$	ln $(g(\alpha)/T)^2$
200	3.33	473	–	0	0	0	–
210	3.30	483	2.07039	0.03	0.01240	0.01255	–16.73788
220	3.08	493	2.02840	0.25	0.10331	0.11521	–14.56204
230	2.24	503	1.98807	1.09	0.45041	0.81955	–12.64018
240	1.58	513	1.94932	1.75	0.72314	2.61194	–11.52046
250	1.03	523	1.91205	2.30	0.95041	19.1667	–9.56599
260	0.96	533	1.87617	2.37	0.97934	47.4	–8.69842
270	0.93	543	1.84162	2.40	0.99174	120	–7.80673
280	0.91	553	1.80832	2.42	1	–	–

TABLE IV. Computational data for the thermal decomposition of $[ThL_2(C_2O_4)_2]$ (n = 1.7; r = 0.99566)

t / °C	m / mg	T/ K	T / 10^{-3} K^{-1}	Weight loss, %	α	$g(\alpha)$	ln $(g(\alpha)/T)^2$
220	3.45	493	2.0284	0	0	0	–-
230	3.42	503	1.98807	0.03	0.01240	0.01253	–16.82091
240	3.35	513	1.94932	0.10	0.04132	0.04283	–15.63107
250	3.25	523	1.91205	0.20	0.08264	0.08892	–14.93921
260	2.70	533	1.87617	0.75	0.30992	0.42356	–13.41611
270	1.76	543	1.84162	1.69	0.69835	1.8770	–11.96454
280	1.21	553	1.80832	2.24	0.92562	7.37952	–10.63201
290	1.08	563	1.77620	2.37	0.97934	20.16347	–9.66269
300	1.05	573	1.74520	2.40	0.99174	39.57784	–9.02350
310	1.03	583	1.71527	2.42	1	–	–

The kinetic parameters determined for the thermal decomposition are listed in Table V. The positive value of the entropy of activation in both cases indicates that the activated state was less ordered than the reactants.[33]

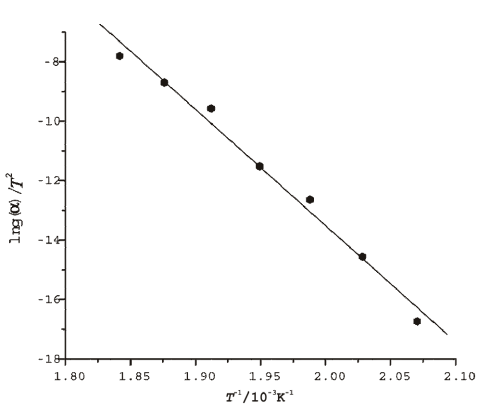

Fig. 8. Coats-Redfern plot for $[ThL_2(NO_3)_4]$.

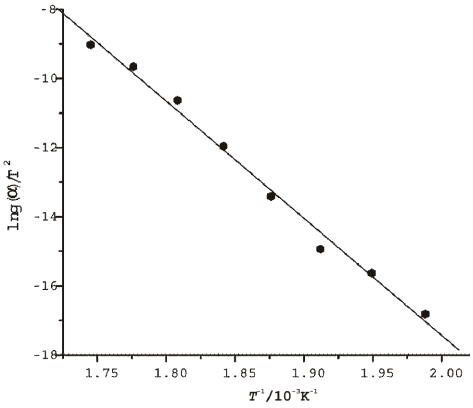

Fig. 9. Coats-Redfern plot for $[ThL_2(C_2O_4)_2]$.

TABLE V. Kinetic parameters for the thermal decomposition of the complexes

Complex	Peak temp. t_s/ °C	Correlation coefficient	Order n	Activation energy E / kJ mol^{-1}	Pre-exponential term A / s^{-1}	Entropy of activation ΔS / J K^{-1} mol^{-1}
$[ThL_2(NO_3)_4]$	247	0.99295	2	325	8.6×10^{31}	362
$[ThL_2(C_2O_4)_2]$	265	0.99566	1.7	282	4.4×10^{25}	241

Antitumour activity

The cell viability over the untreated control was determined using the MTT assay, which is a very convenient method for assessing drug sensitivity even through it does not discriminate between apoptosis and necrosis. The results showed that both the ligand and complex possessed antitumour activity. The results are summarized in Table VI.

The pharmacological properties of the metal complex must primarily be attributed to the thiosemicarbazone ligand since the metal complex shows an activity of the same order of magnitude as that of the ligand. Ribonucleotide reductase, RR, the enzyme that catalyzes the conversion of ribonucleotides to deoxyribonucleotides, is produced as a prerequisite for DNA replication and is highly expressed in tumour cells.[34] A strong positive correlation was established between RR activity and the rate of replication of tumour cells.[35,36] The inhibition of RR prevents the production of deoxyribonucleotides. As a consequence these compounds interfere with DNA synthesis[37] thus decreasing the rate of replication

of tumour cells and inhibiting tumour growth. The antitumour activity seems to be due to an inhibition of DNA synthesis in cancer cells produced by modification in reductive conversion of ribonucleotides to deoxyribonucleotides.[38]

TABLE VI. Antitumour activity of the ligand and complex

Compound	Concentration, μg ml^{-1}	Relative cell viability, %
L	10	88.2
	25	85.5
	50	89.4
	100	83.3
$[ThL_2(NO_3)_4]$	10	85.64
	25	80.6
	50	86.78
	100	82.8

CONCLUSIONS

The coordination sites of the ligand and the coordination number of the metal in the prepared complexes were confirmed by physicochemical studies. Spectral analysis showed that the ligand in the thioketo tatutomer form acts as neutral bidentate with N and S atoms as the coordination sites. All the complexes were neutral, amorphous solids stable at room temperature. From the research findings, the composition of the complexes can be ascertained as $[ThL_2X_4]$ and $[ThL_2Y_2]$, where X represents NO_3^-, NCS^-, CH_3COO^-, $CH_3CHOHCOO^-$ and ClO_4^-, and Y SO_4^{2-} and $C_2O_4^{2-}$. A coordination number of 8 is proposed in all these complexes. Antitumour studies indicated that complexation of the thiosemicarbazone with the metal ion lead to an enhancement of the activity of the thiosemicarbazone.

ИЗВОД

СИНТЕЗА, ТЕРМИЧКА И АНТИТУМОРСКА ПРОУЧАВАЊА Th(IV) КОМПЛЕКСА СА ФУРАН-2-КАРБОКСАЛДЕХИД-4-ФЕНИЛ-3-ТИОСЕМИКАРБАЗОНОМ

G. RAJENDRAN[1], C. S. AMRITHA[1], RUBY JOHN ANTO[2] и VINO T. CHERIYAN[2]

[1]Department of Chemistry, University College, Thiruvananthapuram-695034, Kerala, India, [2]Molecular medicine and Cancer research division, Rajiv Gandhi Centre for Biotechnology, Thiruvananthapuram-695014, Kerala, India

Добијени су и окарактерисани комплекси торијума(IV) са Шифовом базом фуран-2-карбоксалдехид-4-фенил-3-тиосемикарбазоном (L). Састав и структура металних комплекса су предложени на основу елементалне анализе, мерења моларне проводљивости, FT-IR и ^{1}H-NMR спектара. Шифова база се понаша као неутрални бидентатни лиганд координујући се преко азометинског N и тиокето S атома. Из различитих студија комплексима су установљене опште формуле $[ThL_2X_4]$ и $[ThL_2Y_2]$, где X представља NO_3^-, NCS^-, CH_3COO^-, $CH_3CHOHCOO^-$ и ClO_4^-, а Y SO_4^{2-} и $C_2O_4^{2-}$. Проучавано је термичко понашање нитрато и оксалато комплекса, а кинетички и термодинамички параметри су израчунати применом Coats–Redfern-ове једначине. Лиганд и одабрани комплекс $[ThL_2(NO_3)_4]$ су тестирани *in vitro* на антитуморску активноост према ћелијским линијама рака грлића материце (HeLa).

(Примљено 29. јула 2009, ревидирано 2. фебруара 2010)

REFERENCES

1. T. S. Lobana, Rekha, R. J. Butcher, A. Castineiras, C. Bermejo, P. V. Bharatam, *Inorg. Chem.* **45** (2006) 1535
2. M. Ruan, Y. Ye, Y. Song, Q. Mauricio, F. Erben, C. O. D. Vedova, *Spectrochim. Acta* **72 A** (2009) 26
3. P. I. Das, M. F. Fernando, R. Pavan, C. Q. F. Leite, F. D. Sousa, A. A. Batista, O. R. Ascimento, J. E. Eduardo, E. Castellano, E. Niquet, V. M. Deflon, *Polyhedron* **28** (2009) 205
4. Z. H. Chohan, *Transition Met. Chem.* **34** (2009) 153
5. D. P. Saha, S. Padhye, E. Sinn, C. Newton, *Indian J. Chem.* **41A** (2002) 279
6. A. G. Quiroga, C. N. Ranninger, *Coord. Chem. Rev.* **248** (2004) 119
7. H. Zhang, R. Thomas, D. Oupicky, F. Peng, *J. Biol. Inorg. Chem.* **13** (2008) 47
8. E. M. Jouad, G. Larcher, M. Allain, A. Riou, G. M. Bouet, A. M. Khan, X. D. Thanh, *J. Inorg. Biochem.* **86** (2001) 565
9. S. Chandra, M. Tyagi, M. S. Refat, *J. Serb. Chem. Soc.* **74** (2009) 907
10. M. J. M. Campbell, *Coord. Chem. Rev.* **15** (1975) 279
11. M. A. Ali, S. E. Livingstone, *Coord. Chem. Rev.* **13** (1974) 101
12. S. Padhye, G. B. Kauffman, *Coord. Chem. Rev.* **63** (1985) 127
13. J. S. Casas, M. S. Garcia-Tasenda, J. Sorda, *Coord. Chem. Rev.* **209** (2000) 197
14. G. Rajendran, C. S. Amritha, *Asian J. Chem.* **18** (2006) 2695
15. G. Rajendran, C. S. Amritha, *Oriental, J. Chem.* **22** (2006) 365
16. I. M. Kolthoff, P. J. Elving, *Treatise on Analytical Chemistry*, Interscience, New York, 1963
17. A. I. Vogel, *A Textbook of Quantitative Inorganic Analysis*, 4th ed., ELBS, London, 1978
18. E. Kurz, G. Kober, M. Berl, *Anal. Chem.* **30** (1958) 1983
19. P. Indrasean, G. Rajendran, *Synth. React. Inorg. Met. Org. Chem.* **22** (1992) 715
20. T. Mosmann, *J. Immunol. Methods* **65** (1983) 55
21. A. P. Wilson, *Cytotoxicity and Viability Assays in Animal Cell Culture: A Practical Approach*, 3rd ed., Vol. 1, Oxford University Press, Oxford, 2000
22. W. J. Geary, *Coord. Chem. Rev.* **7** (1971) 81
23. A. K. Sen, G. Singh, K. Singh, R. K. Noren, R. M. Handa, S. N. Dubey, *Indian J. Chem.* **36A** (1977) 891
24. K. S. A. Melha, *J. Enzym. Inhib. Med. Chem.* **23** (2008) 493
25. P. Bindu, M. R. P. Kurup, *Transition Met. Chem.* **22** (1997) 578
26. S. G. Devi, P. Indrasenan, *Inorg. Chim. Acta* **133** (1987) 157
27. B. W. Mistry, *A Hand Book of Spectroscopic Data Chemistry*, 1st ed., ABD Publishers, Jaipur, India, 2000
28. D. N. Sathyanarayana, *Vibrational Spectroscopy, Theory and Applications*, New Age International (P) Ltd., India, 2004
29. R. K. Agarwal, P. Kumar, H. K. Rawat, *Thermochim. Acta* **88** (1985) 397
30. K. Nakamoto, *Infrared and Raman Spectra of Inorganic and Coordination Compounds*, Wiley, New York, 1987
31. M. Viswanathan, *J. Indian Chem. Soc.* **82** (2005) 871
32. K. K. Aravindakshan, K. Muraleedharan, *Thermochim. Acta* **155** (1989) 247
33. A. A. Frost, R. G. Pearson, *Kinetics and Mechanism*, Wiley, New York, 1961
34. C. R. Kowol, R. Berger, R. Eichinger, A. Roller, M. A. Jakupee, P. P. Schmidt, V. B. Arion, B. K. Keppler, *J. Med. Chem.* **50** (2007) 1254

35. R. A. Finch, M. C. Liu, S. P. Grill, W. C. Rose, R. Loomis, K. M. Vasquez, Y. C. Cheng, A. C. Sartorelli, *Biochem. Pharmacol*. **59** (2000) 983
36. F. A. French, J. E. Blanz, *J. Med. Chem.* **17** (1974) 172
37. M. B. Ferrari, F. Bisceglie, C. Casoli, S. Durot, I. M. Badarau, G. Pelosi, E. Pilotti, S. Pinelli, P. Tarasconi, *J. Med. Chem.* **48** (2005) 1671
38. W. X. Hu, W. Zhou, C. Xia, X. Wen, *Bioorg. Med. Chem. Lett.* **16** (2006) 2213.

Journal of the Serbian Chemical Society
JSCS@tmf.bg.ac.rs • www.shd.org.rs/JSCS

J. Serb. Chem. Soc. 75 (6) 763–772 (2010)
JSCS–4005

UDC 546.732'742'562'472'482+
546.913:543.42:615.28
Original scientific paper

Template synthesis of macrocyclic complexes of Co(II), Ni(II), Cu(II), Zn(II) and Cd(II): spectroscopic, antibacterial and antifungal studies

DHARAM PAL SINGH*, VANDNA MALIK, RAMESH KUMAR and KRISHAN KUMAR

Department of Chemistry, National Institute of Technology, Kurukshetra-136 119, India

(Received 1 September 2009, revised 19 January 2010)

Abstract: A new series of macrocyclic complexes of the type $[M(C_{17}H_{14}N_4O_2)X_2]$, where M = Co(II), Ni(II), Cu(II), Zn(II) or Cd(II) and X = Cl^-, NO_3^- or CH_3COO^-, was synthesized by the condensation reaction of malonyldihydrazide with benzil in the presence of divalent metal ions. The complexes were characterized with the aid of elemental analyses, conductance measurements, magnetic susceptibilities, electronic, NMR and infrared spectral studies. On the basis of these studies, a six-coordinate distorted octahedral geometry, in which two nitrogen and two carbonyl oxygen atoms are suitably placed for coordination towards metal ion, is proposed for all the complexes. The complexes were tested for their *in vitro* antibacterial activity and antifungal activities. The minimum inhibitory concentration shown by these complexes were compared with the minimum inhibitory concentration shown by standard drugs.

Keywords: macrocyclic complexes; MIC; antibacterial; antifungal.

INTRODUCTION

During recent years, macrocyclic chemistry has attracted much attention and has become a growing class of research. Macrocyclic complexes are of great importance due to their resemblance to many naturally occurring macrocycles, such as porphyrins and cobalamines. A number of nitrogen donor macrocyclic derivatives have long been used in analytical, industrial and medical applications.[1–3] Macrocyclic metal complexes of lanthanides, *e.g.*, Gd^{3+}, are used as MRI contrast agents.[4] Macrocyclic metal chelating agents are useful for detecting tumor lesions.[5] The chemistry of macrocyclic complexes is also important due to their use as dyes and pigments[6] as well as NMR shift reagents.[3] Furthermore, some macrocyclic complexes have been found to exhibit potential antibacterial activities.[7]

* Corresponding author. E-mail: dpsinghchem@yahoo.co.in
doi: 10.2298/JSC090901050S

Prompted by these facts, in the present paper, a series of macrocyclic complexes of Co(II), Ni(II), Cu(II), Zn(II) and Cd(II) obtained by template condensation reaction of malonyldihydrazide and benzil are reported. The complexes were characterized with the help of various physico-chemical techniques, such as elemental analyses, IR, NMR and electronic spectral studies and magnetic susceptibility and molar conductance measurements. These macrocyclic complexes were also screened for their *in vitro* antibacterial and antifungal activity.

EXPERIMENTAL

Synthesis of the complexes

All the reported macrocyclic complexes were prepared by the template method. To a stirring methanolic solution (≈50 cm^3) of malonyldihydrazide (10 mmol) was added divalent cobalt, nickel, copper, zinc and cadmium salts (Cl^-, NO_3^-, CH_3COO^-) (10 mmol) dissolved in a minimum quantity of methanol (20 cm^3). The resulting solution was refluxed for 0.5 h. Then benzil (10 mmol) dissolved in ≈20 cm^3 methanol was added to the refluxing mixture and the refluxing was continued for 6–8 h. On overnight cooling, light colored complexes formed, which were filtered, washed with methanol, acetone, and ether and dried *in vacuo* (yield: 55––60 %). The complexes were soluble in DMF and DMSO, but were insoluble in water. They were found to be thermally stable up to ≈250 °C and then decomposed.

In vitro *antibacterial assay*

Primary screening. The antibacterial activities of the newly synthesized compounds were evaluated by the agar well diffusion assay technique against two Gram-positive bacteria, *i.e.*, *Bacillus subtilis* (MTCC 8509) and *Bacillus stearothermophilus* (MTCC 8508), and two Gram--negative bacteria, *i.e.*, *E. coli* (MTCC 51) and *Pseudomonas putida* (MTCC 121). The bacterial cultures were maintained on the nutrient agar media by sub-culturing them on the fresh slants after every 4–6 weeks and incubating them at the appropriate temperature for 24 h. All stock cultures were stored at 4 °C. For the evaluation of antimicrobial activity of the synthetic compounds, suspension of each test microorganism was prepared. The turbidity of each suspension was adjusted to 0.5 McFarland units by suspending the cultures in sterile distilled water. The size of final inoculum was adjusted to 5×10^7 cfu/ml.

Agar medium (20 ml) was poured into each Petri plate and plates were swabbed with broth cultures of the respective micro-organisms and kept for 15 min for adsorption to take place. Using a punch, ≈8 mm diameter wells were bored in the seeded agar plates and 100 µl of each test compound reconstituted in DMSO was added into the wells. DMSO was used as the control for all the test compounds. After holding the plates at room temperature for 2 h to allow diffusion of the compounds into the agar, the plates were incubated at 37 °C for 24 h. The antibacterial activity was determined by measuring the diameter of the inhibition zone. The entire tests were made in triplicates and the mean of the diameter of inhibition was calculated. The antimicrobial activities of the complexes were compared against the standard drugs.

Minimum inhibitory concentration. Nutrient broth adjusted to pH 7.0 was used for the determination of the *MIC* of synthesized complexes.[8] The *MIC* is the lowest concentration of the antimicrobial agents that prevents the development of visible growth of a micro-organism after overnight incubation. The inoculum of the test microorganisms were prepared using 16 h old cultures adjusted by reference to the 0.5 McFarland standards (10^8 cells/ml).[9] These cultures were further diluted up to 10-fold with nutrient broth to obtain an inoculum size of 1.2×10^7 CFU/ml. A positive control (containing inoculum but no compound) and a negative

control (containing compound but no inoculum) were also prepared. A stock solution of 4 mg/ml of each complex was prepared in DMSO and further appropriately diluted to obtain a final concentration ranging from 250 to 0.03 µg/ml.[10] The requisite quantity of the antifungal drug (cyclohexamide) was added to the broth to obtain its desirable final concentration of 100 µg/ml. Separate flasks was taken for each test dilution. To each flask was added the 100 µl of inoculum. Then an appropriately diluted test sample was added to each flask having broth and microbial inoculum. The contents of the flask were mixed and incubated for 24 to 48 h at 37 °C. The test bacterial cultures were spotted in a predefined pattern by aseptically transferring 5 µl of each bacterial culture onto the surface of the solidified agar-agar plates and incubated at 37 °C for 24 h for determining the *MIC* value.

In vitro *antifungal activity*

Potato dextrose medium (PDA) was prepared in a flask and sterilized. To check the growth of the bacterial culture in the medium, the requisite quantity of a standard antibiotic (ampicillin) was added, so as to obtain their desired final concentration of 100 µg/ml of the medium. Test samples were prepared in different concentrations (10, 50 and 100 µg/ml) in DMSO and 200 µl of each sample was spread on PDA medium contained in sterilized Petri plates. Mycelial discs taken from the standard cultures (*Aspergillus flavus* and *A. niger*) of fungi, were grown on PDA medium for 5–7 days. These cultures were used for aseptic inoculation in the sterilized Petri dish. Standard cultures, inoculated at 28±1 °C, were used as the control. The efficacy of each sample was determined by measuring the radial mycelial growth. The radial growth of the colony was measured in two directions at right angle to each other, and the average of two replicates was recorded in each case. Data were expressed as percent inhibition over the control from the size of the colonies. The percent inhibition was calculated using the formulae: %Inhibition = $((C–T)/C)\times100$, where C is the diameter of the fungus colony in the control plate after 96 h incubation and T is the diameter of the fungus colony in the tested plate after the same incubation period.

RESULTS AND DISCUSSION

The analytical data suggest the formula of the macrocyclic complexes as: $[M(C_{17}H_{14}N_4O_2)X_2]$, where M = Co(II), Ni(II), Cu(II) Zn(II) or Cd(II) and X = = $Cl^–$, $NO_3^–$ or $CH_3COO^–$. The test for the anions was positive after decomposition of the complexes, indicating their presence inside the coordination sphere (Fig. 1). The conductivity measurements (10–20 S cm^2 $mol^{–1}$) in DMSO indicate them to be non-electrolytic in nature.[11] All complexes give satisfactory elemental analyses results, as shown in Table I.

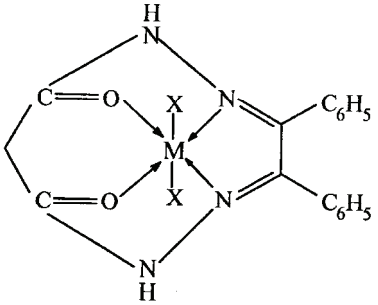

Fig. 1. Proposed structure of the synthesized complexes, where, M = Co(II), Ni(II), Cu(II), Zn(II) or Cd(II); X = Cl^-, NO_3^- or CH_3COO^-.

TABLE I. Analytical data of divalent Co, Ni, Cu, Zn and Cd complexes derived from malonyldihydrazide and benzil

No.	Complex	Found (Calcd.), %				Color	MW
		M	C	H	N		
1	$[Co(C_{17}H_{14}N_4O_2)Cl_2]$	13.27 (13.53)	46.15 (46.78)	3.09 (3.21)	12.37 (12.84)	Reddish brown	436
2	$[Co(C_{17}H_{14}N_4O_2)(NO_3)_2]$	11.97 (12.06)	41.42 (41.71)	2.76 (2.86)	17.12 (17.17)	Reddish brown	489
3	$[Co(C_{17}H_{14}N_4O_2)(OAc)_2]$	12.03 (12.21)	52.06 (52.17)	4.11 (4.14)	11.28 (11.59)	Dark brown	483
4	$[Ni(C_{17}H_{14}N_4O_2)Cl_2]$	13.19 (13.33)	46.85 (46.89)	3.19 (3.21)	12.64 (12.87)	Dark brown	435
5	$[Ni(C_{17}H_{14}N_4O_2)(NO_3)_2]$	11.79 (11.88)	41.58 (41.80)	2.73 (2.86)	17.24 (17.21)	Green	488
6	$[Ni(C_{17}H_{14}N_4O_2)(OAc)_2]$	11.91 (12.03)	52.07 (52.28)	4.08 (4.14)	11.42 (11.61)	Green	482
7	$[Cu(C_{17}H_{14}N_4O_2)Cl_2]$	14.13 (14.31)	46.17 (46.36)	3.04 (3.18)	12.51 (12.72)	Brown	440
8	$[Cu(C_{17}H_{14}N_4O_2)(NO_3)_2]$	12.68 (12.77)	41.22 (41.37)	2.75 (2.83)	17.01 (17.03)	Yellow	493
9	$[Cu(C_{17}H_{14}N_4O_2)(OAc)_2]$	12.52 (12.93)	51.29 (51.74)	4.03 (4.10)	11.17 (11.49)	Dark green	487
10	$[Zn(C_{17}H_{14}N_4O_2)(OAc)_2]$	13.21 (13.29)	51.39 (51.53)	4.02 (4.08)	11.23 (11.45)	Dark green	489
11	$[Cd(C_{17}H_{14}N_4O_2)(OAc)_2]$	20.74 (20.89)	46.89 (47.01)	3.62 (3.73)	10.21 (10.44)	Reddish Orange	536

IR Spectra

In the IR spectrum of malonyldihydrazide, a pair of bands corresponding to $\nu(NH_2)$ was present at ≈3210 and ≈3270 cm^{-1} but was absent in the IR spectra of all the complexes.[12] However, a single broad medium band at ≈3360–3450 cm^{-1} was observed in the spectra of all the complexes, which may be assigned to ν(NH).[13,14] A strong peak at ≈1660cm^{-1} in the IR spectrum of malonyldihydrazide was assigned to the >C=O group of the CONH moiety. This peak was shifted to a lower frequency (≈1620–1640 cm^{-1})[15,16] in the spectra of all the complexes, suggesting the coordination of the oxygen of the carbonyl group with the metal. Furthermore, no strong absorption band was observed near 1700 cm^{-1} in the IR spectra of all complexes as was observed in spectrum of benzil. This indicates the absence of >C=O groups of the benzil moiety in the complexes. These facts confirm the condensation of carbonyl groups of benzil and the amino groups of malonyldihydrazide.[17,18] The IR spectra of the complexes showed a new strong absorption band in the region ≈1595–1610 cm^{-1}, which may be attributed due to ν(C=N).[19,20] These results provide strong evidence for the formation of the macrocyclic frame.[21] The lower value of ν(C=N) indicates coordination of

the nitrogens of azomethine to the metal.[22] The bands present at ≈1300–1000 cm^{-1} were assigned to ν(C–N) vibrations. The bands presents at ≈3080 cm^{-1} may be assigned to ν(C–H) vibrations of the benzil moiety.

The far IR spectra showed bands in the region ≈420–450 cm^{-1} corresponding to ν(M–N) vibrations in all the complexes.[23] The presence of these bands support the fact concerning the coordination of the azomethine nitrogen with the metal.[24] The bands present at ≈310–315 cm^{-1} were due to ν(M–Cl)[23] and the bands present at ≈210–240 cm^{-1} in all nitrate complexes were due to ν(M–O).[23]

NMR Spectra

The ^{1}H-NMR spectrum of the Zn(II) complex showed a broad singlet at 8.45 ppm due to protons of the –CONH moiety.[13,25] A singlet peak at 2.43 ppm may be due to $–CH_2$ protons.[15] The multiplets in the region 6.9–7.5 ppm may be assigned to aromatic protons.[26]

Magnetic measurements and electronic spectra

Cobalt complexes. The magnetic moments of the cobalt complexes were measured at room temperature and lay in the range 4.85–4.90 μ_B which corresponds to 3 unpaired electrons. The solution spectra of the cobalt(II) complexes exhibited absorption in the region 8100–9160 (ν_1), 12500–15700 (ν_2) and 18600––20500 cm^{-1} (ν_3), respectively. The spectra resemble those reported for octahedral complexes.[27] Thus, the various bands can be assigned to: $^4T_{1g} \rightarrow {}^4T_{2g}(F)$, ($\nu_1$); $^4T_{1g} \rightarrow {}^4A_{2g}(F)$, ($\nu_2$) and $^4T_{1g} \rightarrow {}^4T_{1g}(P)$, ($\nu_3$), respectively. It appears that the symmetry of these complexes was not idealized O_h, but distorted octahedral. The assignment of the first spin-allowed band seems plausible since the first band appears at approximately half the energy of the visible band.[28]

Nickel complexes. The magnetic moments of the nickel complexes at room temperature lay in the range 2.91–2.95 μ_B, showing an octahedral environment around the Ni(II) ion in all complexes. The solution spectra of the Ni(II) complexes exhibited a well-discernable band with a shoulder on the low energy side. The other two bands, generally observed in the region at *ca*. 16,570–17,240 cm^{-1} (ν_2), and 26,860–28000 cm^{-1} (ν_3), were assigned to $^3A_{2g} \rightarrow {}^3T_{1g}(F)$ (ν_2) and $^3A_{2g} \rightarrow {}^3T_{1g}(P)$ (ν_3), respectively. The first two bands resulted from the splitting of one band, ν_1, and are in the range ≈9700–10000 and 11800–12440 cm^{-1}, which can be assigned to $^3B_{1g} \rightarrow {}^3E_g$ and $^3B_{1g} \rightarrow {}^3B_{2g}$, assuming the effective symmetry to be D_{4h} (component of $^3T_{2g}$ in O_h symmetry).[28] The intense higher energy band at *ca*. 34000 cm^{-1} may be due to a π–π* transition of the (C=N) group. Various bands do not follow any regular pattern and seem to be anion independent. The spectra are consistent with the distorted octahedral nature of these complexes.

Copper complexes. The magnetic moments of the copper complexes lay in the range 1.77–1.82 μ_B. The electronic spectra of the copper complexes exhibited

bands in the region ≈17780–19000 cm^{-1} with a shoulder on the low energy side at ≈14600–16000 cm^{-1}, which showed that these complexes were distorted octahedral.[27,28] Assuming tetragonal distortion in the molecule, the d-orbital energy level sequence for these complexes may be: $x^2 - y^2 > z^2 > xy > xz > yz$ and the shoulder can be assigned to $z^2 \rightarrow x^2 - y^2$ ($^2B_{1g} \rightarrow {}^2B_{2g}$) and the broad band contained both the $xy \rightarrow x^2 - y^2$ ($^2B_{1g} \rightarrow {}^2E_g$) and $xz, yz \rightarrow x^2 - y^2$ ($^2B_{1g} \rightarrow {}^2A_{2g}$) transitions.[29] The band separation of the spectra of the complexes was of the order 2500 cm^{-1}, which is consistent with the proposed geometry of the complexes.[29] Therefore, it may be concluded that all the complexes formed by the macrocycles with Cu(II) metals are distorted octahedral.

Biological results and discussion

In this study, all the chemically synthesized complexes were evaluated against Gram-positive and Gram-negative bacteria. The minimum inhibitory concentrations (*MIC*) of these synthetic complexes were determined by the method given by Andrews.[30] The standard antibiotic, namely streptomycin and chloramphenicol were used for comparison with the antibacterial activities shown by these complexes. All the complexes of the tested series possessed some antibacterial activity against Gram-positive bacteria and Gram-negative bacteria (Table II). Complexes **2**, **3** and **9** exhibited good activities against all the tested bacterial strains with a zone of inhibition ranging from 29 to 47 mm. Complex **6** showed the highest zone of inhibition (47 and 44) against *E. coli* and *P. putida* (Table II).

TABLE II. *In vitro* antibacterial activity of the complexes obtained by the agar well diffusion method for a concentration of 100 μg/ml

No.	Complex	Diameter of the zone of growth inhibition[a], mm			
		B. subtilis (MTCC 8509)	*B. stearothermophilus* (MTCC 8508)	*E. coli* (MTCC 51)	*P. putida* (MTCC 121)
1	$[Co(C_{17}H_{14}N_4O_2)Cl_2]$	17	13	16	12
2	$[Co(C_{17}H_{14}N_4O_2)(NO_3)_2]$	37	29	37	40
3	$[Co(C_{17}H_{14}N_4O_2)(OAc)_2]$	40	37	32	36
4	$[Ni(C_{17}H_{14}N_4O_2)Cl_2]$	14	17	14	20
5	$[Ni(C_{17}H_{14}N_4O_2)(NO_3)_2]$	14	18	21	14
6	$[Ni(C_{17}H_{14}N_4O_2)(OAc)_2]$	36	36	47	44
7	$[Cu(C_{17}H_{14}N_4O_2)Cl_2]$	27	26	25	28
8	$[Cu(C_{17}H_{14}N_4O_2)(NO_3)_2]$	10	17	17	17
9	$[Cu(C_{17}H_{14}N_4O_2)(OAc)_2]$	32	36	37	33
10	$[Zn(C_{17}H_{14}N_4O_2)(OAc)_2]$	29	27	27	24
11	$[Cd(C_{17}H_{14}N_4O_2)(OAc)_2]$	11	10	12	11
Chloramphenicol		64	77	65	71
Streptomycin		63	77	79	82

[a]Mean of three replicates

Based on the *MIC* values shown by these complexes against bacteria, complexes **2**, **3** and **6** were found to be the most effective by showing an *MIC* of 8 μg/ml for *P. putida*, *B. subtilis* and *E. coli*, respectively (Table III). In the whole series, the *MIC* of complexes **3**, **6** and **9** was found to be 32 μg/ml for *B. stearothermophilus*, whereas the *MIC* of complexes **2** and **6** was found to be 32 μg/ml for *B. subtilis.* The complexes **2** and **9** also showed an *MIC* of 32 μg/ml for *E. coli* (Table III).

TABLE III. Minimum inhibitory concentration (*MIC*, μg/ml) shown by the complexes against the test bacteria obtained by the agar dilution assay

No.	Complex	*B. subtilis* (MTCC 8509)	*B. stearothermophilus* (MTCC 8508)	*E. coli* (MTCC 51)	*P. putida* (MTCC 121)
1	$[Co(C_{17}H_{14}N_4O_2)Cl_2]$	>250	>250	>250	>250
2	$[Co(C_{17}H_{14}N_4O_2)(NO_3)_2]$	32	64	32	08
3	$[Co(C_{17}H_{14}N_4O_2)(OAc)_2]$	8	32	64	32
4	$[Ni(C_{17}H_{14}N_4O_2)Cl_2]$	>250	>250	>250	>250
5	$[Ni(C_{17}H_{14}N_4O_2)(NO_3)_2]$	>250	>250	>250	>250
6	$[Ni(C_{17}H_{14}N_4O_2)(OAc)_2]$	32	32	8	16
7	$[Cu(C_{17}H_{14}N_4O_2)Cl_2]$	>128	>128	>128	>128
8	$[Cu(C_{17}H_{14}N_4O_2)(NO_3)_2]$	>250	>250	>250	>250
9	$[Cu(C_{17}H_{14}N_4O_2)(OAc)_2]$	64	32	32	64
10	$[Zn(C_{17}H_{14}N_4O_2)(OAc)_2]$	>128	>128	>128	>128
11	$[Cd(C_{17}H_{14}N_4O_2)(OAc)_2]$	>250	>250	>250	>250
Chloramphenicol		64.20	2	2	4
Streptomycin		63.24	2	2	4

The antifungal activities of all the complexes were determined against two fungal strains, *i.e.*, *Aspergillus niger* and *A. flavus*, and then compared with the standard antifungal drug cyclohexamide (Table IV). In the whole series, complex **3** showed the highest percentage inhibition (34–35 %) against both fungal strains, but none of the tested complexes restricted the fungal growth excellently. However, of all the tested complexes, complex **6** showed nearly 33–34 % inhibition of mycelial growth against both fungal strains *A. flavus* and *A. niger*, whereas complexes **7**, **9** and **10** showed nearly 25–27 % inhibition of mycelial growth against *A. flavus* and *A. niger* (Table IV).

TABLE IV. Antifungal (inhibition, %) activities of the complexes against the tested fungal strains (for a concentration of 100 μg/ml)

No.	Complex	*A. flavus*	*A. niger*
1	$[Co(C_{17}H_{14}N_4O_2)Cl_2]$	17.7	12.8
2	$[Co(C_{17}H_{14}N_4O_2)(NO_3)_2]$	27.8	22.4
3	$[Co(C_{17}H_{14}N_4O_2)(OAc)_2]$	34.2	35.3
4	$[Ni(C_{17}H_{14}N_4O_2)Cl_2]$	18.5	19.8
5	$[Ni(C_{17}H_{14}N_4O_2)(NO_3)_2]$	13.7	17.2

TABLE IV. Continued

No.	Complex	*A. flavus*	*A. niger*
6	$[Ni(C_{17}H_{14}N_4O_2)(OAc)_2]$	33.8	34.5
7	$[Cu(C_{17}H_{14}N_4O_2)Cl_2]$	24.5	22.5
8	$[Cu(C_{17}H_{14}N_4O_2)(NO_3)_2]$	10.5	16.5
9	$[Cu(C_{17}H_{14}N_4O_2)(OAc)_2]$	26.1	21.5
10	$[Zn(C_{17}H_{14}N_4O_2)(OAc)_2]$	27.5	23.9
11	$[Cd(C_{17}H_{14}N_4O_2)(OAc)_2]$	10.7	09.8
Cyclohexamide		87.3	89.9

CONCLUSIONS

Based on elemental analyses, conductivity and magnetic measurements, and electronic, IR, far IR and NMR spectral studies, the structure as shown in Fig. 1 may be proposed for all the prepared complexes.

However, none of the synthesized macrocyclic metal complexes showed good antibacterial activities against the tested bacterial strains, but some of the cobalt, nickel and copper complexes were reported to show some antibacterial activities against various bacterial strains. It has been suggested that chelation/coordination reduces the polarity of the metal ion mainly because of the partial sharing of its positive charge with the donor group within the whole chelate ring system.[31] This process of chelation thus increases the lipophilic nature of the central metal atom, which in turn, favors its permeation through the lipoid layer of membranes, thus causing the metal complex to cross the bacterial membrane more effectively thus increasing the activity of the complexes. In addition to this, many other factors such as solubility, dipole moment and conductivity influenced by the metal ion may be the possible reasons for the antibacterial activities of these metal complexes.[32] It was also observed that some moieties, such as an azomethine linkage or a heteroaromatic nucleus, introduced into such compounds exhibit extensive biological activities that may be responsible for the increase in hydrophobic character and liposolubility of the molecules in crossing the cell membrane of the microorganism and thus enhance the biological utilization ratio and activity of complexes.[33]

Abbreviations. *MIC* – Minimum inhibitory concentration; MTCC – microbial type culture collection; CFU – colony forming unit; DMF – *N*,*N*-dimethylformamide; DMSO – dimethylsulphoxide; PDA – potato dextrose medium.

Acknowledgements. DPS thanks the University Grants Commission, New Delhi, for financial support in the form of a Major Research Project (MRP-F. No. 32-196/2006(SR)) and Krishan Kumar for the award of Project Fellowship under the above project. Thanks are also due to the authorities of N.I.T., Kurukshetra, for providing the necessary research facilities.

ИЗВОД

ТЕМПЛАТНА СИНТЕЗА МАКРОЦИКЛИЧНИХ КОМПЛЕКСА Co(II), Ni(II), Cu(II), Zn(II) И Cd(II): СПЕКТРОСКОПСКО, АНТИБАКТЕРИЈСКО И АНТИФУГАЛНО ПРОУЧАВАЊЕ

DHARAM PAL SINGH, VANDNA MALIK, RAMESH KUMAR и KRISHAN KUMAR

Department of Chemistry, National Institute of Technology, Kurukshetra-136 119, India

Кондензационом реакцијом малонилдихидразида са бензилом у присуству двовалентних металних јона синтетисана је нова серија макроцикличних комплекса типа $[M(C_{17}H_{14}N_4O_2)X_2]$, где је M = Co(II), Ni(II), Cu(II), Zn(II) или Cd(II) и X = Cl^-, NO_3^- или CH_3COO^-. Комплекси су окарактерисани помоћу елементалне анализе, мерења проводљивости, магнетних сусцептибилности, електронских, NMR и IR спектралних проучавања. На основу овога предложена је дисторгована октаедарска геометрија за све комплексе у којима су два азотова атома и два карбонилна кисеоникова атома у повољном положају за координацију са металним јонима. Комплекси су тестирани на *in vitro* антибактеријске и антифугалне активности. Минимале инхибиторне концентрације ових комплекса су упоређене са онима које дају стандардни лекови.

(Примљено 1. септембра 2009, ревидирано 19. јануара 2010)

REFERENCES

1. a) E. C. Constable, *Coordination Chemistry of Macrocyclic Compounds*, Oxford University Press, Oxford, 1999; b) K. Gloe, Ed., *Current Trends and Future Perspectives*, Springer, Berlin, 2005
2. D. P. Singh, R. Kumar, V. Malik, P. Tyagi, *Transition Met. Chem.* **32** (2007) 1051
3. D. P. Singh, R. Kumar, V. Malik, P. Tyagi, *J. Enzym. Inhib. Med. Chem.* **22** (2007) 177
4. A. D. Watson, S. M. Rockladge, in *Magnetic Resonance Imaging of the Body*, C. B. Higgins, Ed., Raven Press, New York, 1992
5. C. Kosmos, D. Snook, C. S. Gooden, N. S. Courtenay-Luck, M. J. McCall, C. F. Meares, A. A. Epenetos, *Cancer Res.* **52** (1992) 904
6. J. Seto, S. Tamura, N. Asai, N. Kishii, Y. Kijima, N. Matsuzawa, *Pure Appl. Chem.* **68** (1996) 1429
7. D. P. Singh, R. Kumar, P. Tyagi, *Transition Met. Chem.* **31** (2006) 970
8. D. Greenwood, R. Slack, J. Peutherer, *Medical Microbiology: A Guide to Microbial Infections: Pathogensis, Immunity, Laboratory Diagnosis and Control*, 15th ed., ELST Publishers, Edinburgh, 1997
9. J. McFarland, *J. Am. Med. Assoc.* **14** (1907) 1176
10. NCCLS, *Method for dilution antimicrobial susceptibility test for bacteria that grow aerobically*, Approved Standards, 5th ed., M7-A5, National Committee for Clinical Laboratory Standards, Villanova, PA, 2000
11. S. Chandra, S. D. Sharma, *Transition Met. Chem.* **27** (2002) 732
12. R. N. Prasad, M. Mathur, A. Upadhayay, *J. Indian Chem. Soc.* **84** (2007) 1202
13. T. A. Khan, M. A. Rather, N. Jahan, S. P. Varkey, M. Shakir, *Transition Met. Chem.* **23** (1998) 283
14. A. K. Singh, A. Panwar, R. Singh, S. Beniwal, *Transition Met. Chem.* **28** (2003) 160
15. D. L. Pavia, G. M. Lampman, G. S. Kriz, *Introduction to Spectroscopy*, 3rd ed., Harcourt College Publishers, New York, 2007
16. N. Nishat, Rahis-ud-din, M. M. Haq, K. S. Siddiqi, *Transition Met. Chem.* **28** (2003) 948

17. R. N. Prasad, M. Mathur, *J. Indian Chem. Soc*. **83** (2006) 1208
18. Q. Zeng, J. Sun, S. Gou, K. Zhou, J. Fang, H. Chen, *Transition Met. Chem*. **23** (1998) 371
19. A. K. Singh, R. Singh, P. Saxena, *Transition Met. Chem*. **29** (2004) 867
20. L. K. Gupta, S. Chandra, *Transition Met. Chem.* **31** (2006) 368
21. A. K. Mohamed, K. S. Islam, S. S. Hasan, M. Shakir, *Transition Met. Chem.* **24** (1999) 198
22. C. Lodeiro, R. Basitida, E. Bertolo, A. Macias, R. Rodriguez, *Transition Met. Chem*. **28** (2003) 388
23. D. P. Singh, V. Malik, R. Kumar, K. Kumar, J. Singh, *Russ. J. Coord. Chem*. **35** (2009) 740
24. S. Chandra, R. Kumar, *Transition Met. Chem*. **29** (2004) 269
25. Z. A. Siddiqi, S. M. Shadab, *Indian J. Chem*. **43A** (2004) 2274
26. D. P. Singh, R. Kumar, J. Singh, *Eur. J. Med. Chem.* **44** (2009) 1731
27. D. P. Singh, K. Kumar, S. S. Dhiman, J. Sharma, *J. Enzym. Inhib. Med. Chem*. **24** (2009) 795
28. A. B. P. Lever, *Inorganic Electronic Spectroscopy*, Elsevier, Amsterdam, 1984
29. A. B. P. Lever, E. Mantovani, *Inorg. Chem.* **10** (1971) 40
30. J. M. Andrew, *J. Antimicrob. Chemother*. **48** (2001) 5
31. N. Raman, S. Johnson Raja, A. Sakthivel, *J. Coord. Chem*. **62** (2009) 691
32. Z. H. Chohan, M. U. Hassan, K. M. Khan, C. T. Supuran, *J. Enzym. Inhib. Med. Chem*. **20** (2005) 183
33. K. Singh, D. P. Singh, M. S. Barwa, P. Tyagi, Y. Mirza, *J. Enzym. Inhib. Med. Chem.* **21** (2006) 749.

Journal of the Serbian Chemical Society
JSCS@tmf.bg.ac.rs • www.shd.org.rs/JSCS

J. Serb. Chem. Soc. 75 (6) 773–788 (2010)
JSCS–4006

UDC 546.562'472+542.913+
547.477.2+547.963.32:615.28
Original scientific paper

Synthesis, characterization, DNA interaction and antimicrobial screening of isatin-based polypyridyl mixed-ligand Cu(II) and Zn(II) complexes

NATARAJAN RAMAN* and SIVASANGU SOBHA

Research Department of Chemistry, VHNSN College, Virudhunagar-626 001, India

(Received 20 October 2009, revised 17 March 2010)

Abstract: Several mixed ligand Cu(II)/Zn(II) complexes using 3-(phenylimino)-1,3-dihydro-2*H*-indol-2-one (obtained by the condensation of isatin and aniline) as the primary ligand and 1,10-phenanthroline (phen)/2,2'-bipyridine (bpy) as an additional ligand were synthesized and characterized analytically and spectroscopically by elemental analyses, magnetic susceptibility and molar conductance measurements, as well as by UV–Vis, IR, NMR and FAB mass spectroscopy. The interaction of the complexes with calf thymus (CT) DNA was studied using absorption spectra, cyclic voltammetric and viscosity measurements. They exhibit absorption hypochromicity, and the specific viscosity increased during the binding of the complexes to calf thymus DNA. The shifts in the oxidation–reduction potential and changes in peak current on addition of DNA were shown by CV measurements. The Cu(II)/Zn(II) complexes were found to promote cleavage of pUC19 DNA from the supercoiled form I to the open circular form II and linear form III. The complexes show enhanced antifungal and antibacterial activities compared with the free ligand.

Keywords: 1,10-phenanthroline/2,2'-bipyridine; Cu(II) and Zn(II) complexes; antimicrobial activity; DNA binding and cleavage.

INTRODUCTION

The therapeutic and diagnostic properties of transition metal complexes have attracted considerable attention leading to their application in many areas of modern medicine.[1] Many coordination compounds of transition metal ions accomplish nucleolytic cleavage.[2] In this regard, mixed-ligand metal complexes were found to be particularly useful because of their potential to bind DNA *via* a multitude of interactions and to cleave the duplex by virtue of their intrinsic chemical, electrochemical, and photochemical reactivities.[3–8] A recent study on the incorporation of good intercalators, such as phen (1,10-phenanthroline), bpy

* Corresponding author. E-mail: drn_raman@yahoo.co.in
doi: 10.2298/JSC091020054R

(2,2'-bipyridine), *etc.* found high affinity between DNA base pairs and their planar structure through stacking interaction.[9] A singular advantage in the use of these metallo-intercalators for such studies is that the ligands or the metal ion in them can be varied in an easily controlled manner to facilitate individual applications.[10,11] Although DNA interactions of number of mixed-ligand complexes previously appeared in the literature, there is still scope to design and study isatin-based Schiff base containing 1,10-phenantroline/2,2'-bipyridine with the Cu(II) and Zn(II) as new chemical nucleases. Bearing these facts in mind, the nuclease activity of mixed-ligand complexes of Cu(II) and Zn(II) containing 1,10-phenantroline/2,2'-bipyridine is reported herein. DNA binding was also researched. Hence, the present study is very valuable in understanding the mode of complex binding to DNA, as well as laying the foundation for the rational design of DNA structure probes and antitumor drugs.

EXPERIMENTAL

All chemicals used in the present work, *viz.*, isatin, aniline, 1,10-phenanthroline, 2,2'-bipyridine and copper and zinc chlorides were of analytical reagent grade (produced by Merck, Germany). Commercial solvents were distilled and then used for the preparation of the ligand and its complexes. CT DNA and pUC19 DNA was purchased from Bangalore Genei (India). Microanalyses (C, H and N) were performed using a Carlo Erba 1108 analyzer at the sophisticated analytical instrument facility (SAIF), Central Drug Research Institute (CDRI), Lucknow, India. Molar conductivities in DMSO (10^{-2} mol/dm^3) at room temperature were measured using a Systronic model-304 digital conductivity meter. Magnetic susceptibility measurements of the complexes were realized by a Gouy balance using copper sulfate pentahydrate as the calibrant. The IR spectra were recorded on a Perkin–Elmer 783 spectrophotometer in the 4000–400 cm^{-1} range using KBr pellets. The NMR spectra were recorded on a Bruker Avance Dry 300 FT-NMR spectrometer in DMSO-d_6 with TMS as the internal reference. The FAB-MS spectra were recorded using a VGZAB-HS spectrometer at room temperature in a 3-nitrobenzyl alcohol matrix. Electron paramagnetic resonance spectra (EPR) of the mixed ligand complexes of copper(II) were recorded on a Varian E 112 EPR spectrometer in DMSO solution both at room temperature and liquid nitrogen temperature (77 K) using TCNE (tetracyanoethylene) as the g-marker. The absorption spectra were recorded using a Shimadzu model UV-1601 spectrophotometer at room temperature. Electrochemical studies were realized using a CHI Electrochemical analyzer, controlled by CHI620C software. The CV measurements were performed using a glassy carbon working electrode and an Ag/AgCl reference electrode (all potentials refer to this reference electrode) and the supporting electrolyte was 50 mmol/L NaCl–5 mmol/L Tris-HCl buffer (pH 7.2). All solutions were deoxygenated by purging with N_2 for 30 min prior to the measurements.

Preparation of ligand (L)

The Schiff base was synthesized according to a literature procedure.[12] A methanolic solution of aniline (0.040 mol, 3.65 mL) was added to a methanolic solution (25 mL) of isatin (0.040 mol, 5.8 g) and the reaction mixture was refluxed for *ca.* 6 h. The end of the reaction was monitored by TLC. In this technique, a small quantity of a solution of the Schiff base to be analyzed was deposited as a small spot on a TLC plate which had a thin layer of silica gel

(SiO_2) coated on a glass plate as the absorbent. It was used as the stationary phase and the mobile phase was toluene:ethanol (9:1). The observed R_f value was 0.68.

The formed yellowish orange product (L) was filtered and washed with methanol and dried *in vacuo*. Yield: 86 %. The preparation of the Schiff base is schematically presented in Fig. 1.

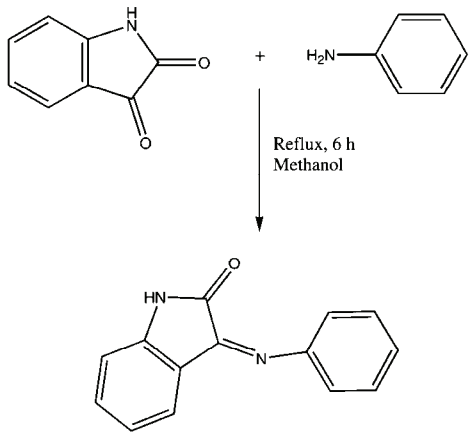

Fig. 1. Synthesis of the Schiff base.

Synthesis of the $[ML(Phen)_2]Cl_2$/$[ML(bpy)_2]Cl_2$ complexes

The complexes were prepared by mixing the appropriate molar quantities of the ligand and the metal salts using the following procedure. A methanolic solution of Schiff base (0.0030 mol) was stirred with a methanolic solution (5 mL) of the required anhydrous metal(II) chloride (0.0030 mol) for *ca.*1 h. To the above mixture, a methanolic solution (5 mL) of 1,10-phenanthroline (phen)/2,2'-bipyridine (bpy) (0.0060 mol) was added in a 1:1:2 molar ratio and the stirring was continued for *ca*. 1 h. The obtained solid product was filtered and washed with methanol.

DNA binding experiments

The interactions between the metal complexes and DNA were studied using electrochemical and electronic absorption methods. The disodium salt of calf thymus DNA was stored at 4 °C. A solution of DNA in the buffer 50 mmol/L NaCl–5 mmol/L Tris-HCl (pH 7.2) in water gave a ratio 1.9 of the UV absorbance at 260 and 280 nm, A_{260}/A_{280}, indicating that the DNA was sufficiently free from protein.[13] The concentration of DNA was measured using its extinction coefficient at 260 nm (6600 mol^{-1} L cm^{-1}) after a 1:100 dilution. Stock solutions were stored at 4 °C and used no more than 4 days. Doubly distilled water was used to prepare the solutions. Concentrated stock solutions of the complexes were prepared by dissolving the complexes in DMSO and diluting suitably with the corresponding buffer to the required concentration for all the experiments. The data were then fitted to Eq. (1) to obtain the intrinsic binding constant (K_b) values for the interaction of the complexes with DNA:

$$[DNA]/(\varepsilon_a - \varepsilon_f) = [DNA]/(\varepsilon_b - \varepsilon_f) + 1/K_b(\varepsilon_b - \varepsilon_f) \quad (1)$$

where ε_a, ε_f, and ε_b are the apparent, free and bound metal complex extinction coefficients, respectively. A plot of $[DNA]/(\varepsilon_b - \varepsilon_f)$ *vs*. [DNA] gave a slope of $1/(\varepsilon_b - \varepsilon_f)$ and a *y*-intercept equal to $[K_b/(\varepsilon_b - \varepsilon_f)]^{-1}$; thus, K_b is the ratio of the slope to the *y*-intercept. Viscosity mea-

surements at room temperature were performed using a semi-micro dilution capillary viscometer. Each experiment was performed three times and an average flow time was calculated. The data are presented as $(\eta/\eta_0)^{1/3}$ *vs*. the binding ratio, where η is the viscosity of a DNA solution in the presence of a complex and η_0 is the viscosity of DNA in solution alone.

pUC19 DNA cleavage study

The cleavage of pUC19 DNA was determined by agarose gel electrophoresis. The gel--electrophoresis experiments were performed by incubation of the samples containing 30 μmol/L pUC19 DNA, 50 μmol/L copper complex and 50 μmol/L hydrogen peroxide (H_2O_2) in Tris-HCl/NaCl buffer (pH 7.2) at 37 °C for 2 h. After incubation, the samples were electrophoresed for 2 h at 50 V on 1 % agarose gel using Tris-acetic acid–EDTA buffer (pH 7.2). The gel was then stained using 1 μg cm^{-3} ethidium bromide (EB) and photographed under 360 nm ultraviolet light. All experiments were performed at room temperature unless otherwise stated.

Antimicrobial activity studies

The *in vitro* antibacterial activity of the ligand and its complexes were tested against the bacteria *Staphylococcus aureus*, *Pseudomonas aeruginosa*, *Escherichia coli*, *Staphylococcus epidermidis*, *Klebsiella pneumoniae* by the paper disc method using nutrient agar as the medium. The antifungal activity was evaluated by the paper disc method against the fungi *Aspergillus niger*, *Fusarium solani*, *Culvularia lunata*, *Rhizoctonia bataticola* and *Candida albicans* cultured on potato dextrose agar medium. Streptomycin and nystatin were used as standards for bacteria and fungi, respectively. A stock solution (10^{-2} mol L^{-1}) was prepared by dissolving the compound in DMSO and the solution was serially diluted in order to find the minimum inhibitory concentration *(MIC)* value. Test extract loaded discs inoculated with microorganisms were incubated at 30 °C for 24 h for the bacteria and 72 h for fungi. During the incubation period, the test solution diffused and the growth of the inoculated microorganisms was affected. The concentration at which an inhibition zone developed was noted.

RESULTS AND DISCUSSION

The ligand (L) and the mixed ligand complexes containing L and phen/bpy were stable in air. L is soluble in common organic solvents but the complexes are soluble only in DMF and DMSO. Elemental analyses of L and the complexes were in agreement with the assigned formula. The higher molar conductance values of the complexes in DMSO show their electrolytic nature. The elemental analysis and FAB-mass data, together with other properties, are given in Table I.

Mass spectra

The FAB-mass spectra of L and its complexes having phen were recorded and the obtained molecular ion peaks confirmed the proposed formulae. The mass spectrum of L ($C_{14}H_{10}N_2O$) exhibited peaks at 222 (M^+), 223 (M+1) and 224 (M+2) with 68, 100 and 49 % abundances, respectively. The most abundant peak at *m*/*z* 223 represents the molecular ion peak of L. The mass spectrum of the copper complex $[CuC_{38}H_{26}N_6O]Cl_2$ showed peaks at 717 (M^+), 718 (M+1), 719 (M+2) with 8.7, 9.2 and 9.9 % abundances, respectively. The most abundant peak at *m*/*z* 719 represents the molecular ion peak of the complex and the other peaks are isotopic species. In addition, the spectrum exhibited fragments at *m/z*

180 and 77, which represent phen and phenyl moieties, respectively. The *m*/*z* of all the fragments of L and the mixed ligand complexes, together with the relative intensities confirmed the stoichiometry of the complexes to be of the type $[ML(phen)_2/(bpy)_2]Cl_2$ (where L = isatin-based Schiff base).The structural formulas of the complexes are shown in Fig. 2. Thus, the mass spectral data reinforced the conclusion drawn from the analytical and conductance values.

TABLE I. Physical and analytical data of the synthesized Schiff base and its complexes

Compound	Yield %	Color	Found (Calcd.), %				MW	Λ_M S cm^2 mol^{-1}	μ_{eff} / μ_B
			M	C	H	N			
L	86	Yellowish orange	–	72.7 (72.9)	5.0 (5.0)	14.1 (14.4)	222.0	–	–
$[CuL(phen)_2]Cl_2$	71	Pale green	8.8 (8.5)	63.6 (63.1)	3.6 (3.5)	11.7 (11.2)	717.1	104.5	1.89
$[CuL(bpy)_2]Cl_2$	67	Pale green	9.5 (8.9)	61.0 (59.2)	3.9 (3.3)	12.5 (12.1)	669.0	115.2	1.86
$[ZnL(phen)_2]Cl_2$	79	Pale brown	9.0 (8.7)	63.4 (59.7)	3.6 (3.1)	11.6 (11.4)	718.9	102.9	Diamagnetic
$[ZnL(bpy)_2]Cl_2$	83	Pale brown	9.7 (9.3)	60.8 (60.6)	3.9 (3.8)	12.5 (12.0)	670.9	112.6	Diamagnetic

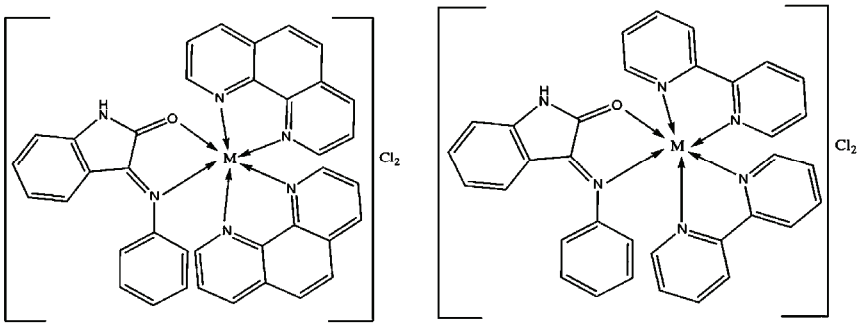

(a) (b)

Fig. 2. The structural formulas of the complexes a) $[ML(phen)_2]Cl_2$ and b) $[ML(bpy)_2]Cl_2$; M = Cu(II) or Zn(II).

IR Spectra

The IR spectrum of the free ligand (L) showed a broad band around 3257 cm^{-1}, which can be attributed to NH stretching vibration of the isatin moiety. The position of this band remained at nearly the same frequency in spectra of the metal complexes, suggesting the uncoordination of this group. The band at 1763 cm^{-1} in the spectrum of the free ligand, assigned to $\nu_{C=O}$ of isatin moiety, shifted towards lower values, around 1719–1710 cm^{-1}, in the complexes, indicating the coordination of the carbonyl oxygen atom of the isatin residue. The C=N stretching frequency of the Schiff base ligand appears in the region 1613–1608 cm^{-1},

which was shifted towards lower values in all the complexes, indicating the involvement of the –C=N nitrogen in coordination to the central metal ion. All the complexes showed bands in the regions 1090–1100 and 700–750 cm^{-1}. These can be assigned to phen/bpy ring –C–H and –C=N stretching vibrations, respectively. The appearance of two new bands in the regions 486–472 and 547–533 cm^{-1} in the spectra of the complexes, due to ν_{M-N} and ν_{M-O} stretching vibrations, respectively, also confirmed the formation of metal complexes. The characteristic IR data are presented in Table II.

TABLE II. IR spectral data (cm^{-1}) of the ligand and its complexes

Compound	ν_{N-H}	$\nu_{C=O}$	$\nu_{C=N}$	ν_{M-N}	ν_{M-O}
L	3257	1763	1645	–	–
$[CuL(phen)_2]Cl_2$	3262	1711	1613	472	533
$[CuL(bpy)_2]Cl_2$	3267	1710	1608	481	536
$[ZnL(phen)_2]Cl_2$	3268	1717	1611	476	537
$[ZnL(bpy)_2]Cl_2$	3265	1719	1619	486	547

^{1}H-NMR Spectra

^{1}H-NMR (300 MHz, DMSO-d_6, δ / ppm) spectrum of the Schiff base exhibited the following signals: the signal at 10.92 (1H, *s*) was assigned to the NH proton of isatin and the multiplet signal around 6.43–7.10 (4H, *m*) to aromatic protons. In addition to these, one singlet peak observed at 7.21 was ascribed to aniline ring protons. In the ^{1}H-NMR spectra of the Zn(II) complexes, the protons of L are shifted downfield due to coordination to the metal ions. The resonance peaks observed in the spectrum of the $[ZnL(phen)_2]Cl_2$ complex at 7.34–7.40 and 7.81–8.37 were assigned to phen protons and the signals at 7.54–7.73 and 8.23––8.37 in the spectrum of $[ZnL(bpy)_2]Cl_2$ were assigned to bpy protons.

EPR Spectra

The EPR spectra of the copper complexes exhibited an auxiliary symmetric g-tensor parameters with $g_\parallel > g_\perp > 2.0023$, indicating that the copper site had a $d_{x^2}–d_{y^2}$ ground state, characteristic of octahedral geometry.[14] According to Hathaway,[15] if the value of *G* is greater than four, the exchange interaction between the copper(II) centers in the solid state is negligible, whereas when *G* is less than four, there is considerable exchange interaction from the polypyridyl nitrogen atom. The *G* values calculated for the present copper complexes lie within the range 2.936–3.277, which are consistent with a $d_{x^2}–d_{y^2}$ ground state.

Apart from this, the covalency parameters α^2 (covalent in-plane σ-bonding) and β^2 (covalent in-plane π-bonding) were calculated using a simplified MO theory and the results are summarized in Table III.

The α^2 and β^2 values indicated a greater interaction in the in-plane π-bonding than in the covalent in-plane σ-bonding, whereas the in-plane π-bonding is

almost ionic. The higher value of α^2 compared to β^2 indicates that the in-plane σ-bonding is more covalent than the in-plane π-bonding. Based on these observations, a distorted octahedral geometry is proposed for both the copper complexes.

TABLE III. The spin Hamiltonian parameters of the copper complexes in DMSO solution at 300 and 77 K

Compound	$g_{\parallel}$	$g_{\perp}$	$A_{\parallel}\times10^4$ / cm^{-1}	$A_{\perp}\times10^4$ / cm^{-1}	α^2	β^2	G
$[CuL(phen)_2]Cl_2$	2.232	2.071	169.0	66.0	0.767	0.615	3.2
$[CuL(bpy)_2]Cl_2$	2.351	2.072	171.3	64.3	0.724	0.518	2.9

Electronic absorption spectra

The UV–Vis spectra of the copper complexes were recorded in DMSO solution. They show a d–d band at around 734–737 nm. This band may be assigned to $^2E_g \rightarrow {}^2T_{2g}$ transitions, characteristics for a distorted octahedral structure. In addition, the complexes exhibited intense bands in the 395–398 nm region, which are attributed to charge transfer transitions. The intense higher energy bands at around 272 and 285 nm can be attributed to intra-ligand π–π* transitions. The copper complexes showed magnetic moment values in the range of 1.87–1.89 μ_B which indicate the monomeric nature of the complexes. The zinc(II) complexes showed bands at 375 and 378.5 nm, assigned to intra-ligand charge transfer transitions. They are diamagnetic.

Based on the elemental analysis, magnetic moments, mass, EPR spectra, electronic, IR and ^{1}H-NMR data, the proposed structures of the complexes are given in Fig. 2.

CT-DNA binding studies

Electronic absorption titration. The binding interaction of the metal complexes with DNA was monitored by UV–Vis spectroscopy. The absorption spectra of the complexes in the presence or without DNA were mutually compared, which is shown in Fig. 3. In the UV region of the spectra, all the copper complexes exhibited an intense absorption around 395–398 nm and zinc complexes showed a band at 375–378.5 nm, which are attributed to n–π* transitions. With increasing concentration of DNA, both the copper and zinc complexes showed hypochromicity and a red-shifted charge transfer peak maxima in the absorption spectra.

The hypochromicity values of the complexes $[CuL(phen)_2]Cl_2$, $[CuL(bpy)_2]Cl_2$, $[ZnL(phen)_2]Cl_2$ and $[ZnL(bpy)_2]Cl_2$ observed in the presence of DNA were 2.16, 1.08, 1.07 and 1.05 respectively, and their hypsochromic shifts were 8.6, 4.2 and 4.0, 5.6 nm, respectively. The change in the absorbance values with increasing amount of DNA was used to evaluate the intrinsic binding constant K_b for the present complexes, the values of which are given in Table IV. The change in hypochromicity may be attributed to the nature of the binding of

the mixed ligand complexes with DNA, which is significant due to π-stacking or hydrophobic interactions of the aromatic phenyl rings. However, the metal ions play crucial role in DNA binding by these complexes. In general, the DNA binding abilities seem to follow the order: $[CuL(phen)_2]Cl_2$ > $[CuL(bpy)_2]Cl_2$ > > $[ZnL(bpy)_2]Cl_2$ > $[ZnL(phen)_2]Cl_2$. The high binding nature of the metal complexes may be due to additional π-π interaction through the aromatic phenyl rings.

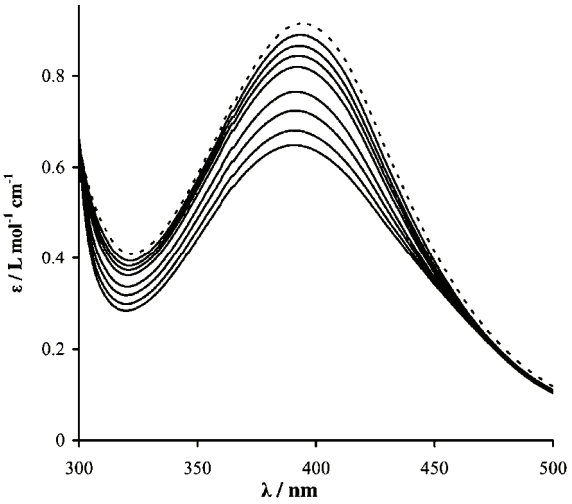

Fig. 3. Electronic absorption spectrum of $[CuL(phen)_2]$ in the absence (dash line) and presence (dark line) of different concentrations (0 to 400 μM) of DNA.

TABLE IV. Electronic absorption spectral properties of the Cu(II) and Zn(II) complexes

Compound	λ_{max} / nm		$\Delta\lambda_{max}$ / nm	H / %	$K_b \times 10^{-5}$ / mol^{-1} dm^3
	Free	Bound			
$[CuL(phen)_2]Cl_2$	397.8	389.2	8.6	2.16	5.84
$[CuL(bpy)_2]Cl_2$	393.2	389.0	4.2	1.08	5.36
$[ZnL(phen)_2]Cl_2$	375.0	371.0	4.0	1.07	2.74
$[ZnL(bpy)_2]Cl_2$	378.4	372.8	5.6	1.50	3.34

Viscosity studies. A useful technique to prove intercalation is viscosity measurements, which are sensitive to change in length of the DNA and are regarded as the least ambiguous and the most critical tests of binding mode in solution in the absence of crystallographic structural data or NMR spectra.[16] Under appropriate conditions, intercalation of drugs, such as ethidium bromide [EB], causes a significant increase in the viscosity of a DNA solution due to the increase in the separation of the base pairs of the intercalation sites and hence, result in an increase in the overall DNA contour length, as shown in Fig. 4. On the other hand, drug molecular binding exclusively in the DNA grooves causes a less pronounced or no changes in the viscosity of a DNA solution.[17] The viscosity of the DNA solution increased with increasing ratio of both the copper and zinc complexes to DNA. This result further suggests an intercalating binding mode of the

complexes with DNA and also parallels the above spectroscopic results, such as hypochromism and bathochromism of the complexes in the presence of DNA.

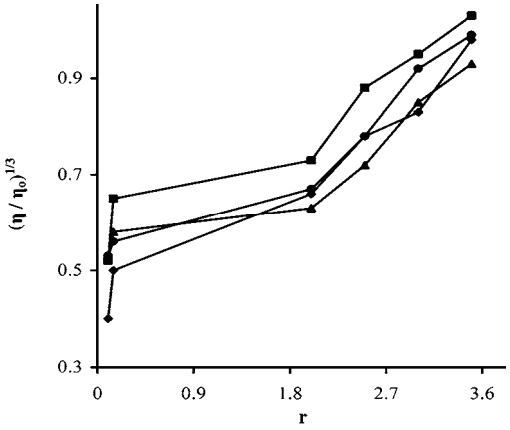

Fig.4. Change in the relative viscosity $(\eta/4_0)^{1/3}$ of CT DNA as a function of *r*, the molar ratio of the compound to the DNA base pairs. The effect of increasing amounts of:
$[CuL(phen)_2]Cl_2$ (▲),
$[CuL(bpy)_2]Cl_2$ (■),
$[ZnL(phen)_2]Cl_2$ (♦) and
$[ZnL(bpy)_2]Cl_2$ (●)
on the relative viscosity of DNA.

Redox studies. The application of cyclic voltammetry to the studies of the complexes bound to DNA provides a useful complement to the previously used investigation methods, *i.e.*, UV–Vis spectroscopy and viscosity measurements. The cyclic voltammograms of the glassy carbon electrode in solutions containing $[CuL(phen)_2]Cl_2$ in the absence and in the presence of varying amounts of DNA are shown in Fig. 5.

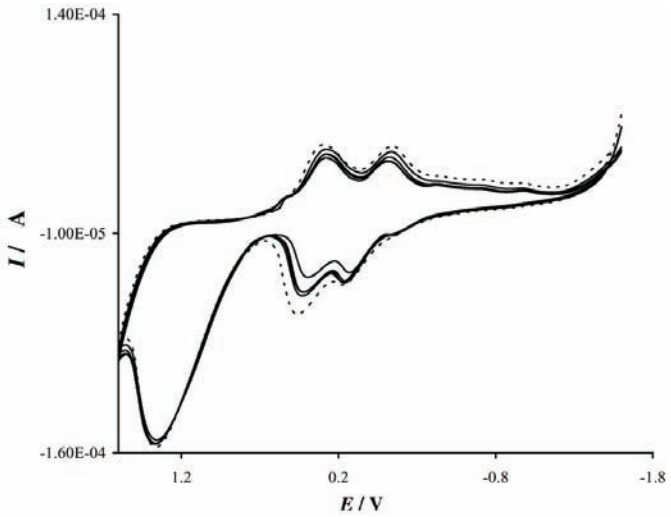

Fig.5. Cyclic voltammograms of the glassy carbon electrode in solutions containing $[CuL(phen)_2]Cl_2$ in the absence (dash line) and presence (dark lines) of different concentrations (0 to 400 μM) of DNA.

In the absence of DNA, the first redox couple cathodic peak appeared at 0.29 V for Cu(III) → Cu(II) (E_{pa} = 0.49 V, E_{pc} = 0.29 V, ΔE_p = 0.20 V, and $E_{1/2}$ = = 0.39 V) and the second redox couple cathodic peak appeared at –0.16 V for Cu(II) → Cu(I), (E_{pa} = 0.17 V, E_{pc} = –0.16 V, ΔE_p = 0.33 V, and $E_{1/2}$ = 0.17 V). The ratio of cathodic to anodic peak currents, I_{pa}/I_{pc} = 0.95, indicated a quasi-reversible redox process. The formal potential ($E_{1/2}$), taken as the average of E_{pc} and E_{pa}, was 0.39 V for the first redox couple in the absence of DNA. The presence of DNA in the solution at the same concentration as $[CuL(phen)_2]Cl_2$ caused a negative shift in the potential ΔE_p by 0.160 V and a decrease in $E_{1/2}$ by 0.35 V, Table V. The value of I_{pa}/I_{pc} also decreased with increasing DNA concentration. The decrease of the anodic and cathodic peak currents of the complex in the presence DNA is due to a decrease in the apparent diffusion coefficient of the Cu(II) complex upon complexation with the DNA macromolecules. These results show that $[CuL(phen)_2]Cl_2$ stabilizes the duplex (GC pairs) by intercalation.

TABLE V. Electrochemical parameters for the interaction of DNA with the Cu(II) complexes

Compound	Redox couple	$E_{1/2}$ / V		ΔE_p / V		K_+/K_{2+}	I_{pc}/I_{pa}
		Free	Bound	Free	Bound		
$[CuL(phen)_2]Cl_2$	Cu(III) → Cu(II)	0.39	0.35	0.20	0.16	0.0965	0.95
	Cu(II) → Cu(I)	0.005	0.014	0.33	0.28	0.4081	0.93
$[CuL(bpy)_2]Cl_2$	Cu(III) → Cu(II)	0.42	0.27	0.16	0.14	0.0826	0.84
	Cu(II) → Cu(I)	0.02	0.07	0.06	0.12	0.7042	0.75

Considering the CV behavior of the glassy carbon electrode in solutions containing $[CuL(bpy)_2]Cl_2$ in the absence of DNA, the first redox couple cathodic peak appeared at 0.338 V for Cu(III) → Cu(II), (E_{pa} = 0.50 V, E_{pc} = 0.34 V, ΔE_p = 0.16 V and $E_{1/2}$ = 0.42 V), while the second cathodic peak appeared at 0.17 V for Cu(II) → Cu(I) (E_{pa} = 0.23 V, E_{pc} = 0.17 V, ΔE_p = 0.06 V and $E_{1/2}$ = = 0.20 V). The I_{pa}/I_{pc} ratios of these two redox couples were approximately unity. This indicates that the reaction of the complex on the working electrode surface was a quasi-reversible redox process. The incremental addition of DNA to the complex caused a negative shift in the potential of the second cathodic peak and a decrease in the current intensity. The changes in the voltammetric currents in the presence of CT DNA can be attributed to the slow diffusion of the metal complex bound to the large, slowly diffusing DNA molecule. The changes of the peak currents observed for the complexes upon addition of CT DNA may indicate that the complexes possess a higher DNA binding affinity. The results lead conclusions similar to those deduced from the spectroscopic and viscosity data of the complexes in the presence of DNA.

The Zn(II) complexes showed only a reduction peak from –0.99 to –0.80 V (E_{pc}) and no oxidation peak in the absence of DNA. The incremental addition of DNA to the Zn(II) complexes increased the current intensity and there was a po-

sitive shift of the reduction peak potential. This result changes the reduction current which indicates interaction of Zn(II) with CT DNA.

Differential pulse voltammogram study. The differential pulse voltammograms of the glassy carbon electrode in solutions containing $[CuL(phen)_2]Cl_2$ both in the absence and presence of varying amounts of DNA are shown in Fig. 6.

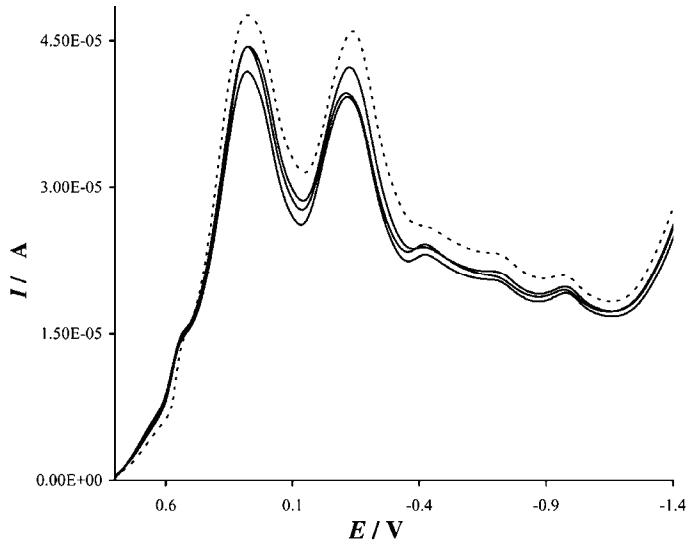

Fig.6. Differential pulse voltammograms of the glassy carbon electrode in solutions containing $[CuL(phen)_2]Cl_2$ in the absence (dash line) and presence (dark lines) of different concentrations (0 to 400 μM) of DNA.

The differential pulse voltammograms of the the glassy carbon electrode in solutions containing $[CuL(phen)_2]Cl_2$ showed that increasing the concentration of DNA resulted in a negative potential shift together with a significant decrease of the current intensity. The shift in potential is related to the ratio of the binding constants:

$$E_b - E_f = 0.0591\log (K_+/K_{2+}) \quad (2)$$

where E_b and E_f are the formal potential of the Cu(II)/Cu(I) complex couple in the bound and free forms, respectively. The ratio of the binding constants (K_+/K_{2+}) for DNA binding of the Cu(II)/Cu(I) couple of the complex was calculated and found to be less than unity. This indicates that the binding of the Cu(I) complex to DNA is small compared to that of the Cu(II) complex. The above electrochemical experimental results indicate that the Cu(II) complex binds to DNA molecules. The possible mechanism is:

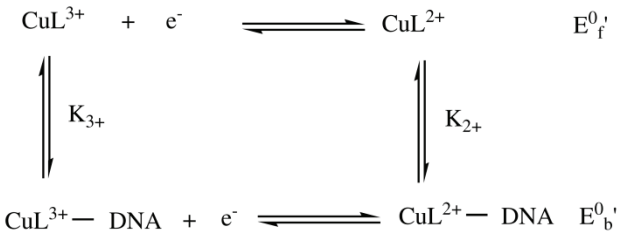

For a complex of the electro-active substance Zn^{2+} with DNA, the electrochemical reduction reactions can be divided into two steps:

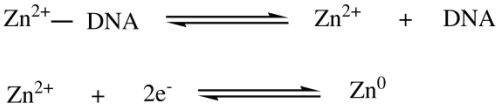

The dissociation constant (K_d) of the Zn^{2+}–CT-DNA complex was obtained using the following equation:

$$I_p^2 = \frac{K_d(I_{po}^2 - I_p^2)}{[DNA]} + I_{po}^2 - [DNA] \quad (3)$$

where K_d is the dissociation constant of the complex Zn(II)–DNA; I_{po}^2 is the reduction current of Zn(II) in the absence of CT-DNA; I_p^2 is the reduction current of Zn(II) in the presence of CT DNA; [DNA] is the concentration of added DNA in the solution. Using the above equation, the dissociation constant was determined (Table VI).

TABLE VI. Electrochemical parameters for the interaction of DNA with the Zn(II) complexes

Compound	E_p / V		I_p / A		$K_d \times 10^9$ / M^{-1}
	Free	Bound	Free	bound	
$[ZnL(phen)_2]Cl_2$	–0.989	–0.931	0.83	0.71	5.41
$[ZnL(bpy)_2]Cl_2$	–0.801	–0.789	0.89	0.78	5.44

The low values of the dissociation constant (Table VI) of Zn(II) ions are indispensable for the catalytic function and structural stability of zinc enzymes which participate in the replication, degradation, and translation of genetics of all species. Moreover, the Zn(II) ion probably not only interacted with the active site of the enzyme during these processes, as is already known in the literature,[18] but also with DNA.

Chemical nuclease activity

The cleavage efficiency of the complexes compared to that of the control is due to their efficient DNA-binding ability. DNA cleavage was controlled by relaxation of the supercoiled form of pUC19 DNA into the nicked circular form

and linear form. When pUC19 DNA is subjected to electrophoresis, the fastest migration will be observed for the supercoiled form (form I). If one strand is cleaved, the supercoils relax to produce the slower-moving open circular form (form II). If both strands are cleaved, the linear form (form III) will be generated that migrates between the other two forms.

DNA cleavage was analyzed by monitoring the conversion of supercoiled DNA (form I) to nicked DNA (form II) and linear DNA (form III) in the presence of the oxidant H_2O_2. The electrophoresis results are shown in Fig. 7.

From Fig. 7, it is evident that the complexes cleave DNA more efficiently in the presence of an oxidant (H_2O_2). This may be attributed to the formation of hydroxyl free radicals. The production of a hydroxyl radical due to the reaction between the metal complex and oxidant may be explained as shown below:

$$(\text{Ligand})Cu^{2+} + H_2O_2 \rightarrow (\text{Ligand})Cu^{3+} + OH\cdot + OH^-$$

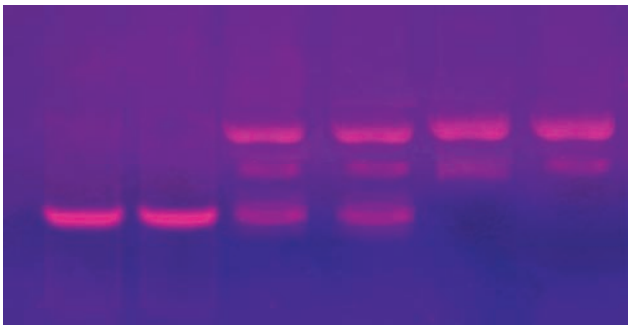

Fig. 7. Changes in the agarose gel electrophoretic pattern of pUC19 DNA induced by H_2O_2 and the Cu(II)/Zn(II) complexes. Lane 1, DNA alone; Lane 2, DNA + Ligand+ H_2O_2; Lane 3, DNA + $[CuL(phen)_2]Cl_2$ complex + H_2O_2; Lane 4, DNA + $[CuL(bpy)_2]Cl_2$ complex + H_2O_2; Lane 5, DNA + $[ZnL(phen)_2]Cl_2$ complex + H_2O_2; Lane 6, DNA + $[ZnL(bpy)_2]Cl_2$ complex + H_2O_2.

The OH· free radicals participate in the oxidation of the deoxyribose moiety, followed by hydrolytic cleavage of a sugar phosphate backbone. All the complexes showed pronounced nuclease activity in the presence of the oxidant H_2O_2, which may be due to the increased production of hydroxyl radicals. Control experiments using DNA alone resulted in no significant cleavage of pUC19 DNA, even after longer exposure times. From the observed results, it was concluded that all the complexes effectively cleaved the DNA as compared to control DNA. Furthermore, the presence of a smear in the gel diagram indicates the presence of radical cleavage.[19]

Antimicrobial screening

The synthesized ligand and its complexes were tested for their *in vitro* antimicrobial activity. They were tested against the bacteria S*taphylococcus aureus*,

Pseudomonas aeruginosa, *Escherichia coli*, *Staphylococcus epidermidis*, *Klebsiella pneumoniae* and the fungi *Aspergillus niger*, *Fusarium solani*, *Culvularia lunata*, *Rhizoctonia bataticola* and *Candida albicans*. The minimum inhibitory concentration *(MIC)* values of the investigated compounds are summarized in Tables VII and VIII. A comparison of the *MIC* value of L with those of the complexes indicates that the metal complexes exhibited higher antimicrobial activity than L and the control sample. Such increased activity of the complexes can be explained based on the Overtone's concept[20] and the Tweedy chelation theory.[21] According to the Overtone's concept of cell permeability, the lipid membrane that surrounds the cell favors the passage of only lipid-soluble materials, due to which liposolubility is an important factor that controls antimicrobial activity. On chelation, the polarity of the metal ion will be reduced due to the partial sharing of positive charges with donor groups. Furthermore, it increases the delocalization of π-electrons over the whole chelate ring and enhances the lipophilicity of the complexes. This increased lipophilicity enhances the penetration of the complexes into lipid membranes and the blocking of the metal binding sites in the enzymes of microorganisms. The results obtained from the antifungal and antibacterial tests showed that all the tested complexes were more active towards bacteria than fungi. Moreover, the copper complexes were more active than the zinc complexes against the tested microorganisms.

TABLE VII. Antibacterial studies of the investigated compounds (minimum inhibitory concentration×10^4, μmol/L)

Compound	*S. aureus*	*P. aeruginosa*	*E. coli*	*S. epidermidis*	*K. pneumoniae*
L	16.3	14.8	16.6	16.2	14.5
$[CuL(phen)_2]Cl_2$	1.4	1.6	1.2	1.0	1.9
$[CuL(bpy)_2]Cl2$	2.1	2.5	2.0	1.7	2.2
$[ZnL(phen)_2]Cl_2$	2.7	3.4	2.4	3.1	4.2
[ZnL(bpy)2]Cl2	3.6	4.8	2.5	3.9	4.4
Streptomycin	1.7	1.9	1.8	1.3	2.6

TABLE VIII. Antifungal studies of the investigated compounds (minimum inhibitory concentration×10^4, μmol/L)

Compound	*A. niger*	*F. solani*	*C. lunata*	*R. bataticola*	*C. albicans*
L	12.8	13.1	14.3	11.5	15.7
$[CuL(phen)_2]Cl_2$	2.0	2.6	3.9	3.8	4.9
$[CuL(bpy)_2]Cl_2$	3.2	3.4	4.3	4.1	5.3
$[ZnL(phen)_2]Cl_2$	5.1	5.3	5.9	6.1	6.4
$[CuL(phen)_2]Cl_2$	6.3	6.7	6.1	6.5	6.9
Nystatin	1.1	1.6	1.2	1.0	1.5

CONCLUSIONS

Four mixed ligand Cu(II) and Zn(II) complexes of an isatin-based Schiff base (L) and 1,10-phenanthroline/2,2'-bipyridine were synthesized and characterized. Elemental analyses, conductivity measurements and FAB-Mass spectrometry revealed the stoichiometry and composition of the complexes to be $[ML(bpy)_2/(phen)_2]Cl_2$. The FTIR, UV–Vis, ^{1}H-NMR, EPR spectra and magnetic measurements data confirmed the bonding features of the studied mixed ligand complexes. Electronic absorption spectroscopy, cyclic voltammetry, differential pulse voltammetry and viscometric studies demonstrated a considerable interaction between the complexes and calf-thymus DNA. The results of cleavage studies using pUC19 DNA showed that the complexes had higher nuclease activities than the isatin-based ligand. The *MIC* values against the growth of microorganisms are much larger for the complexes than those of the ligand and the control sample.

Acknowledgements. The authors express their sincere thanks to the College Managing Board, Principal and Head of the Department of Chemistry, VHNSN College, and Virudhunagar, India, for providing the necessary research facilities.

И З В О Д

СИНТЕЗА, КАРАКТЕРИЗАЦИЈА, ИНТЕРАКЦИЈА СА ДНК И АНТИМИКРОБНО ИЗУЧАВАЊЕ Cu(II) И Zn(II) КОМПЛЕКСА СА МЕШОВИТИМ ЛИГАНДИМА НА БАЗИ ИЗАТИНСКЕ И ПОЛИПИРИДИЛНЕ СТРУКТУРЕ

NATARAJAN RAMAN и SIVASANGU SOBHA

Research Department of Chemistry, VHNSN College, Virudhunagar-626 001, India

Синтетисано је неколико мешовито лигандних Cu(II)/Zn(II) комплекса коришћењем 3-(фенилимино)-1,3-дихидроиндол-2*H*-она (добијеног кондензацијом изатина и анилина) као примарног лиганда и 1,10-фенантролина (phen)/2,2'-бипиридина (bpy) као додатног лиганда и окарактерисано аналитички и спектроскопски елементалном анализом, мерењима магнетне сусцептибилности и моларне проводљивости, UV–Vis, IR, NMR и FAB масеним спектрима. Интеракција комплекса са ДНК телећег тимуса (CT) је изучавана помоћу апсорпционих спектара, мерењима цикличне волтаметрије, вискозности и гел-електрофорезом. Они имају апсорпциони хипохромизам и специфична вискозност расте у току везивања комплекса за ДНК телећег тимуса. Померања оксидо-редукционог потенцијала и промене у пиковима струје додатком ДНК су показане CV мерењима. Cu(II)/Zn(II) комплекси изазивају раскидање pUC19 ДНК из суперувијеног облика I у отворени кружни облик II и линеарни облик III. Комплекси су показали повећану антифунгалну и антибактеријску активност у односу на слободни лиганд.

(Примљено 20. октобра 2009, ревидирано 17. марта 2010)

REFERENCES

1. C. B. Spillane, M. N. V. Dabo, N. C. F. Fletcher, J. L. Morgan, R. Keen, I. Haq, N. J. Buurma, *J. Biol. Inorg. Chem.* **102** (2008) 673

2. M. S. Surendra Babu, P. G. Krishna, K. Hussain Reddy, G. H. Philip, *J. Serb. Chem. Soc.* 75 (2010) 61
3. D. S. Sigman, A. Mazumder, D. M. Perrin, *Chem. Rev*. **96** (1993) 2295
4. T. Ghosh, B. G. Maiya, A. Samanta, *J. Biol. Inorg. Chem*. **10** (2005) 496
5. N. J. Turro, J. K. Barton, D. A. Tomalia, *Acc. Chem. Res*. **24** (1991) 332
6. F. Q. Liu, Q. X. Wang, K. Jiao, F. F. Jian, G. Y. Liu, R. X. Li, *Inorg. Chim. Acta* **395** (2006) 1524
7. T. F. Tullis, *Metal–DNA chemistry*, ACS Symposium Series No. 402, American Chemical Society, Washington DC, 1989
8. J. K. Barton, *Science* **233** (1986) 727
9. S. P. Singh, S. K. Shukla, L. P. Awasthi, *Curr. Sci*. **52** (1983) 766
10. S. Arounaguiri, B. G. Maiya, *Inorg. Chem.* **38** (1999) 842
11. R. Pulimamidi, R. Nomula, R. Karnativ *Indian J. Chem.* **48** (2009) 1638
12. A. Kriza, C. Parnau, *Acta Chim. Slov*. **48** (2001) 445
13. J. A. Marmur, *J. Mol. Biol*. **3** (1961) 208
14. G. Speir, J. Csihony, J. M. Whalen, C. G. Pierpont, *Inorg. Chem.* **3** (1996) 3519
15. B. J. Hathaway, D. E. Billing, *Coord. Chem. Rev*. **5** (1970) 143
16. S. Sathyanarayana, J. C. Dabroniak, J. B. Chaires, *Biochemistry* **31** (1992) 9319
17. S. Sathyanarayana, J. C. Dabroniak, J. B. Chaires, *Biochemistry* **32** (1993) 2573
18. G. M. Blackburn, M. J. Gait, *Nucleic acid in chemistry and biology*, 2nd ed., Oxford University Press, New York, 1996
19. C. X. Zhang, S. J. Lippard, *Curr. Op. Chem. Biol*. **7** (2003) 481
20. Y. Anjaneyalu, R. P. Rao, *Synth. React. Inorg.-Org. Chem.* **16** (1986) 257
21. L. Mishra, V. H. Singh, *Indian J. Chem*. **32A** (1993) 446.

Journal of the Serbian Chemical Society
JSCS@tmf.bg.ac.rs • www.shd.org.rs/JSCS

J. Serb. Chem. Soc. 75 (6) 789–801 (2010)
JSCS–4007

UDC 665.75.001.57+542.913+661.332+
661.183.7/.8+544.774.2:544.478
Original scientific paper

Biodiesel synthesis using K_2CO_3/Al–O–Si aerogel catalysts

IVANA LUKIĆ[1]*, JUGOSLAV KRSTIĆ[2], SANDRA GLIŠIĆ[1], DUŠAN JOVANOVIĆ[2] and DEJAN SKALA[1]

[1]*Faculty of Technology and Metallurgy, Karnegijeva 4, 11000 Belgrade and* [2]*Institute of Chemistry, Technology and Metallurgy, Department of Catalysis and Chemical Engineering, Njegoševa 12, 11000 Belgrade, Serbia*

(Received 7 July 2009, revised 1 February 2010)

Abstract: In this study, catalysts for fatty acid methyl esters (FAME or biodiesel) synthesis with K_2CO_3 as the active component on an alumina/silica support were synthesized using the sol–gel method, which was followed by drying the "dense" wet gels with supercritical carbon dioxide to obtain the aerogels. The prepared catalysts were characterized by XRD analysis, FTIR spectroscopy and N_2 physisorption at 77 K, and tested in the methanolysis of sunflower oil. The effects of reaction variables, such as reaction time, temperature and methanol to oil molar ratio, on the yield of FAME were investigated. The aerogel catalysts with K_2CO_3 as the active component on an alumina/silica support exhibited good activity in the methanolysis of sunflower oil. The leaching of potassium when the catalyst was in contact with pure methanol under the working conditions of methanolysis was also tested in this study, indicating that it occurred only at higher temperatures, while at lower ones, it was negligible.

Keywords: biodiesel; aerogel; alumina/silica; K_2CO_3.

INTRODUCTION

Biodiesel, consisting of FAME, produced by the alcoholysis of vegetable oils or animal fats, is an excellent substitute for conventional diesel fuels. It is non-toxic, biodegradable and made from renewable sources. Increasing biodiesel consumption requires optimized production processes allowing high production capacities, simplified operations, high yields, and the absence of special chemical requirements and wastes. The development of solid catalysts has recently gained much attention because a successful heterogeneous catalyst alleviate most of the economic and environmental drawbacks of a homogeneous process, such as neu-

* Corresponding author. E-mail: ivanal888@yahoo.co.uk
doi: 10.2298/JSC090707047L

tralization of alkali catalysts after reaction and creation of large amount of wastewater produced during washing and separation of the final products.

To date, only one industrial application, developed by the French Institute of Petroleum (IFP), employs heterogeneous based catalysts for the methanolysis of vegetable oils to produce biodiesel.[1] The IFP has announced the construction of further similar industrial plants in Europe based on the use of a heterogeneous catalyst consisting of a mixed oxide of zinc and aluminum with a spinel structure.

On the laboratory scale, many different heterogeneous catalysts have been developed to catalyze the alcoholysis of vegetable oils. Alumina loaded with alkali metal salts or different potassium compounds were demonstrated to be efficient solid-base catalysts.[2] Alumina exhibited no activity, but when loaded with KI, KF, KNO_3, K_2CO_3 or KOH and activated at high temperatures, the supported catalyst showed catalytic activities.[3–9] A good activity of K_2CO_3/Al_2O_3 xerogel catalyst was previously reported, but undesired leaching of the active components was also observed.[9] Xie and Li[7] reported lower activity of K_2CO_3/Al_2O_3 due to its lower basicity compared to other potassium compounds on alumina. Namely, a catalyst with 35 wt. % KI loading on Al_2O_3 (calcined at 500 °C for 3 h) had the highest basicity and the best catalytic activity. Other catalysts that showed efficiency as heterogeneous catalysts for the alcoholysis of vegetable oil are commercial hydrotalcite,[10] zeolites and modified zeolites[11,12] and Na/ /NaOH/γ-Al_2O_3[13] but they are either quite expensive or complicated to prepare, which has limited their industrial application. At temperature above 250 °C, a high conversion of soybean oil (90 %) was obtained after 20 hours of reaction using WO_3/ZrO_2, TiO_2/ZrO_2 or Al_2O_3/ZrO_2 as catalysts.[14,15] The catalytic ability of CaO and MgO was found to be quite weak at lower temperatures, but increasing the reaction temperature had a favorable influence on the methyl ester yield.[16–21] Veljković *et al.*[22] determined 550 °C to be the optimal CaO calcination temperature and studied the kinetics of CaO catalyzed methanolysis. In order to improve the catalytic activity of CaO, it was promoted with Li salts[23,24] or lanthanum,[25] which both increased the basic strength and led to an enhancement of the catalyst activity.

Different techniques have been used for the preparation of catalysts. Sol–gel chemistry was usually applied having many advantages over other methods of catalyst synthesis. It allows control of homogeneity on the nanoscale and results in high surface areas and pore volumes. After dissolution of the reactants in an appropriate solvent and subsequent gelation of the sol, the formed wet gel can be dried using different methods. An available drying method is the extraction of the solvent using the supercritical drying process (SCD), which was performed in this study. Namely, supercritical drying preserves the original gel structure by eliminating capillary pressure while, at the same time, the solvent and sol–gel reaction byproducts present in the gel pores are extracted at a temperature and pres-

sure higher than the critical temperature and pressure of the solvent, thereby producing a material known as an aerogel.[26] Supercritical drying can also be realized using another supercritical extracting fluid with moderate values of the critical parameters (commonly carbon dioxide). Due to their unique morphological and physicochemical properties, aerogels are being widely studied for potential applications in heterogeneous catalysis.[27]

In this study, a new type of heterogeneous catalyst with K_2CO_3 as the active component on an alumina/silica support was synthesized using the sol–gel method, which was followed by drying the wet gel with supercritical carbon dioxide. The characteristics of the obtained aerogels and their activity in the methanolysis reaction were studied. The activity of the prepared aerogel catalysts was tested in the methanolysis of sunflower oil and the efficiency of process at different temperatures (80–200 °C) and molar ratios of methanol to oil (6:1–30:1) was also analyzed. Eventual leaching of K_2CO_3 from the catalyst would reduce the activity of the catalyst and decrease its activity in the second repeated process of methanolysis. For this reason, the leaching of potassium on contact of the catalyst with pure methanol under working conditions of methanolysis was also tested in this study.

EXPERIMENTAL

Catalyst preparation

The catalysts were synthesized by a one-step sol–gel procedure. Aluminum tri-*sec*-butoxide, tetraethoxy orthosilane (TEOS), 1-butanol, anhydrous potassium carbonate (all Fluka) were used as reagents. Aluminum tri-*sec*-butoxide (29.1 g, 0.120 mol) was mixed with 1-butanol (200 cm^3) and then TEOS (8.32 g, 0.0400 mol) was added. The mixture was stirred vigorously and heated to 70 °C for 5 min until a clear solution was obtained. The solution was cooled to room temperature and then hydrolyzed with water (37.5 cm^3, 2.08 mol) containing dissolved potassium carbonate (2.86 g; 0.0210 mol). The solution was stirred for 15 min and left to stand overnight (gelation). Water and a certain amount of 1-butanol (excess) were then removed by heating the gel to 150 °C, and a "densed" wet gel was obtained. The above procedure describes the wet gel synthesis of samples with ratio Al/Si = 3/1 and an amount of K_2CO_3 which was calculated to be 45 wt. % based on the support.

Aerogels were obtained by drying the "dense" wet gels with supercritical carbon dioxide in a previously described 300 cm^3 tubular extractor, Autoclave Engineers SCE Screening System.[28] During the supercritical drying, the extractor was filled with liquid CO_2 at the beginning of drying process, then the pressure was increased above the critical value for CO_2 and finally the temperature was raised to the desired value. After reaching the working conditions of pressure and temperature, the flow of CO_2 was maintained and kept constant at about 100 g CO_2/h. This procedure was necessary to avoid the presence of two CO_2 phases of in the extractor. The duration of the SCD depended on the employed drying conditions. The parameters of sol–gel synthesis and gel drying are presented in Table I, together with the experimental conditions used for calcination of the prepared catalysts (four samples defined as AG1–AG4).

TABLE I. The experimental conditions for the SCD process performed at 100 bar

Condition	AG1	AG2	AG3	AG4
Drying temperature, °C	40	40	200	200
Duration of SCD, h	9	9	5	5
Total consumption of CO_2, kg	0.9	0.9	0.5	0.5
Temperature of calcinations, °C (t = 12h)	600	300	600	300

Catalyst characterization

The XRD measurements were performed on a Philips PW1710 powder X-ray diffractometer using Cu Kα radiation, over the 2θ range 4–90 ° in the scan mode (step size 0.02°, counting 0.5 s per step).

The nitrogen adsorption–desorption isotherms were determined using a Sorptomatic 1990 Thermo Electron instrument at –196 °C. All samples were degassed at 120 °C for 12 h under reduced pressure (< 1 torr) prior to the sorption measurements. Various models and appropriate software – ADP, Thermo Electron, version 5.1, were used to analyze the obtained isotherms. The specific surface area of samples (S_{BET}) was calculated according to the Brunauer, Emmett, Teller (BET) method from the linear part of the nitrogen adsorption isotherms.[29] The total pore volume (V_{tot}) was taken at p/p_0 = 0.998. The mesopores volume and pore size distribution was calculated according to the Barrett, Joyner and Halenda method from the desorption branch of the isotherm.[30] The micropores were analyzed using the Dubinin–Radushkevich method.[31]

The Fourier-transform infrared (FTIR) spectra were recorded in the transmission mode using a BOMEM (Hartmann & Braun) spectrometer. All measurements were conducted at room temperature in the wave number range 400–4000 cm^{-1}, with a 2 cm^{-1} resolution.

Methanolysis reaction

Synthesized catalysts were tested in the methanolysis of sunflower oil. Commercial edible sunflower oil (Sunce, Sombor, Serbia) was used for the experimental studies. The experiments were performed in a 300 cm^3 batch autoclave (Autoclave Engineers, Country), equipped with an electrical heater and a mixer. Prior to the reaction, the catalyst samples (fraction <500 μm) were activated by heating in an oven at 120 °C for 2 h. The preliminary tests of the activity of the prepared aerogel catalysts (AG1–AG4; 2 wt. % catalyst based on the oil) were realized at 200 °C and 37 bar using an agitation speed of 400 rpm and a molar ratio of sunflower oil to methanol of 1:30. The pressure in the autoclave was resulted from the vapor pressure methanol at the working conditions. The time when the reaction temperature was achieved was taken as zero reaction time. Reaction samples were withdrawn periodically, without stopping of the reaction, and after filtration and separation of the residual methanol using a rotational evaporator, the samples were analyzed by gas chromatography (Varian 3400; FID detector, a fused silica capillary column 5 m×0.53 mm, film thickness 0.5 μm and an on-column injector). Quantitative analysis of FAME was realized using correction factors for FAME, tri-, di- and monoglycerides and glycerol. The calculated correction factors were used for calculating the mass percentage of FAME. The catalyst sample AG2 was used to study the influence of different working conditions (temperature, ratio of methanol to oil) on the synthesis of FAME.

The leaching of potassium from the catalyst was tested by contacting catalyst AG2 with methanol for 2 h at 120 °C, and then the methanol solution after filtering to remove solids was used in the reaction with vegetable oil.

RESULTS AND DISCUSSION

Catalyst characterization

X-Ray diffraction analysis was conducted to investigate the structure and crystallinity of the catalysts. The XRD patterns of the aerogels presented no sharp diffraction peaks. A similar effect was observed and recently reported in literature.[9] This fact indicated that the synthesized catalysts were amorphous, regardless of the preparation procedure. The XRD pattern for aerogel AG2 is presented in Fig. 1.

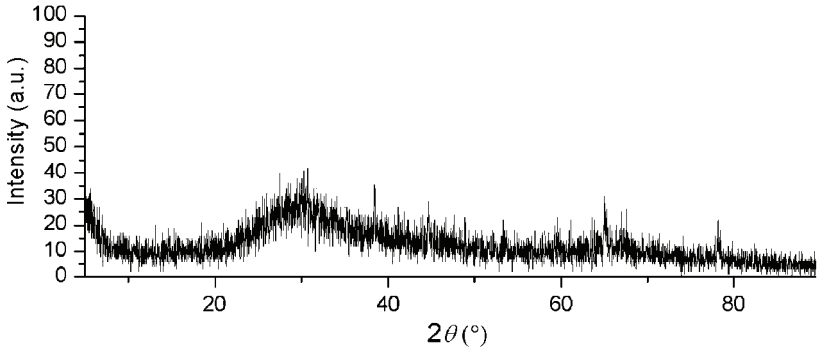

Fig. 1. XRD Pattern for aerogel AG2.

The measured BET surface area, the volumes of the mesopores and micropores, the overall pore volume, D_{max}, the pore diameter where the maximum of the derivative cumulative volume curve is reached, and D, the average pore diameter, are given in Table II, and the pore size distribution in Fig. 2.

TABLE II. Textural properties of the catalysts

Catalyst	S_{BET} / m^2 g^{-1}	V_{tot} / cm^3 g^{-1}	V_{meso} / cm^3 g^{-1}	V_{mic} / cm^3 g^{-1}	D_{max} / nm	D / nm
AG1	114	0.225	0.182	0.039	3.808	4.925
AG2	107	0.144	0.137	0.036	3.764	3.838
AG3	122	0.206	0.202	0.042	3.734	4.979
AG4	113	0.175	0.172	0.035	3.786	4.427

The results of the BET analyses indicated that the synthesized catalysts were mesoporous, while the D_{max} values were similar around 3.8 nm and the D values were between 3.8 and 4.9 nm. The aerogel AG2 had a value of D_{max} very similar to that of D, which means that the sizes of all pores were equally distributed around D_{max}. A very slight shift of the pore sizes to larger pore diameters was observed for the other 3 catalysts. When calcination of the prepared catalysts was realized at higher temperature (AG1 and AG3), a slightly larger surface area and pore volume was observed than for aerogels AG2 and AG4. The BET analysis

indicated that the different SCD conditions had only a moderate influence on the porous structure of the prepared aerogels.

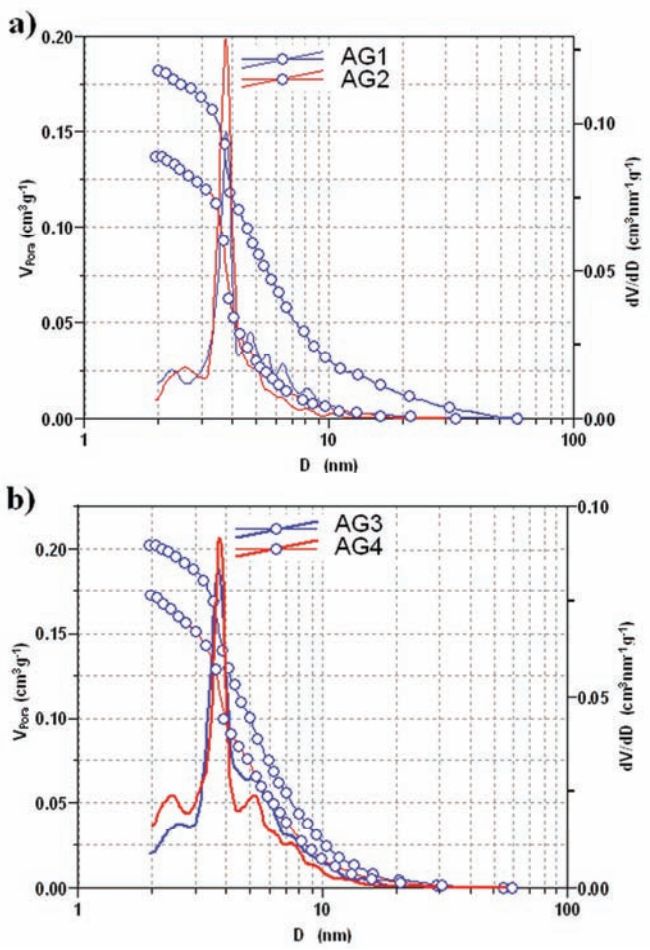

Fig. 2. Pore size distribution of the catalysts a) AG1 and AG2; b) AG3 and AG4.

As can be seen from Fig. 2 and Table II, the major part of the catalyst volume was occupied by pores with an average diameter of 3.8–4.9 nm, which is common for samples of aerogels. According to Fernandez *et al.*,[34] the critical diameter of the triglyceride molecule, defined as the diameter of the smallest cylinder through which the molecule can pass without distortion, is around 2 nm; Lopez Granados *et al.*[19] reported that methyl oleate has a diameter around 2.5 nm, and the diameter of triglycerides is certainly at least two times larger. A number of studies showed that restricted diffusion, which transpires when the dimensions of the reactant molecule and the pore are comparable, occurs in silica–

–alumina catalysts with pore diameters less than 5 nm.[35]. For a narrow pore catalyst (mean pore diameter ≈ 4 nm), a 50 % decrease in catalytic activity relative to the activity of a catalyst with medium (d ≈ 6 nm) and wide pore (d ≈ 8 nm) size could be expected.[36] The problem of the access of the voluminous triglycerides molecules to the active sites within the pores of a catalyst were calculated for a xerogel catalyst taking into account the mean pore size diameter (3.8 nm) and the dimensions of the triglycerides molecule and the results indicated that internal diffusion resistance obviously exists.[9] Taking into account that space occupation by triglyceride could be represented by 5 nm in diameter,[19] which is larger than the pore diameter, molecules of triglycerides obviously cannot easily diffuse through the pores of the major part of the catalyst and that efficient contact between reactant and active site is mainly possible only on the external surface of the catalyst.

FTIR Spectra of the catalyst samples are shown in Fig. 3. The characteristic bands are: a band at about 1000 cm^{-1}, attributed to the Si–O stretching vibration; a band at around 460 cm^{-1}, attributed to Si–O bending;[37,38] bands in the range 500–700 cm^{-1}, attributed to octahedral Al–O, and 700–900 cm^{-1}, attributed to tetrahedral Al–O.[39] The shift of the absorption band of Si–O stretching from 1000 cm^{-1} to lower wavenumbers indicates the presence of Al–O–Si bonds in the investigated samples and the intensity of the shifting indicates the level of mixing of Al and Si in the alumina/silica network.[38] The band at about 3430 cm^{-1} is associated with stretching vibrations due to OH groups of water molecules adsorbed onto the surface of the catalyst but, according to Xie and Li[7], this band could be partly assigned to the stretching vibrations of Al–O–K groups. Another band associated with the presence of water is located at 1635 cm^{-1}.[40] Supported K_2CO_3 and bulk K_2CO_3 give slightly different absorption bands.[41] Bands at

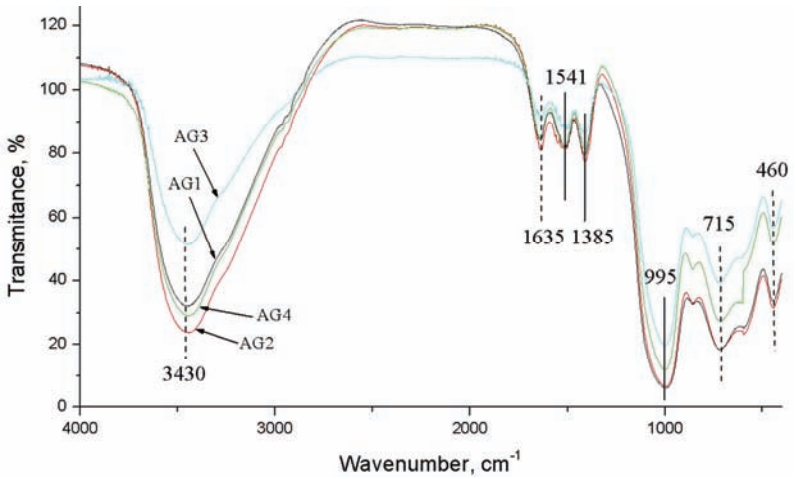

Fig. 3. FTIR Spectra of prepared catalysts.

1541 and 1385 cm^{-1} were observed for all catalyst samples and are attributed to carbonate species,[41,42] whereby the band at 1385 cm^{-1} indicates the presence of bulk K_2CO_3,[41] the part of the catalyst which is the main reason for its activity.[9]

Influence of various parameters on the yield of FAME

Yield of FAME achieved in the methanolysis reaction is shown in Fig. 4. As can be seen, all the prepared aerogel catalysts with K_2CO_3 as the active component showed very good catalytic activity, with yields of FAME over 90 % after 15 min in the batch process for all catalysts except for AG1, which expressed a slightly lower activity. All four aerogels had very similar textural and structural characteristics and the only difference observed for AG1 which could be the explanation for the lower activity is its smaller fraction of mesopores in the total pore volume.

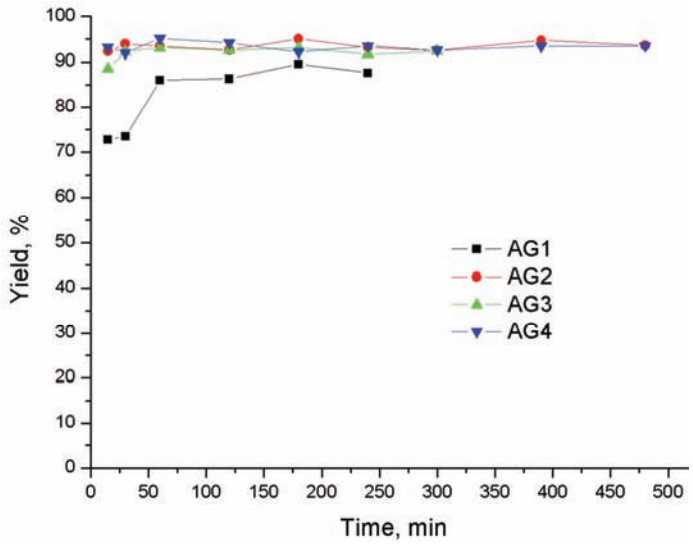

Fig. 4. Effect of reaction time on the yield of FAME synthesized at 200 °C and under 37 bar, using a molar ratio of methanol:oil = 30:1 and 2 wt. % of catalyst based on oil.

The influence of the reaction temperature on the yield of FAME in the methanolysis performed using catalyst AG2 is shown in Fig. 5. The rate of the methanolysis reaction of the vegetable oil was strongly influenced by the reaction temperature and the yield of FAME increased with increasing temperature. At the lower temperature (80 °C), several hours were necessary to achieve the desired high yield of FAME. However, in the batch process at 120 °C, approximately 92 % conversion of the triglycerides giving the desired yield of FAME could be achieved after 15 min of methanolysis.

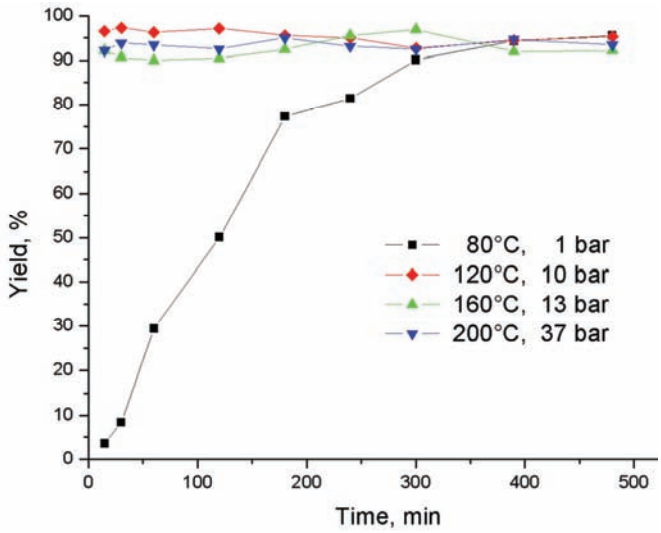

Fig. 5. Influence of reaction temperature on the yield of FAME, using a methanol to oil molar ratio of 30:1 and 2 wt. % of catalyst sample AG2 (based on oil).

The molar ratio of methanol to vegetable oil is also a very important parameter which affects the conversion of triglycerides to methyl esters. The influence of the molar ratio was examined in the methanolysis of sunflower oil with aerogel AG2 at 120 °C using 2 wt. % of catalyst based on oil and the obtained results are shown in Fig. 6.

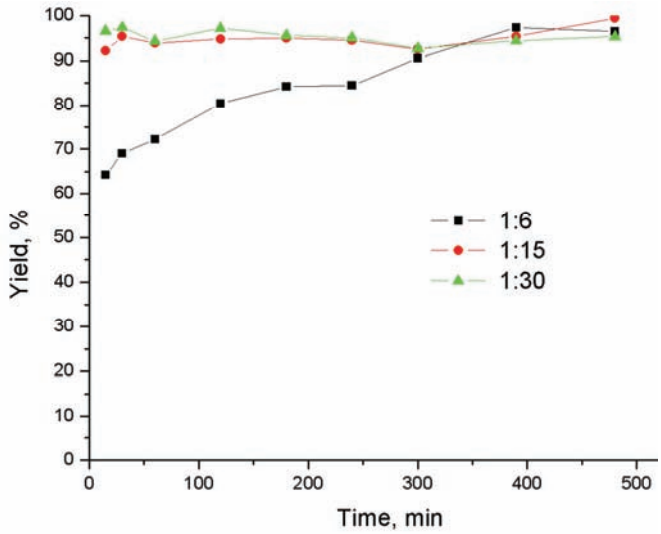

Fig. 6. Influence of the methanol to oil molar ratio on the yield of FAME at 120 °C and with 2 wt. % of catalyst sample AG2 (based on oil).

Stoichiometrically, the methanolysis of vegetable oil requires three moles of methanol for each mole of oil. However, in practice a higher molar ratio is employed in order to shift the reaction equilibrium towards the products side and produce more methyl esters. As shown in Fig. 6, the syntheses realized with larger methanol to oil ratios (15:1 and 30:1) were followed by higher rates of the methanolysis reaction and, thus, the desired high conversions of the triglycerides were observed in shorter times. According to the results of this study, it can be concluded that a molar ratio of methanol to oil of 15:1 was sufficient for a good yield of FAME to be achieved in a relatively short reaction time.

The obtained results were compared to the catalytic activity of a K_2CO_3/Al–O–Si xerogel (2 wt. % based on oil)[9] used for the methanolysis of sunflower oil at 120 °C with a methanol to oil molar ratio of 15:1. The comparison indicated that the applied drying process gave a catalyst with similar activity.

A kinetic model for the reaction between methanol and triglycerides was determined assuming that a first order irreversible reaction could be used for the prediction the yield of FAME. Simultaneously, solution of the energy and mole balances were realized for a batch, non-isothermal process using Polymath software and the results of the calculation together with the experimentally determined FAME content in the reaction mixture are presented in Fig. 7. The model was described in detail and the parameters defined by Glišić *et al.*[43] As can be seen, this model fits well the experimental data for the performed methanolysis of triglycerides using the studied aerogel catalyst.

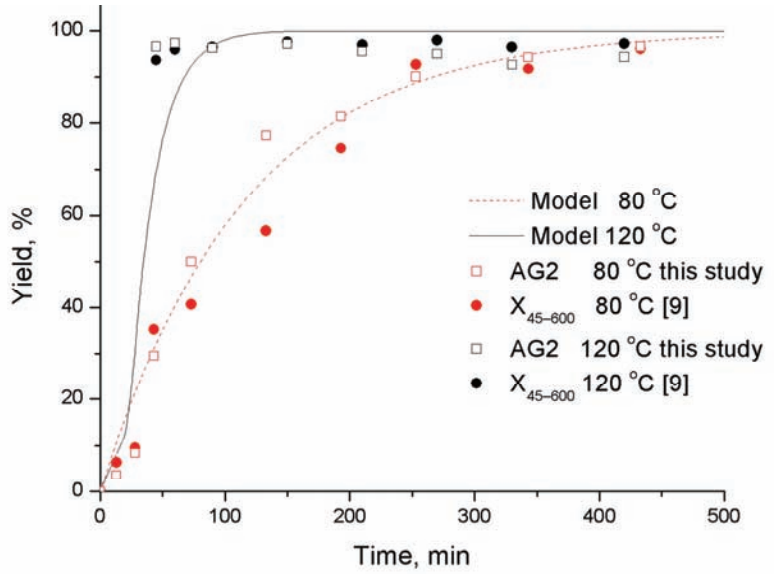

Fig. 7. Comparison of the experimental and simulated data.

An additional experiment was performed to check whether leaching of the active phase from aerogel catalyst occurred. The activated catalyst was placed in contact with methanol for 2 h at 120 °C, filtered to remove the solids and then the vegetable oil was placed in contact with the clear methanol solution. The yield of FAME was 43.9 %, after 2 h at 120 °C, indicating that leaching of some amount of active phase had occurred.

The amount of leached potassium carbonate in methanol was measured and the results are shown in Table III. The potassium content at higher temperature is quite high, as expected – 210 mg/l when 120 °C was reached and 390 mg/l after 2 h at 120 °C, confirming that at this temperature the aerogel used in the reaction of triglyceride methanolysis showed activity which could be mainly contributed to the effect of homogeneous–heterogeneous catalyst. However, at temperatures below 100 °C, the leaching of potassium species was negligible with only 7 mg/l. This fact is very important because a high yield could be also achieved at 80 °C but after a longer time of reaction (Fig. 5). Finally, according to these investigations, it can be concluded that at lower temperatures, 100 °C or below, the prepared aerogel catalyst acted as a heterogeneous one.

Table III. Determined amount of K in methanol at different temperatures

Temperature, °C	K amount, mg/l
60	4
100	7
120	210
120 (after 2 h)	390

CONCLUSIONS

The experiments performed in this study showed that the synthesized aerogel catalysts with potassium carbonate as the active component on an alumina/silica support are very active in the methanolysis of sunflower oil. It was also shown that leaching of some amount of potassium species to the methanol phase during FAME synthesis occurred when the reaction was performed at 120 °C, but when the temperature was below 100 °C, the leaching was negligible and, thus, the catalyst acts as a heterogeneous one under such conditions.

The analysis of different working conditions indicated that the temperature of the reaction and methanol:oil molar ratio mainly affected the reaction rate of methanolysis. Although at 120 °C with a methanol:oil molar ratio of 15:1 a yield of over 92 % was achieved after 15 min, the performed investigation of the catalytic activity of K_2CO_3/(alumina–silica support) showed that at lower temperatures, a heterogeneously catalyzed methanolysis of triglycerides was possible and that similar conversion of the triglycerides could be achieved but after a longer reaction time.

Acknowledgements. The financial support of the Ministry of Science and Technological Development of the Republic of Serbia, Projects Nos. TR 19062 and 166001, is gratefully acknowledged.

И З В О Д

СИНТЕЗА БИОДИЗЕЛА КАТАЛИЗОВАНА АЛУМОСИЛИКАТНИМ АЕРОГЕЛОМ СА K_2CO_3

ИВАНА ЛУКИЋ[1], ЈУГОСЛАВ КРСТИЋ[2], САНДРА ГЛИШИЋ[1], ДУШАН ЈОВАНОВИЋ[2] и ДЕЈАН СКАЛА[1]

[1]Технолошко–металуршки факултет, Карнегијева 4, 11000 Београд и [2]Институт за хемију, технологију и металургију, Центар за катализу и хемијско инжењерство, Његошева 12, 11000 Београд

У овом раду катализатор за синтезу метил естара масних киселина (МЕМК или биодизел) са K_2CO_3 као активном компонентом на алумосиликатном носачу синтетизован је сол–гел методом након чега је добијени гел сушен уз присуство наткритичног угљен диоксида да би се добио аерогел. За карактеризацију синтетизованих катализатора коришћене су методе XRD, FTIR и N_2 физисорпција на 77 K и катализатори су тестирани у реакцији метанолизе сунцокретовог уља. Катализатор је тестиран у реакцији метанолизе сунцекротовог уља и синтези МЕМК. Испитан је утицај различитих параметара као што су време, температура и моларни однос метанол:уље на принос МЕМК. Аерогел катализатор са K_2CO_3 као активном компонентом на алумосиликатном носачу показао је добру каталитичку активност у реакцији метанолизе сунцокретовог уља. Излуживање калијума у контакту са метанолом на радним условима метанолизе такође је тестирано у овом раду, показујући да оно постоји на вишим температурама, док је на нижим занемарљиво.

(Примљено 7. јула 2009, ревидирано 1. фебруара 2010)

REFERENCES

1. L. Bournay, D. Casanave, B. Delfort, G. Hillion, J. A. Chodorge, *Catal. Today* **106** (2005) 190
2. S. Benjapornkulaphong, C. Ngamcharussrivichai, K. Bunyakiat, *Chem. Eng. J.* **145** (2009) 468
3. T. Ebiura, T. Echizen, A. Ishikawa, K. Murai, T. Baba, *Appl. Catal. A Gen.* **283** (2005) 111
4. D. Martın Alonso, R. Mariscal, R. Moreno-Tost, M. D. Zafra Poves, M. Lopez Granados, *Catal. Comm.* **8** (2007) 2074
5. K. Noiroj, P. Intarapong, A. Luengnaruemitchai, S. Jai-In, *Renew. Energy* **34** (2009) 1145
6. A. P. Vyas, N. Subrahmanyam, P. A. Patel, *Fuel* **88** (2009) 625
7. W. Xie, H. Li, *J. Mol. Catal. A Chem.* **255** (2006) 1
8. W. Xie, H. Peng, L. Chen, *Appl. Catal. A Gen.* **300** (2006) 67
9. I. Lukić, J. Krstić, D. Jovanović, D. Skala, *Bioresour. Technol.* **100** (2009) 4690
10. W. Xie, H. Peng, L. Chen, *J. Mol. Catal. A Chem.* **246** (2006) 24
11. W. Xie, X. Huang, H. Li, *Bioresour. Technol.* **98** (2007) 936
12. G. J. Suppes, M. A. Dasari, E. J. Doskocil, P. J. Mankidy, M. J. Goff, *Appl. Catal. A Gen.* **257** (2004) 213
13. H. J. Kim, B. S. Kang, M. J. Kim, Y. M. Park, D. K. Kim, J. S. Lee, K. Y. Lee, *Catal. Today* **93–95** (2004) 315
14. S. Furuta, H. Matsuhashi, K. Arata, *Catal. Comm.* **5** (2004) 721
15. S. Furuta, H. Matsuhashi, K. Arata, *Biomass Bioenerg.* **30** (2006) 870
16. A. Demirbas, *Energ. Convers. Manag.* **48** (2007) 937

17. M. Di Serio, M. Ledda, M. Cozzolino, G. Minutillo, R. Tesser, E. Santacesaria, *Ind. Eng. Chem. Res.* **45** (2006) 3009
18. S. Gryglewicz, *Bioresour. Technol.* **70** (1999) 249
19. M. Lopez Granados, M. D. Zafra Poves, D. Martin Alonso, R. Mariscal, F. Cabello Galisteo, R. Moreno-Tost, J. Santamarı, J. L. G. Fierro, *Appl. Catal. B Environ.* **73** (2007) 327
20. G. Vicente, A. Coteron, M. Martinez, J. Aracil, *Ind. Crop. Prod*. **8** (1998) 29
21. L. Wang, J. Yang, *Fuel* **86** (2007) 328
22. V. B. Veljković, O. S. Stamenković, Z. B. Todorović, M. L. Lazić, D. U. Skala, *Fuel* **88** (2009) 1554
23. R. S. Watkins, A. F. Lee, K. Wilson, *Green Chem.* **6** (2004) 335
24. D. Martın Alonso, R. Mariscal, M. Lopez Granados, P. Maireles-Torres, *Catal. Today* **143** (2009) 167
25. S. Yan, M. Kim, S. O. Salley, K. Y. Simon Ng, *Appl. Catal. A Gen.* **360** (2009) 163
26. A. Orlović, D. J. Janaćković, S. Drmanić, Z. Marinković, D. Skala, *J. Serb. Chem. Soc.* **66** (2001) 685
27. J. Chen, R. Wang, J. Zhang, F. He, S. Han, *J. Mol. Catal. A Chem.* **235** (2005) 302
28. I. Žižović, M. Stamenić, A. Orlović, D. Skala, *CI&CEQ* **12** (2006) 164
29. F. Rouquerol, J. Rouquerol, K. Sing, *Adsorption by Powders and Porous Solids*, Academic Press, London, 1999
30. E. P. Barrett, L. G. Joyner, P. P. Halenda, *J. Am. Chem. Soc.* **73** (1951) 373
31. M. M. Dubinin, *Progress in Surface and Membrane Science*, Academic Press, New York, 1975
32. E. J. Zanto, S. A. Al-Muhtaseb, J. A. Ritter, *Ind. Eng. Chem. Res.* **41** (2002) 3151
33. F. Silveira, G. P. Pires, C. F. Petry, D. Pozebon, F. C. Stedile, J. H. Z. dos Santos, A. Rigacci, *J. Mol. Catal. A Chem.* **265** (2007) 167
34. M. B. Fernandez, G. M. Tonetto, G. Crapiste, D. E. Damiani, *Int. J. Chem. React. Eng.* **5** (2007) A10
35. E. Ramırez, M. A. Larrayoz, F. Recasens, *AIChE J.* **52** (2005) 1539
36. J. W. E. Coenen, *Ind. Eng. Chem. Fundam.* **25** (1986) 43
37. A. Orlović, *PhD Thesis*, University of Belgrade, 2001
38. B. A. Sava, A. Diaconu, M. Elisa, C. E. A. Grigorescu, I. C. Vasiliu, A. Manea, *Superlattice Microst.* **42** (2007) 314
39. G. Paglia, C. E. Buckley, T. J. Udovic, A. L. Rohl, F. Jones, C. F. Maitland, J. Connolly, *Chem. Mater.* **16** (2004) 1914
40. D. C. L. Vasconcelos, R. L. Orefice, W. L. Vasconcelos, *Mater. Sci. Eng. A* **447** (2007) 77
41. T. Yamaguchi, Y. Wang, M. Komatsu, M. Ookawa, *Catal. Surv. Jpn.* **5** (2002) 81
42. D. Martın Alonso, R. Mariscal, R. Moreno-Tost, M. D. Zafra Poves, M. Lopez Granados, *Catal. Comm.* **8** (2007) 2074
43. S. Glišić, I. Lukić, D. Skala, *Bioresour. Technol.* **100** (2009) 6347.

Journal of the Serbian Chemical Society
JSCS@tmf.bg.ac.rs • www.shd.org.rs/JSCS

J. Serb. Chem. Soc. 75 (6) 803–812 (2010) UDC 665.12+641.3:543.544.3+543.51:66.061
JSCS–4008 *Original scientific paper*

Determination of *trans* fatty acids in foodstuffs by gas chromatography–mass spectrometry after simultaneous microwave-assisted extraction–esterification

SNEŽANA KRAVIĆ[1*#], ZVONIMIR SUTUROVIĆ[1#], JAROSLAVA ŠVARC-GAJIĆ[1#], ZORICA STOJANOVIĆ[1#] and MIRA PUCAREVIĆ[2]

[1]*Faculty of Technology, Department of Applied and Engineering Chemistry, University of Novi Sad, Bulevar cara Lazara 1, 21000 Novi Sad and* [2]*Faculty of Environmental Protection, Educons University, Vojvode Putnika bb, 21202 Sremska Kamenica, Serbia*

(Received 17 July 2009, revised 15 February 2010)

Abstract: A sample preparation method based on the simultaneous microwave-assisted extraction–esterification (SMAEE) was developed for the determination of the fatty acid composition of foodstuffs by gas chromatography–mass spectrometry. The proposed sample preparation method was validated by comparison with the reference Soxhlet extraction method followed by derivatisation by ester formation and the same determination step. The fatty acid compositions and the extraction efficiencies obtained using the proposed SMAEE method and the reference method were statistically similar. The results showed that compared to the conventional method, the SMAEE method offered the advantages of short sample preparation time, low consumption of expensive organic solvents and lower energy consumption. This good agreement between results provided by both the SMAEE and the reference method demonstrates the usefulness of the former as a routine method for the treatment of food samples prior to *trans* fatty analysis.

Keywords: *trans* fatty acids; microwave-assisted extraction–esterification; gas chromatography; mass spectrometry; foodstuffs.

INTRODUCTION

The determination of fatty acid profiles is a basic requirement in the testing of food material as a response to the demand of consumers for improved fat quality in food.[1] Moreover, interest in dietary fat has grown in the last years due to *trans* fatty acids (TFA), which are produced in the hydrogenation process that solidifies liquid oils.[2] Their consumption has been associated with an increase in serum cholesterol levels and the risk of cardiovascular heart diseases. Parallel to

* Corresponding author. E-mail: sne@uns.ac.rs
# Serbian Chemical Society member.
doi: 10.2298/JSC090717051K

this, other researchers have reported that *trans* fatty acids decrease the serum levels of the high-density lipoprotein cholesterol.[3–5]

These concerns moved Food and Agriculture, and the World Health Organization to recommend that fats for human consumption should contain less than 4 % of the total fats as *trans* and urged the food industry to reduce the presence of *trans* fats in their products to these levels. The Food and Drug Administration also decreed that by 1 January, 2006, manufacturers must itemize the *trans* fats category separately from the total fat listing. For this purpose, the FDA and Health Canada proposed food-labelling rules that require the amount of *trans* fat per serving to be given. Specifically, products that contain >0.5 g per serving would have the asterisked footnote, "*Includes – g *trans* fat".[6] This is also a concern in Europe, as demonstrated by the Danish legislation that established a lower content of these lipids, < 2 % (w/w), and the general trend in the EU to include the content of *trans* fatty acids on the label as a quality index.[7]

Methods employed to analyse the TFA in foods of natural origin or formed during the processing of fats and oils are of two types. Methods based on infrared spectroscopy only measure the total amount of TFA in a sample, while separation of the different isomers containing one or more double bonds may be achieved only using methods based on gas liquid chromatography (GLC) or high performance liquid chromatography (HPLC). Currently, capillary gas chromatography, with flame ionization (FID) or mass spectroscopy (MS) detectors, is the most appropriate technique for quantifying the composition of fatty acids, including *trans* fatty acids.[8] This separation technique requires the analyte to be volatile, so transesterification to fatty acid methyl esters (FAMEs) is usually performed.

In general, the analytical procedure for the determination of oils or fats from food products comprises three steps: extraction of the fat, esterification and GC analysis. Whereas the last step is completed in 30 to 60 min, extraction takes at least several hours. It is frequently realized by the Soxhlet extraction method, based on iterative percolation of fresh solvent, generally *n*-hexane.[9] After the extraction, most of the solvent is removed in a vacuum rotary evaporator. Much work has been performed to improve the Soxhlet extraction to decrease the operation time and solvent use, and to eliminate the need for evaporation and concentration at the end of the extraction.[10]

Microwave-assisted extraction (MAE) is a relatively novel method of extracting soluble products into a fluid from a wide range of materials using microwave energy. MAE provides a technique whereby compounds can be extracted selectively and in a shorter time compared to those required for conventional extraction methods.[11] MAE supports sustainable development as it consumes less energy than convectional extraction processes while providing in many instance for a reduction in wastes.[12] Liquid-phase MAE is based on the ability of a matrix to absorb microwave energy. This varies with the chemical nature of the species

being exposed to the microwave irradiation. Under MAE conditions, solvents are chosen for their ability to dissolve the target compound and their relative transparency to microwaves. Chemical substances absorb microwave energy at different levels. The parameter generally used as a measure of this physical property is the dielectric constant. Liquid-phase extraction using microwave energy is based on the fact that is possible to immerse the matrix to be extracted in a solvent that is characterized by a small dielectric constant and that is relatively transparent to microwaves.[13] The application of microwave energy as a heat source causes selective heating of the matrix over the extractant. The high, localized temperature and increase in pressure cause a selective migration of target compounds from the material to the solvent at a faster rate and with a similar or better recovery compared with conventional extraction methods.[12]

Recently, much attention has been given to the application of microwave dielectric heating in analytical chemistry because of the reduced analysis time, simplified manipulation and higher purity of the final product. Several classes of compounds, such as fats and oils, essential oils, aromas, pesticides, phenols, dioxins and other organic compounds, have been efficiently extracted from a variety of matrices (mainly soils, sediments, animal tissues, food or plant materials).[14]

The propose of this research was the development of an analytical method for the fast extraction of fat from food with simultaneous derivatisation to FAMEs, based on the use of auxiliary energies, without extract alterations and independent identification–quantification of fatty acids using GC–MS, including the *trans* compounds. Simultaneous microwave-assisted extraction–esterification was used and the obtained results were compared with those of the Soxhlet reference method in order to demonstrate the advantages of the proposed analysis for *trans* fatty acids. On the other hand, GC–MS allows more accurate peak identification to be achieved, fulfils present and future necessities and provides information in relation to the quality of fat used for food elaboration.

EXPERIMENTAL

Instruments

Microwave-assisted extraction was performed in a modified LG 800 W household microwave oven (China) equipped with solvent-extraction equipment. The household microwave oven had to be modified in order to enable connection of an upright reflux condenser located outside the oven with the extraction flask located inside the oven. A hole of 30 mm diameter was drilled at the oven top and 80 mm of the bottom end of an Allihn condenser was passed through the hole and connected to the extraction vessel located in the microwave irradiation zone. Tap water was used as the cooling fluid. A Petri dish (external dimensions: 190 mm diameter, 45 mm high) was placed upside down instead of a rotation plate in order to eliminate rotation of the extraction vessel coupled with condenser during the microwave-assisted extraction process. Polystyrene positioned on the Petri dish was used as a holder for the extraction flask.

A rotary-evaporator (Rotavapor-R, Büchi) was used to evaporate the solvent after Soxhlet extraction.

A Hewlett-Packard HP 5890 gas chromatograph coupled to a HP 5971A quadrupole mass spectrometer equipped with an SP-2560 fused silica capillary column (100 m×0.25 mm, 0.20 μm) coated with highly polar biscyanopropyl polysiloxane liquid phase, provided by Supelco (Bellefonte, PA, USA), was used for the specific analysis of the *trans* fatty acids in the extracts.

Reagents and samples

A multi-standard from Supelco (Cat. No. 47885-U, Bellefonte, PA, USA) containing the methyl esters of 37 fatty acids was used to confirm the retention times and mass spectra for peak identification, as well as to confirm that the peak areas reflected the actual composition of these mixtures. The reagents used were methanol, potassium hydroxide, hydrochloric acid and *n*-hexane. All reagents were of analytical grade purity.

Eleven food items, all commercial, were used in this study. The samples included different bakery and confectionary products, such as caramel, crackers, chocolates, croissant with filling, cookies and biscuits, as these products mainly contain *trans* fats.

Procedures

All the steps involved in the overall analysis, namely, extraction, derivatisation and separation/determination, are described in this section. In all instances, three replicates were made for each sample.

Soxhlet extraction reference method.[15] A homogenized sample (5 g) was weighed into a cellulose extraction cartridge and the Soxhlet apparatus containing the cartridge was fitted to a distillation flask containing 150 ml of *n*-hexane and a few anti-bumping granules. The samples were extracted for 220 min (30–40 cycles/h). After extraction, the solvent was removed using a vacuum rotary evaporator. The total time required was approximately 4 h.

Microwave-assisted extraction. A sample (1.5 g) and 5 ml of *n*-hexane were placed into the extraction flask placed in the microwave oven equipped with an Allihn condenser and irradiated for 5 min at a fixed power of 800 W. After phase separation, a 2.4 cm^3 aliquot of the extract was taken for further preparation of the fatty acid methyl esters.

Simultaneous microwave-assisted extraction–esterification. A sample (1.5 g), 5 ml of *n*-hexane and 1.2 ml of 2.0 mol/dm^3 methanolic potassium hydroxide solution were placed into the extraction flask placed in the microwave oven furnished with an Allihn condenser. After leaching (5 min of microwave irradiation at 800 W), 2.4 ml of 1.0 mol/dm^3 HCl was added and gently stirred. After phase separation, the upper phase containing the fatty acid methyl esters was decanted off and finally a 1.0 μl aliquot was used for GC–MS analysis. The total time required was approximately 15 min.

Preparation of fatty acid methyl esters. After Soxhlet extraction, approximately 150 mg of fat extract was put into a test tube and dissolved in 2.4 cm^3 of *n*-hexane, while after microwave-assisted extraction, an aliquot of 2.4 cm^3 of *n*-hexane phase was taken. Further, the extracts were treated in the same way. An aliquot (0.60 cm^3) of 2.0 mol/dm^3 methanolic KOH solution was added. The tube was capped and vigorously shaken for 20 s and allowed to boil for one minute in water bath at 70 °C. After 20 s of shaking, 1.2 cm^3 of 1.0 mol/dm^3 HCl was added and gently stirred. After phase separation, 3 cm^3 of *n*-hexane was added and the upper phase containing the fatty acid methyl esters was decanted and dissolved in *n*-hexane to 5.0 cm^3. Finally, 1.0 μl of the thus-obtained solution was injected into the GC–MS.

Gas chromatography–mass spectrometry analyses

Helium at a constant flow rate of 0.58 cm^3/min was used as carrier gas for the GC–MS analysis of the FAME extracts. The following temperature program was used: injector temperature 230 °C, initial column temperature 100 °C (held 5 min), temperature ramp 10 °C/min to 240 °C and held at this temperature for 10 min. The total run time was 30 min. The injection was performed manually, volume 1.0 µl, with a split ratio 1:80.

The mass spectrometer was operated in the electron ionization mode with a quadrupole temperature of 180 °C. Data acquisition was realised in the scan mode (range 40–400 m/z). The instrument was tuned daily by operating the software programs (Autotune) using perfluorotributylamine (PFTBA) as the calibration substance. Mass spectrometer parameters were adjusted so that the masses 69, 219, and 502 and their respective isotopes met the target mass – intensity criteria.

The fatty acids were identified by comparing their retention times and mass spectral data to the mass spectral data obtained by analysis of standard fatty acid methyl esters solution under the same conditions. A commercial database of mass spectra "Wiley" was also used.

The response factor, mean of five injection of the standard solution for each fatty acid methyl ester present in the calibration standard solution, was calculated related to palmitic acid according to Eq. (1):

$$R_i = \frac{m_{0,i} A_{16:0}}{m_{16:0} A_{0,i}} \quad (1)$$

where $m_{0,i}$ is the mass % of $FAME_i$ in the calibration standard solution; $A_{16:0}$ the peak area of 16:0 in the calibration standard solution chromatogram; $m_{16:0}$ the mass % of 16:0 in the calibration standard solution; $A_{0,i}$ the peak area of $FAME_i$ in the calibration standard solution.

The content of each fatty acid expressed by mass percentage was calculated according to relation (2):

$$100 \frac{R_i A_i}{\sum R_i A_i} \quad (2)$$

where R_i is the response factor for each fatty acid and A_i the peak area of the fatty acid methyl ester in the sample solution.

RESULTS AND DISCUSSION

Different microwave-assisted extraction methods have already been proposed for the extraction of the total fat content from a variety matrices, such as food,[9,14] cocoa powder and cocoa nibs,[11] seeds[16] and poultry feeds.[17] MAE has also been suggested for the determination of the fatty acids profile.[7,8,18,19] However, the applicability of the simultaneous microwave-assisted extraction–esterification method for the determination of the fatty acids profile with emphasis on *trans* fatty acids has not been demonstrated.

Optimization of simultaneous microwave-assisted extraction–esterification

When two-step methods are studied, it is difficult to separate the extraction and esterification effects. For this reason, microwave-assisted extraction followed by esterification was compared with classical Soxhlet extraction followed by es-

terification in terms of extraction efficiency. The main factors affecting microwave-assisted extraction in open vessel systems are: solvent nature, extraction time and microwave power. The choice of solvent for MAE is dictated by the solubility of the target analyte, by the interaction between the solvent and matrix, and finally by the microwave absorbing properties of the solvent.[20] Another important aspect is compatibility of the extracting solvent with further chromatographic analytical steps.[21]

The effect of microwave energy is strongly dependent on the nature of both the solvent and the solid matrix. Solvents generally used cover a wide range of polarities, from heptane to water. The microwave-assisted extraction process may occur by a number of mechanisms: the sample could be immersed in a single solvent or mixture of solvents that strongly absorb the microwave energy (mechanism I); the sample could be extracted in a combined solvent containing solvents with both high and low dielectric losses mixed in various proportions (mechanism II); samples that have a high dielectric loss (*e.g.*, with a high water content) can be extracted with a microwave transparent solvent (mechanism III).[22]

It was demonstrated that lipid extraction is highly dependent on the solvent used and, consequently, the choice of solvent is one of the most critical decision in the determination of fat.[16] Thus, the solvent used in all the extraction methods was that proposed in the ISO method, *i.e.*, *n*-hexane.[23] Considering the fact that the main goal of this study was the development of a fast sample preparation method for the determination of the fatty acid composition of foodstuffs by GC–MS, the use of more polar solvents in the microwave-assisted extraction was rejected to avoid differences between the compositions of the extracts and solvent exchange before derivatisation or the chromatographic step.

Most times, the chosen solvent for microwave-assisted extraction possesses a high dielectric constant and strongly absorbs microwave energy, however, the extracting selectivity and the ability of the medium to interact with microwaves can be modulated by the use of a mixture of solvents. In some cases, as in this study, the matrix itself interacts with the microwaves while the surrounding solvent possesses a low dielectric constant and thus remains cold. This is possible since the microwaves interact selectively with the polar water molecules naturally present in foodstuffs. Localized heating leads to the expansion and rupture of the cells, causing a rapid and selective expulsion of the fat into the relatively cool surrounding solvent that solubilises it rapidly. With samples having a high dielectric loss, efficient extractions can be performed using pure, microwave-transparent solvents (mechanism III).[22]

In order to avoid extract evaporation before the derivatisation step, factors such as the amount of solvent in contact with the sample when the microwave irradiation is applied and the amount of sample were fixed to constant values. The

amounts of sample and solvent were calculated in relation to the fat content; hence, the extract contained approximately 150 mg per 2.4 ml *n*-hexane.

Microwave power and irradiation time are two factors that influence each other greatly. Preliminary experiments showed that efficient extraction could not be achieved if the MAE process was stopped before the commencement of rapid boiling of the extraction mixture. The microwave-assisted extraction process was performed with the irradiation power set at 160 (minimum level), 480, 640 and 800 W (maximum level), whereby rapid boiling of the reaction mixture began at 12, 6, 4 and 1.5 min, respectively. In order to achieve an efficient extraction in the shortest possible time, the maximal microwave power (800 W) was selected as the optimal and used for subsequent experiments. The extraction time was changed from 2 to 12 min, in order to determine the optimal time. The results (Fig. 1) indicate that amount of fat extracted initially increased with increasing extraction time, but that a plateau was reached after 5 min, the four longer extractions gave similar analytical signal.

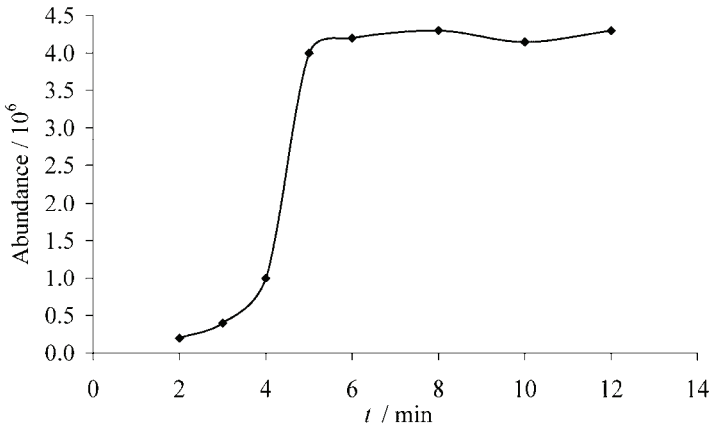

Fig. 1. The dependence of average analytical signal on the extraction time.

In view of these results, 5 min was selected as the optimal extraction time and used for further experiments. The accepted optimal working conditions were those described under “microwave-assisted extraction” and “simultaneous microwave-assisted extraction–esterification”.

Comparison of the composition of the extract obtained by the different method

The optimal working conditions obtained for the proposed method were applied for all samples under study and the results compared with those provided by the reference Soxhlet method in terms of extraction efficiency. The average extraction efficiencies obtained by the three methods provided by each analyte are given in Tables I and II (Supplementary material).

A two-tailed *t*-test was used to compare the means of related (paired) samples in order to evaluate if microwave-assisted extraction followed by esterification and simultaneous microwave-assisted extraction–esterification yielded similar results as Soxhlet method at the 95 % confidence level. The null hypothesis was that both methods yielded the same results or, in other words, that the observed differences between the Soxhlet and the MAE or SMAEE methods were not significant. The calculated *t*-values were compared with the theoretical value at $\alpha = 0.05$ and suitable degrees of freedom. As the calculated values were smaller than the theoretical value, the null hypothesis was accepted. This means that at the chosen significance level, the differences between the values obtained for the different fatty acids were within experimental error. Particularly, the standard deviation for all compounds ranged between 0.00 and 1.80, see Tables I and II. As can be seen, similar extraction efficiencies were provided by both the proposed simultaneous microwave-assisted extraction-esterification method and the Soxhlet reference method. Furthermore, the similar extraction efficiency of *trans* compound indicates that alterations of the double bonds did not occur. The advantages of SMAEE *vs*. Soxhlet extraction (Table III), such as: a drastic reduction of both the procedure time and sample handling, 15 min *vs*. 4 h, and the smaller amount of organic solvent required, make the SMAEE method an alternative with reliable possibilities for replacing the Soxhlet method in routine analysis in view of the imminent policy of mandatory characterisation of the fat content in foodstuffs.

TABLE III. Comparison of the optimal conditions of the simultaneous microwave-assisted extraction–esterification (SMAEE) method with the Soxhlet reference method

Condition	Soxhlet extraction	SMAEE
Solvent volume, ml	150	5
Total time, min	240	15
Special	Extraction 220 min (30–40 cycles/h); solvent evaporation: 10 min; FAMEs preparation: 10 min	–

CONCLUSIONS

Fatty acid analysis, with special emphasis on TFA, was performed on eleven food samples using a very fast and effective sample preparation method – simultaneous microwave-assisted extraction–esterification. The proposed method was compared with the reference method – Soxhlet extraction followed by esterification. Gas chromatography–mass spectrometry was used for individual separation and detection. Similar extraction efficiencies were provided by both the proposed SMAEE method and the Soxhlet reference method. The fatty acid composition obtained by the use of the simultaneous microwave-assisted extraction–esterification method and the Soxhlet reference method can be regarded as statistically equivalent. The SMAEE method provides a substantial reduction in the

sample preparation time (from approximately 15 min to 4 h) with a minimal solvent requirement relative to Soxhlet extraction followed by derivatisation.

The results of this study suggest that the presented SMAEE method could be appropriate for routine quality control analysis of fats in food products.

SUPPLEMENTARY MATERIAL

The average extraction efficiencies obtained by the three methods (Tables I and II) are available electronically from http://www.shd.org.rs/JSCS/ or from the corresponding author on request.

Acknowledgements. The presented research was funded by the Ministry of Science and Technological Development of the Republic of Serbia through Project No. 20023.

ИЗВОД

ОДРЕЂИВАЊЕ *trans* МАСНИХ КИСЕЛИНА У ПРЕХРАМБЕНИМ ПРОИЗВОДИМА ГАСНОМ ХРОМАТОГРАФИЈОМ–МАСЕНОМ СПЕКТРОМЕТРИЈОМ НАКОН ИСТОВРЕМЕНЕ МИКРОТАЛАСНЕ ЕКСТРАКЦИЈЕ И ЕСТЕРИФИКАЦИЈЕ

СНЕЖАНА КРАВИЋ[1], ЗВОНИМИР СУТУРОВИЋ[1], ЈАРОСЛАВА ШВАРЦ-ГАЈИЋ[1], ЗОРИЦА СТОЈАНОВИЋ[1] и МИРА ПУЦАРЕВИЋ[2]

[1]Универзитет у Новом Саду, Технолошки факултет, Катедра за примењене и инжењерске хемије, Булевар цара Лазара 1, 21000 Нови Сад и [2]EDUCONS Универзитет, Факултет за заштиту животне средине,Војводе Путника бб, 21202 Сремска Каменица

У оквиру овог рада развијена је метода за припрему узорака у циљу одређивања састава масних киселина у прехрамбеним производима гасном хроматографијом–масеном спектрометријом заснована на истовременој микроталасној екстракцији и естерификацији (SMAEE). Валидација методе је изведена поређењем са резултатима добијеним гасном хроматографијом–масеном спектрометријом након екстрације по Soxhlet-у и дериватизације масних киселина у метилестре масних киселина. Резултати добијени применом предложене и референтне методе били су статистички исти, како у погледу састава масних киселина, тако и ефикасности екстракције. Резултати су показали да су предности SMAEE у односу на конвеционалну методу следећи: кратко време припреме узорка, и самим тим мања потрошња енергије, као и употреба малих количина скупих органских растварача. Добро слагање резултата добијених применом референтне и методе засноване на истовременој микроталасној екстракцији и естерификацији показује да би се SMAEE могла применити као рутинска метода за припрему узорака прехрамбених производа у циљу одређивања *trans* масних киселина.

(Примљено 17. јула 2009, ревидирано 15. фебруара 2010)

REFERENCES

1. R. R. Chao, S. J. Mulvaney, M. E. Bailey, L. N. Fernando, *J. Food Sci.* **56** (1991) 183
2. P. Khosla, K. C. Hayes, *J. Am. Coll. Nutr.* **15** (1996) 325
3. A. Acherio, W. C. Willet, *Am. J. Clin. Nutr.* **66** (1997) 1006
4. S. Stender, J. Dyerberg, *Ann. Nutr. Metab.* **48** (2004) 61
5. M. Pfeuffer, J. Schrezenmeir, *Inter. Dairy J.* **16** (2006) 1383
6. L. Ruth, *Anal. Chem.* **74** (2002) 312
7. F. Priego-Capote, J. Ruiz-Jiménez, M. D. Luque de Castro, *Food Chem.* **100** (2007) 859

8. J. Ruiz-Jiménez, F. Priego-Capote, M. D. Luque de Castro, *Anal. Bioanal. Chem.* **385** (2006) 1532
9. M. Virot, V. Tomao, G. Colnagui, F. Visinoni, F. Chemat, *J. Chrom. A* **1174** (2007) 138
10. M. D. Luque de Castro, L. E. García-Ayuso, *Anal. Chim. Acta* **369** (1998) 1
11. S. Elkhori, J. R. J. Paré, J. M. R. Bélanger, E. Pérez, *J. Food Eng.* **79** (2007) 1110
12. J. R. J. Paré, J. M. R. Bélanger, *Instrumental methods in food analysis*, Elsevier Science, Amsterdam, 1997, p. 395
13. J. R. J. Paré, J. M. R. Bélanger, S. S. Stafford, *Trends Anal. Chem.* **13** (1994) 176
14. M. Virot, V. Tomao, C. Ginies, F. Visinoni, F. Chemat, *J Chrom. A* **1196–1197** (2008) 57
15. *Official Methods of Analysis of the Association of Official Analytical Chemist (AOAC)*, 17th ed., AOAC International, Gaithersburg, MD, 2000, Official Method 920.39
16. L. E. García-Ayuso, J. Velasco, M. C. Dobarganes, M. D. Luque de Castro, *Chromatographia* **52** (2000) 103
17. S. A. Mahesar, S. T. H. Sherazi, K. Abro, A. Kandhro, M. I. Bhanger, F. R. van de Voort, J. Sedman, *Talanta* **75** (2008) 1240
18. J. A. Pérez-Serradilla, M. C. Ortiz, L. Sarabia, M. D. Luque de Castro, *Anal. Bioanal. Chem.* **388** (2007) 451
19. A. Batista, W. Vetter, B. Lucas, *Eur. Food Res. Technol.* **212** (2001) 377
20. M. Letellier, H. Budzinski, L. Charrier, S. Capes, A. M. Dorthe, *J. Anal. Chem.* **364** (1999) 228
21. M. Vivekananda, M. Yogesh, S. Hemalatha, *Pharmacogn. Rev.* **1** (2007) 7
22. C. S. Eskilsson, E. Bjorklund, *J. Chrom. A* **902** (2000) 227
23. *International Organization for Standardization*, Case postale 56, CH-1211 Genève 20, Switzerland, 1998, ISO 659-1988 (E).

Journal of the Serbian Chemical Society
JSCS@tmf.bg.ac.rs • www.shd.org.rs/JSCS

J. Serb. Chem. Soc. 75 (6) S1–S6 (2010)
JSCS–4008

UDC 665.12+641.3:543.544.3+543.51:66.061
Supplementary material

SUPPLEMENTARY MATERIAL TO

Determination of *trans* fatty acids in foodstuffs by gas chromatography–mass spectrometry after simultaneous microwave-assisted extraction–esterification

SNEŽANA KRAVIĆ[1*#], ZVONIMIR SUTUROVIĆ[1#], JAROSLAVA ŠVARC-GAJIĆ[1], ZORICA STOJANOVIĆ[1#] and MIRA PUCAREVIĆ[2]

[1]Faculty of Technology, Department of Applied and Engineering Chemistry, University of Novi Sad, Bulevar cara Lazara 1, 21000 Novi Sad and [2]Faculty of Environmental Protection, Educons University, Vojvode Putnika bb, 21202 Sremska Kamenica, Serbia

J. Serb. Chem. Soc. 75 (6) (2010) 803–812

* Corresponding author. E-mail: sne@uns.ac.rs
# Serbian Chemical Society member.

TABLE I. Saturated fatty acids composition, as % of total fatty acids, of foodstuffs obtained by Soxhlet, MAE and SMAEE methods (values are the means of three determinations±standard deviation; the shorthand names of the fatty acid are given in the form: number of carbon atoms in the molecule followed by the number of double bonds; the two number are separated by a colon)

Sample	Method	Fatty acid					
		6:0	8:0	10:0	12:0	14:0	15:0
Caramel	SE[a]	0.87±0.07	3.62±0.13	3.96±0.05	27.19±0.00	12.60±0.19	0.61±0.03
	MAE[b]	0.96±0.05	3.77±0.19	3.95±0.09	28.46±0.24	12.61±0.15	0.46±0.03
	SMAEE[c]	1.15±0.04	4.03±0.20	3.87±0.07	28.91±0.11	12.76±0.18	0.53±0.05
Cracker 1	SE	–	1.65±0.11	1.17±0.01	8.11±0.36	2.85±0.06	–
	MAE	–	1.15±0.10	0.80±0.03	6.62±0.26	2.61±0.09	–
	SMAEE	–	0.89±0.02	0.66±0.03	6.82±0.14	2.35±0.03	–
Biscuit	SE	–	2.65±0.12	3.42±0.03	9.14±0.20	10.05±0.10	0.93±0.07
	MAE	–	2.68±0.09	3.33±0.07	8.72±0.21	9.66±0.50	0.94±0.02
	SMAEE	–	2.60±0.05	3.50±0.04	8.76±0.19	9.81±0.23	1.04±0.02
Cookie 1	SE	–	3.00±0.03	2.13±0.09	13.76±0.23	5.65±0.01	–
	MAE	–	3.38±0.11	2.21±0.03	13.01±0.45	5.58±0.03	–
	SMAEE	–	3.73±0.12	2.31±0.02	13.56±0.54	5.58±0.03	–
Cookie 2	SE	–	2.16±0.14	1.49±0.06	10.17±0.15	4.33±0.28	–
	MAE	–	2.65±0.18	1.75±0.10	10.45±0.12	4.31±0.06	–
	SMAEE	–	2.31±0.11	1.60±0.03	10.06±0.11	4.22±0.02	–
Cracker 2	SE	–	3.21±0.00	2.41±0.11	14.09±0.15	5.27±0.10	–
	MAE	–	3.84±0.05	2.60±0.12	14.25±0.21	5.16±0.08	–
	SMAEE	–	3.40±0.07	2.60±0.17	14.05±0.29	4.64±0.06	–
Milk chocolate	SE	–	1.97±0.01	1.52±0.04	8.98±0.02	4.39±0.11	–
	MAE	0.22±0.01	1.83±0.05	1.43±0.06	7.52±0.06	3.97±0.13	0.12±0.01
	SMAEE	0.28±0.02	2.21±0.01	1.68±0.03	8.84±0.14	4.46±0.14	0.16±0.00
Croissant with cocoa	SE	–	–	–	0.56±0.02	1.37±0.05	–
	MAE	–	–	–	0.52±0.01	1.40±0.02	–
	SMAEE	–	–	–	0.53±0.00	1.29±0.07	–

TABLE I. Continued

Sample	Method	Fatty acid					
		6:0	8:0	10:0	12:0	14:0	15:0
Chocolate with coconut	SE	–	9.32±0.41	5.20±0.46	29.25±1.17	9.05±0.33	–
	MAE	–	9.64±0.10	5.26±0.48	30.09±1.80	9.18±0.21	–
	SMAEE	–	9.17±0.50	5.34±0.04	30.77±1.76	9.16±0.28	–
Chocolate with rice	SE	–	–	–	0.33±0.03	0.91±0.06	–
	MAE	–	–	0.41±0.04	0.46±0.02	1.11±0.02	–
	SMAEE	–	–	0.71±0.04	0.67±0.01	1.77±0.02	–
Cookie 3	SE	–	1.71±0.04	1.60±0.01	17.67±0.07	5.96±0.11	–
	MAE	–	1.88±0.01	1.53±0.02	17.01±0.08	5.66±0.10	–
	SMAEE	–	1.92±0.01	1.70±0.02	17.21±0.07	5.92±0.08	–
		16:0	17:0	18:0	20:0	22:0	
Caramel	SE	17.56±0.14	0.40±0.04	15.86±0.30	0.23±0.01	–	
	MAE	17.48±0.00	0.34±0.04	15.94±0.20	0.26±0.02	–	
	SMAEE	17.56±0.19	0.34±0.03	15.19±0.29	0.19±0.00	–	
Cracker 1	SE	19.50±0.32	–	7.38±0.10	0.44±0.02	0.36±0.04	
	MAE	18.26±0.23	–	7.52±0.12	0.36±0.02	0.36±0.01	
	SMAEE	18.91±0.25	–	7.73±0.14	0.40±0.03	0.39±0.01	
Biscuit	SE	32.48±0.36	0.58±0.02	7.38±0.04	–	–	
	MAE	32.13±0.16	0.59±0.03	7.44±0.08	0.24±0.02	–	
	SMAEE	32.03±0.25	0.54±0.03	8.05±0.04	0.20±0.02	–	
Cookie 1	SE	31.77±0.02	–	5.19±0.03	0.31±0.03	–	
	MAE	31.59±0.11	–	5.19±0.05	0.32±0.02	–	
	SMAEE	31.31±0.16	–	4.92±0.07	0.32±0.01	–	
Cookie 2	SE	25.61±0.14	–	4.09±0.01	0.23±0.02	–	
	MAE	26.22±0.09	–	4.12±0.03	0.26±0.01	–	
	SMAEE	26.56±0.10	–	4.22±0.03	0.27±0.02	–	

TABLE I. Continued

Sample	Method	Fatty acid				
		16:0	17:0	18:0	20:0	22:0
Cracker 2	SE	31.68±0.03	–	3.73±0.01	0.30±0.01	–
	MAE	31.22±0.25	–	3.66±0.16	0.27±0.03	–
	SMAEE	31.95±0.39	–	3.71±0.15	0.22±0.03	–
Milk chocolate	SE	30.48±0.11	–	17.82±0.12	0.61±0.03	–
	MAE	29.92±0.39	0.25±0.01	19.52±0.14	0.66±0.06	0.15±0.01
	SMAEE	29.86±0.04	0.23±0.00	18.34±0.24	0.58±0.05	0.08±0.00
Croissant with cocoa	SE	45.13±0.84	0.17±0.02	5.35±0.20	0.40±0.03	0.11±0.01
	MAE	43.20±0.11	0.13±0.00	6.47±0.00	0.45±0.03	0.11±0.01
	SMAEE	43.14±0.24	0.14±0.00	6.53±0.10	0.39±0.03	0.13±0.00
Chocolate with coconut	SE	14.20±0.87	–	16.62±0.82	0.55±0.05	–
	MAE	14.42±1.30	–	14.39±0.98	0.56±0.01	–
	SMAEE	14.29±0.35	–	14.07±0.82	0.52±0.00	–
Chocolate with rice	SE	15.76±1.19	–	10.61±0.21	0.48±0.04	0.28±0.01
	MAE	17.58±0.15	–	9.72±0.15	0.40±0.00	0.21±0.00
	SMAEE	18.68±0.35	–	9.85±0.06	0.41±0.02	0.18±0.02
Cookie 3	SE	30.68±0.91	–	4.28±0.21	0.32±0.02	–
	MAE	30.68±0.95	–	4.11±0.17	0.30±0.03	–
	SMAEE	30.55±0.87	–	4.32±0.14	0.27±0.03	–

[a]Soxhlet extraction; [b]microwave-assisted extraction; [c]microwave-assisted extraction–esterification

TABLE II. Unaturated fatty acids composition, as % of total fatty acids, of foodstuffs obtained by Soxhlet, MAE and SMAEE methods (values are the means of three determinations±standard deviation; the shorthand names of the fatty acid are given in the form: number of carbon atoms in the molecule followed by the number of double bonds and indication of structural configuration; the two number are separated by a colon)

Sample	Method	Fatty acid							
		14:1	16:1	18:1 *trans*	18:1 *cis*	18:2 *trans*	18:2 *cis*	20:1	18:3
Caramel	SE[a]	0.40±0.00	0.79±0.00	1.88±0.02	9.92±0.26	–	3.82±0.02	–	0.29±0.01
	MAE[b]	0.40±0.02	0.69±0.04	1.77±0.02	9.23±0.03	–	3.46±0.02	–	0.22±0.01
	SMAEE[c]	0.35±0.02	0.74±0.04	1.84±0.03	8.59±0.12	–	3.71±0.09	–	0.24±0.00
Cracker 1	SE	–	–	18.36±0.08	29.59±0.71	1.70±0.12	8.89±0.13	–	–
	MAE	–	–	18.26±0.18	31.22±0.01	1.80±0.04	10.74±0.15	0.15±0.01	0.15±0.01
	SMAEE	–	–	18.22±0.15	31.39±0.27	1.85±0.07	10.03±0.05	0.15±0.01	0.21±0.02
Biscuit	SE	0.63±0.05	1.33±0.10	1.19±0.08	22.37±0.11	–	7.42±0.01	–	0.43±0.04
	MAE	0.67±0.00	1.42±0.08	1.24±0.04	22.74±0.78	–	7.75±0.18	–	0.45±0.02
	SMAEE	0.67±0.01	1.25±0.06	1.09±0.07	21.64±0.39	–	8.39±0.17	–	0.43±0.03
Cookie 1	SE	–	–	0.46±0.03	29.05±0.32	–	8.68±0.06	–	–
	MAE	–	–	0.33±0.02	29.57±0.51	–	8.66±0.16	–	0.16±0.01
	SMAEE	–	–	0.34±0.01	28.74±0.41	–	8.98±0.12	–	0.21±0.02
Cookie 2	SE	–	–	–	40.53±0.16	–	11.39±0.05	–	–
	MAE	–	0.13±0.01	–	38.61±0.77	–	11.10±0.03	0.17±0.01	0.23±0.02
	SMAEE	–	0.16±0.01	–	38.46±0.16	–	11.66±0.04	0.22±0.02	0.26±0.02
Cracker 2	SE	–	–	–	25.64±0.13	–	13.67±0.19	–	–
	MAE	–	–	–	25.10±0.25	–	13.90±0.57	–	–
	SMAEE	–	–	–	25.90±0.88	–	13.53±0.43	–	–
Milk chocolate	SE	–	0.22±0.00	–	27.91±0.05	–	6.10±0.01	–	–
	MAE	–	0.29±0.01	–	28.34±0.06	–	5.63±0.11	–	0.15±0.01
	SMAEE	–	0.28±0.00	–	26.82±0.06	–	5.98±0.05	–	0.20±0.01
Croissant with cocoa	SE	–	0.17±0.05	2.15±0.10	31.97±0.54	–	12.28±0.24	0.15±0.02	0.19±0.02
	MAE	–	0.12±0.00	2.13±0.02	31.81±0.02	–	13.34±0.06	0.13±0.02	0.19±0.02
	SMAEE	–	0.11±0.00	2.00±0.03	31.05±0.03	–	14.33±0.12	0.14±0.00	0.22±0.02

TABLE II. Continued

Sample	Method	Fatty acid							
		14:1	16:1	18:1 *trans*	18:1 *cis*	18:2 *trans*	18:2 *cis*	20:1	18:3
Chocolate with coconut	SE[a]	–	–	1.05±0.08	13.70±1.36	–	1.06±0.19	–	–
	MAE[b]	–	–	1.16±0.11	14.30±0.94	–	1.00±0.13	–	–
	SMAEE[c]	–	–	1.10±0.11	14.44±1.08	–	1.14±0.13	–	–
Chocolate with rice	SE	–	–	41.65±0.89	29.31±1.48	–	0.67±0.02	–	–
	MAE	–	–	36.31±0.65	32.28±0.08	–	1.52±0.09	–	–
	SMAEE	–	–	34.94±0.66	31.03±1.04	–	1.76±0.07	–	–
Cookie 3	SE	–	–		28.04±1.03	–	9.74±0.07	–	–
	MAE	–	–		28.72±0.46	–	10.11±0.08	–	–
	SMAEE	–	–		28.36±0.37	–	9.75±0.07	–	–

[a]Soxhlet extraction; [b]microwave-assisted extraction; [c]microwave-assisted extraction–esterification

Journal of the Serbian Chemical Society
JSCS@tmf.bg.ac.rs • www.shd.org.rs/JSCS

J. Serb. Chem. Soc. 75 (6) 813–822 (2010)
JSCS–4009

UDC 546.11'267+546.266'131:
543.632.6+543.26
Original scientific paper

The use of tristimulus colorimetry for the determination of hydrogen cyanide in air by a modified König method

VLADIMÍR PITSCHMANN[1]*, IVANA TUŠAROVÁ[1], EMIL HALÁMEK[2] and ZBYNĚK KOBLIHA[2]

[1]*Oritest spol s.r.o., Staropramenná 17, 150 00 Praha 5 and* [2]*NBC Defence Institute, University of Defence, Kounicova 65, 612 00 Brno, Czech Republic*

(Received 21 May 2009, revised 18 March 2010)

Abstract: A simple visual and tristimulus colorimetric method (three-dimensional system CIE-L*a*b*) for the determination of trace amounts of hydrogen cyanide in air has been developed. The method is based on the suction of hydrogen cyanide through a chlorinating cartridge where cyanogen chloride is formed, which is further driven to an indicator disc made of a modified cotton fabric. This indicator disc is placed into an adapter. Prior to analysis, the disc is saturated with a chromogenic reagent, a solution of 5,5-dimethyl-1,3-cyclohexanedione (dimedone) and 4-benzylpyridine in ethanol. In the presence of hydrogen cyanide (cyanogen chloride), a pink coloration emerges on the indicator disc, the intensity of which is evaluated either visually or by use of a tristimulus colorimeter. The detection limit is 0.1 mg m^{-3}. The method is mainly suitable for mobile field analyses. It was applied for the CHP-5 chemical agent detector introduced into the equipment of the Czech Army corps.

Keywords: atmosphere analysis; hydrogen cyanide; cyanogen chloride; 4-benzylpyridine; dimedone; tristimulus colorimetry.

INTRODUCTION

Hydrogen cyanide (HCN), with an accent to its structural simplicity, ranks among the very important and remarkable chemicals. It is abundant in nature as a part of plant cyanogenic hetero-glycosides. It is essential in organic cyano chemistry, as an effective pesticide in agriculture, in gold and precious metal mining, or in galvanotechnology. It is formed when various materials, mainly synthetic polymeric materials, burn. In the past, it was produced and used as a chemical weapon and misused as a technical instrument of genocide. Its possible role in chemical terrorism has also been a point of discussion for a long time. Given the relative availability and high toxicity of HCN, it is not surprising that extraor-

* Corresponding author. E-mail: pitschmann@oritest.cz
doi: 10.2298/JSC090521046P

dinary attention is dedicated to its analysis throughout the world. So much the more that from the view of how quickly its effects commence to appear, it presents an unequalled poison inhalation hazard.[1] The exposure limit for HCN has been determined and recommended by the National Institute for Occupational Safety and Health (NIOSH) as 5 mg m^{-3}.

The bibliography concerning the analysis of HCN and cyanides is extremely extensive. It comprises a large number of publications dedicated to methods of classic volumetric analysis, electrometric and electrochemical methods, separation methods with an emphasis on chromatographic or optical methods such as spectrophotometry and luminescent analysis. In addition to instrumentally demanding methods, simple methods and means of chemical analysis are also used, which are generally based on an appropriate colour reaction. These on-site analysis methods include, *e.g.*, detection papers, testing strips, tablets, powder, chalks, or detection tubes.[2,3] The predisposition of HCN dispositions to all kinds of colour reactions is well known and frequently used in practice for air analysis. Evidently, the most widespread is the highly sensitive and selective method of HCN conversion to halogencyans, which react with pyridine and its derivatives to form glutacon dialdehyde, which condenses with a series of amines and substances containing active hydrogen as a passive component to give polymethine dyes.[4] This König reaction was employed for HCN detection in air in numerous modifications, *e.g.*, for sensitive detection crayons[5] or tubes.[6] Other methods are based on the reaction of HCN with Cu^{2+} and aromatic amines,[7] sodium picrate,[8] *p*-nitrobenzaldehyde,[9] ninhydrin,[10] aromatic disulphides,[11] and on other reactions.

In this paper, a simple and sensitive method for the determination of HCN in the air using tristimulus colorimetry is reported. The method has recently also found application in industry for controlling surface quality and in analytical chemistry.[12,13] Previously, tristimulus colorimetry was applied in the development of simple methods for the determination of chlorine,[14] sulphur dioxide,[15] formaldehyde[16] and diphosgene.[17] The new method devised for the HCN determination consists in the conversion of HCN to cyanogen chloride (ClCN), which reacts with modified König reagent (4-benzylpyridine, dimedone) to give the corresponding polymethine dye (Fig. 1). The conversion to ClCN occurs in a chlorinating cartridge. The reaction with a chromogenic agent occurs on the indicator disc inserted into an adapter. After taking an air sample, a characteristic coloration emerges on the disc, the intensity of which is measured using a tristimulus colorimeter or assessed visually.

EXPERIMENTAL

Chemicals and equipment

Potassium cyanide p.a. (Lachema, Czech Republic) served as a standard. Dimedone, or 5,5-dimethyl-1,3-cyclohexanedione, 4-benzylpyridine (both Sigma-Aldrich) and absolute etha-

nol (Riedel de Haen) were used for the preparation of the chromogenic reagent. The basic variant of the chromogenic reagent contained 1.5 g of 5,5-dimethyl-1,3-cyclohexanedione and 10 ml of 4-benzylpyridine in 100 ml of ethanol solution.

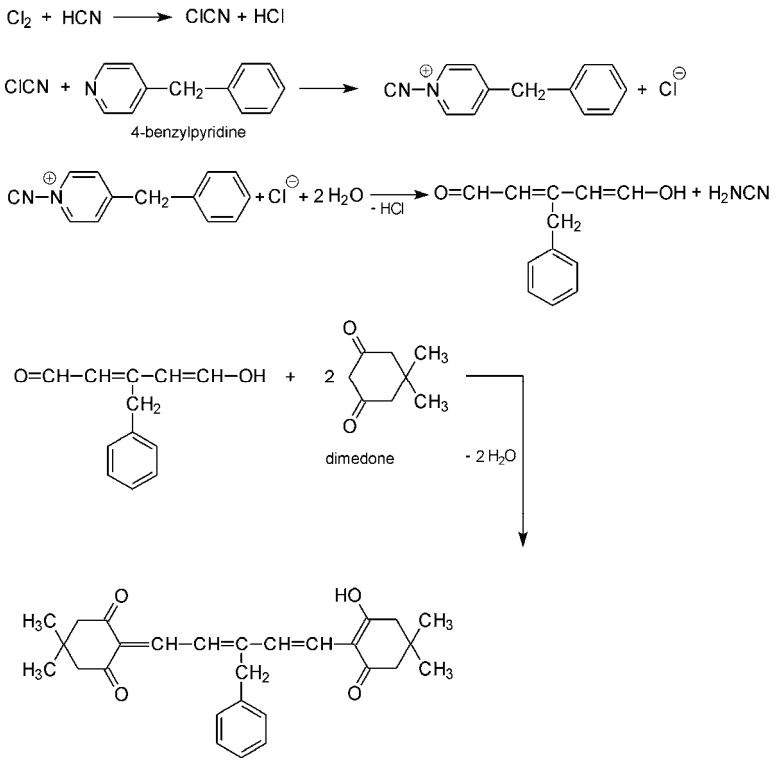

Fig. 1. Mechanism of the analytical reaction.[18]

HCN samples were prepared in a test chamber of 712 dm^3 volume, equipped with a thermostat (Lamon, Czech Republic). HCN samples were taken using an XDS-10C vacuum pump (BOC Edwards, Great Britain) with an attached flow meter and a CHP-5 chemical agent detector equipped with an electric pump (Oritest, Czech Republic). A portable tristimulus colorimeter LMG-173 (Lange, Germany) was used to measure the coloration intensity. A Helios-α UV/Vis spectrophotometer (Hermo Electron, Great Britain) was used to measure the colouring of solutions (HCN concentration control).

Preparation of the indicator disc

The fabric based on a web of cotton threads 0.31–0.33 mm thick was used for the indicator disc. This cotton fabric was impregnated with a solution containing 0.30 g of $Na_2B_4O_7 \cdot 10\ H_2O$, 0.45 g of H_3BO_3, 0.1 g of NaCl, 2.5 g of silica gel (fraction up to 5 μm), and 3.0 g of dextran per 100 ml of water. The impregnated fabric was dried freely in the air. Drying was completed in a desiccator above solid sodium hydroxide. After drying, it was formed in a shape of circle with 45 mm in diameter.

Preparation of the chlorinating cartridge

The chlorinating cartridge contained activated silica gel (purified with hydrochloric acid and dried at 150 °C), which was impregnated with an aqueous solution of 5 % sodium carbonate and 2 % monochloramine B. 100 ml of solution was used for 100 g of silica gel. After impregnation, the charge was dried at 80 °C to constant weight. The thus prepared charge was poured into glass tubing with an inner diameter of 5 mm and anchored against motion by polyethylene distributing pieces. The standard length of the layer was 10 mm. The chlorinating cartridge was hermetically sealed to permit long-term storage.

Sample preparation

Various concentrations of HCN were prepared in a test chamber by heating potassium cyanide solution acidified with H_3PO_4. The actual HCN concentration was determined by a spectrophotometric method. The HCN vapours were pumped from the test chamber by vacuum pump at a rate of 1.0 dm^3 min^{-1} and absorbed for a period of 10 min in an absorption apparatus containing 10 ml of 0.10 M NaOH. To 1ml of absorption solution with HCN, 1.0 ml of HCl, 1.0 ml of chromogenic reagent (1 % barbituric acid in a mixture pyridine–water 10:90), and 0.5 ml of 0.10 % calcium hypochlorite were added and made up to 5 ml with water. After 30 min, the absorbancy of the solution was measured at 581 nm.

The HCN determination procedure by the devised method

The indicator disc was inserted into an adapter with a supply hose connected to the chlorinating cartridge and a device for regulated intake of air. 50 μl of the chromogenic reagent was dosed to the middle of the indicator disc. Then contaminated air was sucked through the system (at a defined flow rate and suction time). After the sampling, the intensity of the colour stain of about 20 mm in diameter was assessed both visually and using a tristimulus colorimeter. The apparatus for the determination of the HCN concentration in the air using the CHP-5 chemical agent detector (electrical pump) is shown in Fig. 2.

Fig. 2. Apparatus photo: CHP-5 with indicator disc and adapter (a); CHP-5 with indicator disc, chlorinating cartridge and adapter (b).

Tristimulus colorimetry

Tristimulus colorimetry is a type of reflectance colorimetry (spectrophotometry) based on the CIE-L*a*b* colour system.[21] In this system, L^* represents the neutral axis of brightness, a^* is the chromatic green–red axis (+a^* red, –a^* green) and b^* is the chromatic blue–yellow axis (+b^* yellow, –b^* blue). In practice, the colour difference, ΔE, is also used, which is defined by the equation:

$$\Delta E = [(\Delta L^*)^2 + (\Delta a^*)^2 + (\Delta b^*)^2]^{1/2}$$

where ΔL^*, Δa^*, and Δb^* are the differences between the obtained values of L^*, a^* and b^* for the standard and for the controlled colours. All these parameters can be used as analytical signals, which enable the course of a colour chemical reaction to be quantified. The colour differences (ΔE) can also be assessed according to Table I.

TABLE I. Evaluation of colour differences (ΔE) – utilisation in the polygraphic industry

Difference ΔE	Visual assessment of colour difference
Below 0.2	Unperceivable
0.2–0.5	Very slight
0.5–1.5	Slight
1.5–3.0	Distinct
3.0–6.0	Very distinct
6.0–12.0	Strong
Above 12.0	Very strong

RESULTS AND DISCUSSION

Colour stability

The passage of HCN-contaminated air practically instantaneously induces a pink coloration on the cotton disc, which can be characterised by a reflection curve (Fig. 3). After the sampling, this coloration remains relatively stable for 10 min minimally. The development of all components of the colour system (parameters ΔE, ΔL^*, Δa^* and Δb^*) for this period are documented in Table II.

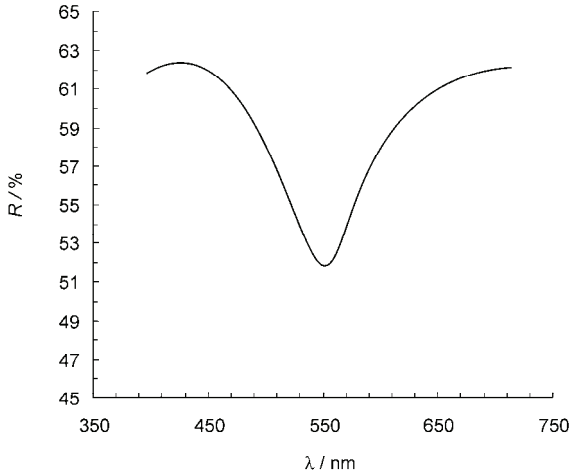

Fig. 3. Dependence of the reflection factor R on the wavelength λ.

Effect of the sampling period

The intensity of stains coloration on the indicator disc is dependent on the volume of the analysed sample (exposition time). The maximum values of the ΔE, ΔL^*, Δa^* and Δb^* parameters were obtained 2 min after air in-take; a longer

exposition resulted in a weaker intensity of coloration. This decrease was caused by oxidation effects of the atmospheric oxygen, drying of the indicator disc and gradual exhaustion of the chlorinating cartridge. The dependence of the individual parameters on the time of HCN sample in-take is given in Table III.

TABLE II. Colour stability – dependence of measured values on time (HCN sampling time: 1 min, flow rate: 1 dm^3 min^{-1}, HCN concentration: 1.6 mg m^{-3})

Time of measurement, min	ΔE	ΔL^*	Δa^*	Δb^*
Immediately	4.79	0.72	3.97	–2.58
1	4.15	1.42	3.22	–2.21
2	4.09	1.58	3.07	–2.25
4	3.84	1.74	2.74	–2.05
6	3.73	1.94	2.50	–2.00
8	3.59	2.08	2.27	–1.84
10	3.53	2.25	2.08	–1.75

TABLE III. Dependence on exposure time (of HCN sampling)

Time of sampling, min	ΔE	ΔL^*	Δa^*	Δb^*
1	9.02	–4.91	6.69	–3.53
2	15.16	–6.89	12.08	–6.02
3	14.28	–6.72	11.56	–5.01
4	12.87	–6.39	10.11	–4.76

Effect of the sampling flow rate

The dependence of monitored parameters on the flow rate of contaminated air is given in Table IV. It is evident that the values of the analytic signals decrease with increasing flow rate. This is probably caused by different periods of contact of the sorption layer of the indicator disc with HCN.

TABLE IV. Dependence on air flow rate (HCN concentration: 1.6 mg m^{-3}, suction time: 1 min)

Flow rate, dm^3 min^{-1}	ΔE	ΔL^*	Δa^*	Δb^*
0.5	6.37	–0.07	5.17	–3.72
1.0	4.79	0.72	3.97	–2.58
2.0	4.52	0.18	3.92	–2.25
3.0	4.32	0.25	3.74	–2.16

Effect of reagent composition and chlorinating cartridge capacity

The dependence of colour response on the composition (concentration) of chromogenic reagent is given in Table V. Any higher concentration of reagent has a demonstrable effect on the potency to capture HCN on the indicator disc and results in an increased sensitivity of the determination.

On the contrary, with higher capacity (length of layer) of the chlorinating cartridge, the sensitivity of the HCN determination decreases as shown in Table

VI. On the other hand, a higher capacity may result in a prolonged effective life of the chlorinating cartridge and improved determination selectivity.

TABLE V. Dependence on reagent composition (A – basic variant reagent, see experimental section, B – twice-diluted reagent, C – twice-concentrated reagent)

Reagent concentration	ΔE	ΔL^*	Δa^*	Δb^*
A	4.79	0.72	3.97	–2.58
B	4.44	0.54	3.58	–2.58
C	8.90	4.50	8.84	–5.58

TABLE VI. Dependence on length of chlorinating cartridge

Cartridge length, mm	ΔE	ΔL^*	Δa^*	Δb^*
10	12.52	–2.79	9.41	–7.77
20	12.46	–2.07	9.02	–8.35
40	8.16	–0.16	5.42	–6.10

Interference

The analytical method based on the conversion of HCN to ClCN, which gives a characteristically coloured polymethine dye with 4-benzylpyridine and dimedone, is highly selective. Only ClCN or BrCN gave results comparable to those of HCN (Table VII). They can be distinguished from HCN performing the detection without insertion of the chlorinating cartridge. Among other interfering substances, a similar pink coloration is produced by phosgene oxime and nitrogen oxides, but at higher concentrations. Chloropicrin gives a yellow-orange coloration. The chemical composition of the chlorinating cartridge ensures the high resistance of this method against the effects of acidic and alkaline pollutants (HCl, SO_2, H_2S, and NH_3). Volatile aldehydes in higher concentrations reduce the sensitivity of the HCN determination because they deplete the chlorinating cartridge.

TABLE VII. Effect of diverse compounds on the detection of 0.40 mg m^{-3} HCN

Compound	Colour	Tolerance limit (visually), mg m^{-3}
Cyanogen chloride	Pink	0.4
Cyanogen bromide	Pink	0.8
Phosgene oxime	Pink	5
Chloropicrin	Yellow	20
Nitrogen dioxide	Pink	50
Hydrogen sulphide	No colour	100
Ammonia	No colour	100
Hydrogen chloride	No colour	200
Sulphur dioxide	No colour	200
Acetonitrile	No colour	200
Benzaldehyde	No colour	200

Calibration graph

The calibration graph for the determination of HCN is shown in Fig. 4. The HCN detection limit attained by the tristimulus colorimeter was 0.10 mg m^{-3}. For the visual method, the HCN detection limit (threshold perception) was 0.40 mg m^{-3}. For visual assessment, it is advisable to compare the intensity of the colour stain with a reference standard representing a colour scale 0–10 mg m^{-3} with a 0.2 mg m^{-3} resolution.

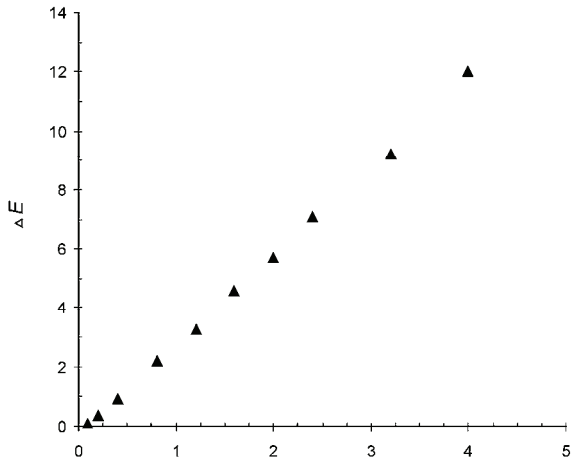

Fig. 4. Calibration graph. Dependence of ΔE on HCN concentration (flow of 1.0 dm^3 min^{-1}, 1 min exposure). Calibration line equation: $y = 2.9249x$, $R^2 = 0.9971$.

The reproducibility of test results for 0.10, 1.0 and 5.0 mg m^{-3} concentrations show that the relative standard deviation of the response (ΔE) ranged from 12 to 17 %.

Application

The elaborated visual and tristimulus colorimetric method for HCN determination can be applied to many different areas of field analysis – military, Industrial disaster recovery, and environment control. The method was devised for application of a CHP-5 chemical agent detector introduced into the equipment of the Chemical Corps of the Czech Army (Fig. 2). The standard airflow rate through this apparatus is 1.0 dm^3 min^{-1}, the suction time is 1 min. Results of HCN determination by the proposed method and of a comparable method are presented in Table VIII. When stored in hermetically sealed containers, the indicator disc can be used for several years. Solutions of the chromogenic reagents are stable; the standard variant showed stability for at least 12 months. The effective life of a closed chlorinating cartridge is several years. When opened, it can be used repeatedly until the charge is exhausted.

Using the devised tristimulus colorimetric method, trace concentrations of HCN in the atmosphere can be proved. As shown in Table IX, the detection limit

is comparable to, and even lower, than those of any known methods and technical means of HCN detection. The developed analysis procedure has universal application, which means that it enables the application of other liquid chromogenic reagents to determine a whole range of toxic substances in air.

TABLE VIII. Determination of HCN in air by the developed and a reported method (detector tube, tristimulus colorimetry)[6]

HCN added mg m^{-3}	HCN found by developed method mg m^{-3}	HCN found by reported method mg m^{-3}
1.2	0.9	1.0
2.4	2.1	2.2
3.6	3.2	3.3
4.8	4.3	4.5

TABLE IX. Comparison with technical means of HCN detection

Name	Principle	Detection limit, mg m^{-3}	Ref.
M256, USA	Indicator paper, colorimetry	9.0	19
HCN-2 Auer, Germany	Detection tube, colorimetry	2.2	20
CMS Dräger, Germany	Chip measurement system, optical sensor	2.2	21
Indicator tape, Japan	Reflectance spectrophotometry	0.2	7
Bruker A2, Germany	Electrochemical sensor	50.0	19
RAID-1, Germany	Ion mobility spectrometry (IMS)	2.2	19
Developed method	Indicator disc, tristimulus colorimetry	0.1	–

ИЗВОД

ПРИМЕНА ТРИСТИМУЛУС КОЛОРИМЕНТРИЈЕ ЗА ОДРЕЂИВАЊЕ ЦИЈАНОВОДОНИКА У ВАЗДУХУ МОДИФИКОВАНОМ KÖNIG МЕТОДОМ

VLADIMÍR PITSCHMANN[1], IVANA TUŠAROVÁ[1], EMIL HALÁMEK[2] и ZBYNĚK KOBLIHA[2]

[1]Oritest spol s.r.o., Staropramenná 17, 150 00 Praha 5 и [2]NBC Defence Institute, University of Defence, Kounicova 65, 612 00 Brno, Czech Republic

Развијена је једноставна тристимулус колориметријска метода (тродимензионални систем CIE-*L*a*b**) за одређивање цијановодоника у ваздуху. Метода се заснива на сукцији цијановодоника кроз хлоровани кертриџ у коме се формира дицијан, који се даље спроводи до индикаторског диска од модификоване памучне тканине. Индикаторски диск је смештен у адаптеру. Пре анализе диск се засити хромогеним реагенсом, раствором 5,5-диметил-1,3--циклохександионом (димедон) и 4-бензилпиридином у етанолу. У присуству дицијана индикаторски диск се обоји љубичасто, а интензитет обојења се може проценити било визуелно било употребом тристимулус колориметрије. Граница детекције износи 0,1 mg m^{-3}. Метода је погодна углавном за теренске анализе и нашла је примену за детекцију хемијског агенса CHP-5 у војсци Чешке Републике.

(Примљено 21. маја 2009, ревидирано 18. марта 2010)

REFERENCES

1. T. C. Marrs, R. L. Maynard, F. R. Sidell, Eds., *Chemical Warfare Agents, Toxicology and Treatment*, Wiley, Chichester, 2007
2. J. A. Zolotov, V. M. Ivanov, V. G. Amelin, *Chemical Test Methods of Analysis*, Elsevier, Amsterdam, 2002
3. J. P. A. Lodge, *Methods of Air Sampling and Analysis*, CRC Press, Boca Raton, FL, 1988
4. W. König, *J. Prakt. Chem.* **69** (1904) 105
5. B. Witten, A. Prostak, *Anal. Chem.* **29** (1957) 885
6. V. Pitschmann, Z. Kobliha, E. Halámek, I. Tušarová, *Chem. Anal.* (*Warsaw*) **53** (2008) 47
7. N. Nakano, A. Yamamoto, Y. Kobayashi, K. Nagashima, *Anal. Chim. Acta* **398** (1999) 305
8. G. Drochioiu, I. Mangalagiu, V. Tataru, *Analyst* **125** (2000) 939
9. J. A. D. Fávero, M. Tubino, *Anal. Sci.* **19** (2003) 1139
10. G. Drochioiu, *Talanta* **56** (2002) 1163
11. S. Spurlin, W. Hinze, D. W. Armstrong, *Anal. Lett*. **10** (1997) 991
12. F. Yokota, S. Abe, *Anal. Commun.* **34** (1997) 11
13. Y. Suzuki, M. Endo, J. Jin, K. Iwase, M. Iwatsuki, *Anal. Sci.* **22** (2006) 411
14. V. Pitschmann, Z. Kobliha, E. Halámek, I. Tušarová, *Science Military* **2** (2006) 69
15. V. Pitschmann, Z. Kobliha, E. Halámek, I. Tušarová, *Pak. J. Anal. Environ. Chem.* **7** (2006) 120
16. V. Pitschmann, Z. Kobliha, E. Halámek, I. Tušarová, *Chem. Listy* **101** (2007) 790
17. V. Pitschmann, Z. Kobliha, E. Halámek, I. Tušarová, *J. Serb. Chem. Soc.* **72** (2007) 1031
18. E. Halámek, Z. Kobliha, V. Pitschmann, *Analysis of Chemical Warfare Agents*, NBC Defence Institute Vyškov, University of Defence, Brno, 2007
19. *Worldwide Chemical Detection Equipment Handbook*, Chemical and Biological Defense Information Analysis Center – Gunpowder Branch Aberdeen Proving Ground, Aberdeen, MD, 1995
20. *Detector Tube Handbook*, Mine Safety Appliances Company, Pittsburgh, PA, 1995
21. *Dräger-Röhrchen-/CMS-Handbuch*, Dräger Safety AG & KGaA, Lübeck, 2003.

Journal of the Serbian Chemical Society
JSCS@tmf.bg.ac.rs • www.shd.org.rs/JSCS

J. Serb. Chem. Soc. 75 (6) 823–831 (2010)
JSCS–4010

UDC 678.745:53.08+532.612+620.168.3
Original scientific paper

Tensiometric investigation of the interaction and phase separation in a polymer mixture–ionic surfactant ternary system

JAROSLAV M. KATONA*, VERICA J. SOVILJ, LIDIJA B. PETROVIĆ and NENAD Z. MUCIĆ

Faculty of Technology, University of Novi Sad, Bul. Cara Lazara 1, 21000 Novi Sad, Serbia

(Received 12 January, revised 18 February 2010)

Abstract: The interaction and phase separation in a ternary mixture composed of hydroxypropyl methyl cellulose (HPMC), sodium carboxymethyl cellulose (NaCMC), and sodium dodecylsulfate (SDS) were investigated by tensiometry. Surface tension measurements of binary mixtures (0.7 % HPMC and 0.00–2.00 % SDS) and of ternary mixtures (0.7 % HPMC, 0.3 % NaCMC, and 0.00–2.00 % SDS) were performed. The measurements indicated interaction between HPMC and SDS, which resulted in HPMC–SDS complex formation. The critical association concentration, *CAC*, and polymer saturation point, *PSP*, were determined. Phase separation of ternary HPMC/SDS/NaCMC mixtures occurs at SDS concentration > CAC, *i.e.*, when the HPMC–SDS complex is formed. The volume of the coacervate increases with increasing SDS concentration, and at SDS concentrations > 1.00 %, the coacervate vanishes. The surface tensions (σ) of ternary HPMC/SDS/NaCMC mixtures in the pre-coacervation region and at the onset of the coacervation region are similar to the σ of the corresponding binary HPMC–SDS mixtures, while in the coacervation and post coacervation region, they are close to the σ of the corresponding SDS solutions.

Keywords: polymer–surfactant interaction; complex formation; coacervation; phase separation; tensiometry; surface tension.

INTRODUCTION

Interaction between macromolecules may result in phase separation of a colloidal system into a coacervate (*i.e.*, liquid precipitate) and an equilibrium solution (supernatant). Depending on whether the interaction is of the associative or segregative type, either complex coacervation or coacervation due to thermodynamic incompatibility occurs, respectively.[1,2] During complex coacervation, a complex of two associative macromolecules (*e.g.*, polycation and polyanion) is formed which separates from the solution as a coacervate, while the equilibrium solution is more or less pure solvent. Thermodynamic incompatibility has been

* Corresponding author. E-mail: jkatona@uns.ac.rs
doi: 10.2298/JSC100112056K

related to the classical Flory–Huggin's theory or to depletion interaction theories, depending on the characteristics of the two macromolecules, where both of the two phases formed are rich in just one of the two macromolecules.[3,4]

Coacervate formation is involved in a number of practical situations: it is of special interest to the food and cosmetic industries, where macromolecules are found in the coacervate state in a wide range of products, and thereby determine their properties, *e.g.*, texture, stability, taste *etc*.;[5] complex formation *via* polymer–polymer interaction occurs in cells and other biological systems, and is important for their functioning;[6] the coacervation method is a common microencapsulation technique,[7] *etc*.

In a ternary mixture composed of two water soluble cellulose ethers, non-ionic hydroxypropylmethyl cellulose (HPMC) and anionic sodium carboxymethyl cellulose (NaCMC), and an anionic surfactant (SDS), various interactions occur (*i.e.*, HPMC–NaCMC, HPMC–SDS, HPMC/SDS–NaCMC) which may result in the formation of a coacervate. The microstructural properties of the coacervate can be varied by controlling the HPMC–SDS–NaCMC interaction.[8] In a recent work, the interactions were successfully employed to obtain oil microcapsules stabilized with coacervate shells of different properties.[9]

The aim of the present work was to investigate how the interactions among the components of HPMC/SDS/NaCMC ternary mixtures of different composition influence the surface tension of the investigated mixtures, especially when phase separation is involved. This is of importance for the understanding of the complex behavior of phase-separated polymer mixture–surfactant systems and provides further insight into the mechanism of microcapsule formation by the previously published method.[9] For this purpose, the surface tensions of different binary HPMC/SDS and ternary HPMC/SDS/NaCMC mixtures were determined, in which the concentrations of the polymers were fixed while the concentration of the surfactant was varied. In addition, the influence of the SDS concentration on the relative volume of the coacervate in the ternary HPMC/SDS/NaCMC system was determined.

EXPERIMENTAL

Chemicals

Hydroxypropylmethyl cellulose, HPMC, (trade name Methocel K4M CR, methoxyl content: 22.7 %, hydroxypropyl content: 8.9 %) was obtained from Colorcon Ltd., England. The viscosity average molar mass of the HPMC was M_v = 91500 g/mol, while the critical overlap concentration was c^* = 0.1269 %, determined at 20 °C. Sodium carboxymethyl cellulose, NaCMC, degree of substitution *DS* = 0.77, purity >96 %, was obtained from "Milan Blagojević", Serbia. The viscosity average molar mass of the NaCMC was M_v = 121000 g/mol, determined at 25 °C and the critical overlap concentration c^* = 0.1927 %. Details of the viscosimetric characterization of the HPMC and NaCMC samples can be found elsewhere.[10] Sodium dodecylsulfate, SDS, purity > 99%, was obtained from Merck, Germany. Critical micelle

concentration was *CMC* = 0.252 % at 30 °C, as determined by conductometric titration.[11] All samples were used without any further purification. Bidistilled water was used as the solvent.

Preparation of the binary and ternary mixtures

Stock solutions of 2.00 % w/w HPMC and 1.00 % w/w NaCMC were prepared by dispersing the required mass of HPMC and NaCMC in water at 80 and 20 °C, respectively, with gentle stirring. The stock solutions were left for 24 h at room temperature prior to further use. A 5% w/v stock solution of SDS was prepared by dispersing the required mass of SDS in bidistilled water at room temperature. Binary mixtures of 0.7 % w/w HPMC and 0.00–2.00 % w/w SDS were prepared by mixing the required masses of HPMC stock solution with a suitably diluted SDS stock solution. The mixtures were left for 24 h at room temperature prior to further use. Ternary mixtures of HPMC/SDS/NaCMC were prepared by mixing water and stock solutions of HPMC, NaCMC and SDS. The ternary mixtures were composed of 0.7 % w/w HPMC, 0.3 % w/w NaCMC and 0.00–2.00 % w/w SDS, and were left for 48 h at room temperature prior to further use.

Tensiometry

The surface tension measurements of the solutions were performed using a KSV Sigma 703D at 25 °C. The *Du Noüy* ring method was employed. Prior to the measurements, the air–liquid surface was disturbed by vigorous mixing, the ring was then immersed in the liquid (below the surface) and the surface was left to equilibrate for 20 min for the binary and ternary mixtures and 3 min for the SDS solution. The reported values of the surface tension are average values of at least three measurements. The surface tension of the bidistilled water used for the preparation of the solutions was σ = 72.1 mN/m.

Phase separation

The phase separation in the ternary mixtures consisting of 0.70 % HPMC, 0.30 % NaCMC and different SDS concentrations (0.00–2.00 %) was followed visually in 10 ml measuring cylinders. The relative volume of the coacervate, $v_{rel} = 100v/V$, in the ternary mixtures containing various concentrations of SDS was calculated, where v is the volume of the coacervate and V the volume of the whole ternary system in the measuring cylinder.

RESULTS AND DISCUSSION

Tensiometric investigation of the interaction between HPMC and SDS

Influence of the SDS concentration on surface tension of the SDS solution and the 0.70 % HPMC solution is shown in Fig. 1.

The surface tension of the SDS solution first decreased with increasing SDS concentration, passed through a minimum, then slightly increases and finally reached a constant value. The decrease in the surface tension is due to adsorption of surface active SDS molecules at the solution surface. The decrease occurs until the critical micelle concentration (*CMC*) is reached, when the surface becomes saturated with surfactant molecules and micelles begins to form in the solution. Above the *CMC*, there is no further adsorption of surfactant to the surface and thus no influence of the surfactant concentration on the surface tension of the solution. Such a dependence of the surface tension on the concentration of a surfactant can be used for the determination of the *CMC*. However, tensiometric de-

termination of the *CMC* is often difficult due to occurrence of a minimum in the surface tension *vs.* surfactant concentration curve around the *CMC*. The minimum in the surface tension curve, which can also be observed in Fig. 1, is typically ascribed to small amount of highly surface active impurities in solution.[12,13,14] In the case of an SDS solution, the occurrence of the minimum is often attributed to the presence of dodecanol in a SDS sample.[13,14] The impurities preferentially adsorb to the surface when compared to the surfactant and additionally lower the surface tension of the solution. Once micelles of SDS molecules are formed in a solution, solubilization of the impurities occurs and they desorb from the surface and are replaced by less surface active surfactant molecules. Consequently, a slight increase in the surface tension occurs. Therefore, the onset of the slight increase in the surface tension of a solution indicates *CMC*, which in the present case was found to occur at 0.23 % SDS. The *CMC* determined by tensiometric measurements (0.23 %) is somewhat lower than the *CMC* determined previously in the same laboratory[11] by conductometric titration (0.252 %). Finally, when all impurities are solubilized and the surface is saturated only with surfactant molecules, the surface tension of a solution becomes constant.

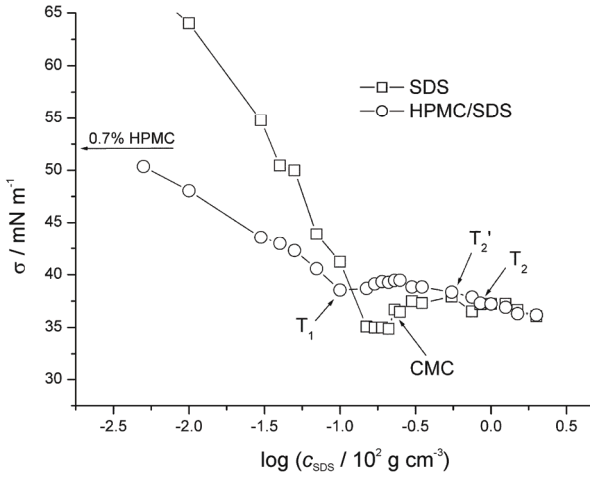

Fig. 1. Influence of the SDS concentration on the surface tension 0.70 % HPMC solutions.

HPMC is a surface active macromolecule;[15] the surface tension of a 0.70 % HPMC solution was found to be 52.32 mN/m, as indicated by the arrow in Fig. 1. On addition of SDS to a 0.70 % HPMC solution, the surface tension of the solution decreased. Due to the adsorption of both HPMC and SDS molecules on the surface, the surface tension of the binary HPMC/SDS mixture was lower than that of the corresponding SDS solution. At $T_1 \approx 0.1$ % of SDS, the first transition point in the surface tension *vs.* SDS concentration curve occurred. The transition

point indicates the onset of HPMC–SDS complex formation as a result of hydrophobic interaction between SDS and HPMC, and is usually referred to as the critical association concentration, *CAC*.[16,17] The HPMC–SDS complex formation was previously detected using different experimental techniques.[8,11,18] On further addition of SDS, surface tension of the binary mixture slightly increased and after reaching a maximum, it decreased. Occurrence of the maximum in surface tension is not typical for a nonionic polymer–ionic surfactant systems,[16] but was also previously observed by *e.g.*, Folmer and Kronberg in a mixture of SDS and poly(vinyl pyrrolidone).[19] Such a behavior is certainly concerned with reorganization of the adsorption layer at the surface, however, details of the surface composition could not be provided solely by tensiometric measurements. At the transition point denoted as $T_2 \approx 0.85$ % SDS, the surface tension of the mixture became the same as the surface tension of the pure SDS solution, indicating the onset of free SDS micelle formation in the bulk. The idealized picture of a nonionic polymer––ionic surfactant interaction predicts the occurrence of one more transition point between T_1 and T_2.[16,17] It is usually denoted as T_2', and represents a surfactant concentration at which all the hydrophobic sites of a polymer are saturated with surfactant molecules (*i.e.*, polymer saturation point, *PSP*). This transition point is typically far less evident than is the case for T_1 and T_2. T_2' is defined as the first SDS concentration at which the surface tension of the binary mixture becomes lower than at T_1, which is ≈0.65 % SDS. The *CAC* and *PSP* values obtained by tensiometric measurements agree with the values obtained in previous investigations using other experimental techniques.[8,11,18]

Tensiometric investigation of the interactions and phase separation in ternary HPMC/SDS/NaCMC mixtures

The addition of NaCMC to a HPMC/SDS mixture brings about phase separation of the ternary HPMC/SDS/NaCMC mixture. The investigated ternary mixture (composed of 0.70 % HPMC, 0.30 % NaCMC and 0.00–2.00 % SDS) phase separated into a coacervate (bottom) and an equilibrium solution (top) when the SDS concentration was between 0.10–1.00 %, Fig. 2.

Coacervate formation began at an SDS concentration which corresponds to the onset of HPMC–SDS complex formation, *i.e.*, at the *CAC*. This indicates that the formation of the HPMC–SDS complex is a prerequisite for phase separation of the ternary HPMC/SDS/NaCMC mixture. Previous rheological measurements indicated that the ternary HPMC/SDS/NaCMC mixture phase separates into an HPMC–SDS complex-rich coacervate phase and a NaCMC-rich equilibrium solution, due to the thermodynamic incompatibility between the HPMC–SDS complex and NaCMC.[8]

The relative volume of the coacervate in the ternary mixture increased with increasing SDS concentration, Fig. 3, and was determined by the governing interactions and a change in the microstructure of the HPMC–SDS complex.

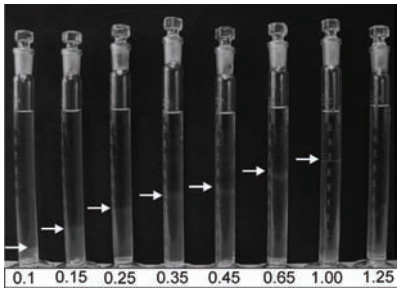

Fig. 2. Phase separation in ternary HPMC/SDS/NaCMC mixtures with varying SDS concentrations. The numbers indicate the SDS concentration (in %).

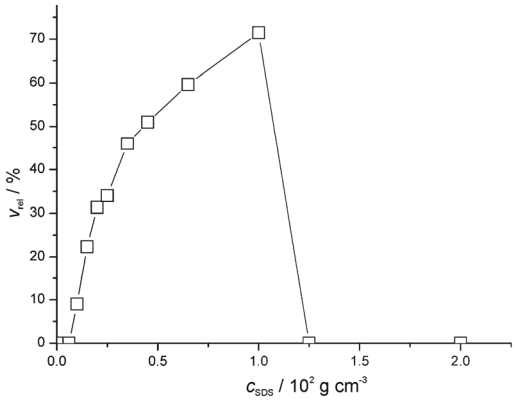

Fig. 3. Influence of SDS concentration on the relative volume of the coacervate in ternary HPMC/SDS/NaCMC mixtures.

The increase in the relative volume indicates an increase in the salvation of the coacervate. This was to be expected since the HPMC–SDS complex becomes increasingly more negatively charged as the SDS concentration is increased, due to the fact that more SDS is bound to the HPMC molecules.[8,9] The binding of SDS continues until the *PSP* is reached. As indicated by viscosimetry,[11] above the *PSP* there are additional conformational changes of the HPMC–SDS complex due to repulsion between the negatively charged complex and the free SDS micelles, which results in shrinkage of the complex. At sufficiently high SDS concentrations, the complex is able to be accommodated in the system, it becomes soluble even in the presence of NaCMC and thus the coacervate disappears when the concentration of SDS is >1.00 %.

The results of the surface tension measurements of the ternary HPMC/SDS/ /NaCMC mixtures are compared with the surface tensions of the corresponding binary HPMC/SDS mixtures and pure SDS solutions in Fig. 4.

In the pre-coacervation region, the surface tensions of the ternary mixtures were slightly lower than of the corresponding binary HPMC/SDS mixtures, indicating a similar composition of the surfaces, *i.e.*, adsorption of both HPMC and SDS molecules. This was expected since NaCMC shows only a small surface activity and contributes only slightly to surface tension of the ternary mixture. The surface tension of a 0.3 % NaCMC solution was found to be σ_{NaCMC} = 70.7 mN/m, which is very close to surface tension of bidistilled water (σ_{water} = 72.1 mN/m). At the onset of the coacervation region, the surface tensions of the binary and ternary mixtures were equal, indicating that phase separation only slightly influenced the balance between the components in the bulk and those adsorbed at the surface. This is somewhat surprising since the HPMC–SDS complex was separated as a coacervate at the bottom of the measuring vessel. It should be noted,

however, that previous rheological measurements[8] indicated the presence of HPMC in the equilibrium solution at the onset of the coacervation region, which also suggests that some of the HPMC molecules could be adsorbed at the surface at the beginning of the coacervate region. On further increase in the SDS concentration, the surface tension of the ternary mixture dropped; it became lower than in the binary mixtures and equaled the surface tension of the corresponding SDS solutions. In this part of the coacervate region, the dependence of the surface tension on the SDS concentration was very similar to the dependence in the pure SDS solution and bore no resemblance to the dependence observed in the binary HPMC/SDS mixtures. This indicates that the HPMC molecules gradually desorbed from the surface and were replaced by SDS molecules, and that the surface of the supernatants of the ternary mixture became free of HPMC molecules and free of the HPMC–SDS complex. The surface became saturated with only SDS molecules, the concentration of free SDS in the bulk was in the vicinity of the *CMC*, while the excess SDS was bound to HPMC and formed HPMC–SDS complexes. This phase separated from the solution. After reaching the *PSP*, in the post-coacervation region, the surface tension of all three systems (SDS solution, the binary and the ternary mixtures) became equal and free micelles of SDS appeared in the solution.[20,21]

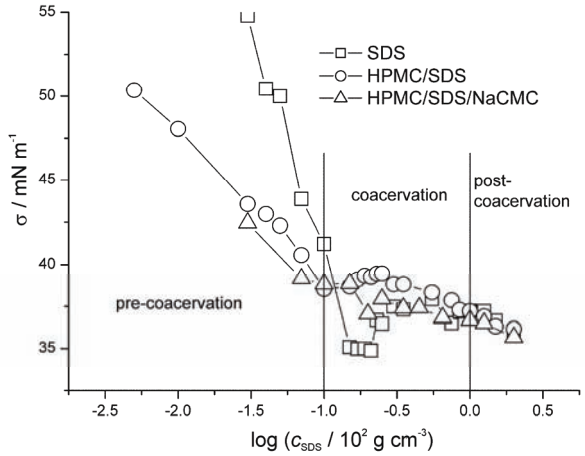

Fig. 4. Influence of the SDS concentration on the surface tension of ternary HPMC/SDS/NaCMC mixtures.

CONCLUSIONS

Tensiometric measurements of the binary HPMC/SDS and ternary HPMC/ /SDS/NaCMC mixtures with constant polymer(s) and different SDS concentrations were carried out in order to investigate interaction and phase separation in the ternary mixture. It was shown that the formation of the HPMC–SDS complex

influenced the surface tension of the binary mixture, and resulted in a characteristic dependence of the surface tension on the SDS concentration. Characteristic transition points of the dependence were used to determine the interaction regions of HPMC–SDS, *i.e.*, *CAC* and *PSP*, which were found to be in agreement with the values obtained previously using other experimental techniques. The ternary HPMC/SDS/NaCMC mixture phase separated when the SDS concentration was above the *CAC*, *i.e.*, when the HPMC–SDS complex was formed. The volume of the coacervate increased with increasing SDS concentration, and at an SDS concentration >1.00 % (*i.e.*, in the post-coacervation region), the coacervate vanished. The surface tension (σ) of the ternary HPMC/SDS/NaCMC mixtures in the pre-coacervation region and at the onset of the coacervation region were similar to the σ values for the corresponding binary HPMC–SDS mixtures, while in the coacervation and post coacervation region, it was close to the σ of the corresponding SDS solutions, indicating that the supernatants became free of HPMC and HPMC–SDS complex.

Acknowledgements. This work was supported by the Ministry of Science and Technological Development of the Republic of Serbia (Grant No. 20022). The authors are thankful to Colorcon Ltd. (England) for their generous gift of the HPMC sample.

И З В О Д

ТЕНЗИОМЕТРИЈСКО ИСПИТИВАЊЕ ИНТЕРАКЦИЈЕ И СЕПАРАЦИЈЕ ФАЗА У ТЕРНЕРНОМ СИСТЕМУ САСТАВЉЕНОМ ОД СМЕШЕ ПОЛИМЕРА И ЈОНСКЕ ПОВРШИНСКИ АКТИВНЕ МАТЕРИЈЕ

ЈАРОСЛАВ М. КАТОНА, ВЕРИЦА Ј. СОВИЉ, ЛИДИЈА Б. ПЕТРОВИЋ и НЕНАД З. МУЦИЋ

Технолошки факултет, Универзитет у Новом Саду, Бул. цара Лазара 1, 21000 Нови Сад

Испитивана је интеракција и сепарација фаза у тернерном систему састављеном од хидроксипропилметил целулозе (HPMC), натријум-карбоксиметил целулозе (NaCMC), и натријум-додецилсулфата (SDS) употребом тензиометрије. Измерени су површински напони HPMC/ /SDS бинарних смеша (0,7 % HPMC и 0,00–2,00 % SDS) и тернерних смеша HPMC/SDS/ /NaCMC (0,7 % HPMC и 0,00–2,00 % SDS). Мерења указују да долази до интеракције између HPMC и SDS, и до формирања HPMC–SDS комплекса. Одређена је критична концентрација асоцијације (*CAC*) и критична концентрација засићења полимера (*PCP*). До сепарације фаза и формирања коацервата у тернерној HPMC/SDS/NaCMC смеши долази при концентрацијама SDS већим од *CAC*, односно када је у смеши формиран комплекс HPMC–SDS. Запремина коацервата се повећава са повећањем концентрације SDS, док при концентрацијама >1,00 % коацерват нестаје. Вредности површинског напона HPMC/SDS/NaCMC тернерне смеше у области пре коацервације као и у области почетка коацервације су блиске вредностима површинског напона одговарајуће HPMC/SDS бинарне смеше. У области коацервације и у области након коацервације вредности површинског напона тернерне смеше се поклапају са вредностима површинског напона чистих раствора SDS.

(Примљено 12. јануара, ревидирано 18. фебруара 2010)

REFERENCES

1. S. L. Turgeon, C. Schmitt, C. Sanchez, *Curr. Opin. Colloid. Interface Sci*. **12** (2007) 166
2. V. Tolstoguzov, *Food Hydrocolloid.* **17** (2003) 1
3. J. L. Doublier, C. Garnier, D. Renard, C. Sanchez, *Curr. Opin. Colloid. Interface Sci*. **5** (2000) 202
4. R. Tuinier, E. ten Grotenhuis, C. Holt, P. A. Timmins, C. G. de Kruif, *Phys. Rev. E*. **60** (1999) 848
5. I. T. Norton, W. J. Frith, *Food Hydrocolloid*. **15** (2001) 543
6. C. G. de Kruiff, F. Weinbreck, R. de Vries, *Curr. Opin. Colloid Interface Sci*. **9** (2004) 340
7. S. Gouin, *Trends Food. Sci. Tech*. **15** (2004) 330
8. J. M. Katona, V. J. Sovilj, L. B. Petrović, *Carbohydr. Polym*. **74** (2008) 193
9. J. M. Katona, V. J. Sovilj, L. B. Petrović, *Carbohydr. Polym*. **79** (2010) 563
10. C. Alvarez-Lorenco, R. Duro, J. L. Gomez-Amoza, R. Martinez-Pacheco, C. Souto, A. Concheiro, *Colloid and Polym. Sci*. **279** (2001) 1045
11. V. J. Sovilj, L. B. Petrović, *Carbohydr. Polym*. **64** (2006) 41
12. A. Patist, in *Handbook of Appled Surface and Colloid Chemistry*, K. Holmberg, Ed., Wiley, Chicester, 2001, p. 239
13. K. Holmberg, B. Jönsson, B. Kronberg, B. Lindman, *Surfactants and Polymers in Aqueous Solution*, Wiley, Chicester, 2002, p. 346
14. M. Umlong, K. Ismail, *Colloids Surf. A* **299** (2007) 8
15. M. W. Kulicke, O. Arendt, M. Berger, *Colloid Polym. Sci*. **276** (1998) 1019
16. E. D. Goddard, *J. Colloid Interface Sci*. **256** (2002) 228
17. D. J. F. Taylor, R. K. Thomas, J. Penfold, *Adv. Colloid Interface Sci*. **132** (2007) 69
18. V. J. Sovilj, L. B. Petrović, *Colloid Polym. Sci*. **284** (2005) 334
19. B. M. Folmer, B. Kronberg, *Langmuir* **16** (2000) 5987
20. E. Minatti, D. Zanette, *Colloid Surf. A* **113** (1996) 237
21. E. D. Goddard, in *Interaction of Surfactants With Polymers and Proteins*, E. D. Goddard, K. P. Ananthapadmanabhan, Eds., CRC, Boca Raton, FL, 1993, p. 123.

J. Serb. Chem. Soc. 75 (6) 833–843 (2010)
JSCS–4011

Journal of the Serbian Chemical Society
JSCS@tmf.bg.ac.rs • www.shd.org.rs/JSCS

UDC 66.017+62–405.8+661.183.8+544.773.42.004.13
Original scientific paper

Pore surface fractal analysis of PEG and La(III)-doped mesoporous alumina obtained by the sol–gel method

TATJANA B. NOVAKOVIĆ[1*#], LJILJANA S. ROŽIĆ[1#], SRĐAN P. PETROVIĆ[1#], ZORICA M. VUKOVIĆ[1#] and VERA T. DONDUR[2#]

[1]*IChTM–Department of Catalysis and Chemical Engineering, University of Belgrade, Njegoševa 12, Belgrade and* [2]*Faculty of Physical Chemistry, University of Belgrade, Studentski trg 12–16, Belgrade, Serbia*

(Received 22 September, revised 10 December 2009)

Abstract: Active porous alumina was prepared *via* a sol–gel method and subjected to thermal treatment in the temperature range 500–1200 °C. The addition of lanthanum effectively inhibited the surface area loss of the aluminas. Fractal analysis from nitrogen adsorption isotherm was used to study the pore surface roughness of alumina samples with different chemical compositions (PEG, PEG and lanthanum) and calcinations conditions in terms of the surface fractal dimension, *d*. The Mahnke and Mögel (MM) model was used to determine the value of *d* of La(III)-doped alumina. Following the MM model, the *d* value of the activated aluminas increased as the calcination temperature increased from 500 to 700 °C but decreased after calcination at 1000, 1100 and 1200 °C. The addition of polyethylene glycol (PEG 5600) to the boehmite sol reduced the surface fractal of the activated alumina due to the heterogeneous distribution of the pores. With increasing La(III) concentration from 0.015 to 0.045 mol La(III)/mol Al(III), the *d* value of La-modified alumina samples decreased, indicating a smoother surface. The obtained PEG+La-doped boehmite sol can be used as a precursor dispersion for the deposition of mesoporous alumina coatings on stainless steel foil, by the spray pyrolysis method.

Keywords: mesoporous alumina; porous structure; surface fractal dimension; sol–gel.

INTRODUCTION

Porous materials are of scientific and technological interest because of their potential applications in separation processes, catalysts, chromatography, low dielectric constant fillers, microelectronics, electro-optics and other emerging nanotechnologies. Active aluminas are prepared mainly by hydrothermal or thermal

* Corresponding author. E-mail: tnovak@nanosys.ihtm.bg.rs
# Serbian Chemical Society member.
doi: 10.2298/JSC090922053N

transformations of aluminum hydroxides or alumogel. They are widely used as catalyst supports, because their high specific surface areas, surface properties and crystalline structures are important in the field of various catalysis.[1,2] Since the temperature of the catalyst can rise to over 1000 °C in a modern engine, thermal stabilization of the catalysts is important. The additive of lanthanum species greatly improves the thermal stability by inhibiting the sintering and phase transformation of alumina.[3,4] In the sol–gel process, calcination plays an important role in determining the performance of the resultant xerogels. During calcination, organic groups are removed and densification of the gel textures might also occur above a certain temperature. The evolution of the gel structure during calcination might also be influenced by the calcination procedures and thermal history.[5,6]. The preparation routes also influence the surface area and pore structure at the operation temperatures.[7] In addition, changes in the phase composition and the degree of alumina dehydration also cause changes of the internal pore structure of the alumina. Therefore, in order to better understand a particular physical process occurring within a porous medium, it is necessary to have detailed knowledge of the internal geometry and topology of the internal pore network. However, the surface area and pore size distribution alone do not meet all requirements to describe the characteristics of the pore structure of alumina. Another parameter to characterize the pore structure is surface fractal analysis, which is characterized by the fractal dimension. Gas adsorption is a method that is frequently used to determine the surface fractal dimension of porous media. Several different theories have been developed to analyze gas adsorption data to obtain the surface fractal dimension, which is an important parameter reflecting the roughness of the pore surface.[8–11] The standard BET equation generally overpredicts the amount adsorbed above the BET region. On a fractal surface, the amount adsorbed on each subsequent layer above the first decreases according to a power law. This principle has been used to derive versions of the BET model for adsorption on a fractal surface, *e.g.*, that derived by Mahnke and Mögel.[12]

In this work, the surface fractal dimensions of activated alumina samples were calculated using the Mahnke and Mögel method (MM). The MM equation provides a relationship between the surface fractal dimension and nitrogen adsorption, that is to say, the pore surface roughness can be probed by nitrogen molecules. The surface fractal dimension by Mahnke and Mögel method yields the following equation:

$$\log\frac{Vp}{p_0} = \log V_{\mathrm{m}} + \log\frac{\frac{Cp}{p_0}}{1-\frac{p}{p_0}(1+C)} - \alpha\log(1-\frac{p}{p_0}) \qquad (1)$$

where Vp is the volume of adsorbed gas at equilibrium pressure (p), p_0 is the saturation pressure, V_m is the volume of a monolayer and C is the BET constant.

This logarithmic version of the Mahnke and Mögel Equation (1) enables the estimation of the optimal values (with respect to mean square error) of α, C and V_m for the measured isotherms using the simplex optimization method.[13] The values of the volume of a monolayer, V_m, and the BET constant, C, can be obtained from the BET model and the surface fractal dimension, d, can be calculated from the relation $\alpha = 3–d$.

In the present work, an effort was make to investigate the influence of poly(ethylene glycol) (PEG), pure or combined with La(III), added to the boehmite sol, and of the calcination temperature on the structure (pore size distribution) and the surface fractal dimension of active porous alumina prepared by the sol––gel method. The surface fractal dimension was used to characterize the pore structure of the active porous alumina. These properties are crucial for the implementation of doped boehmite sol as a precursor solution for the synthesis of γ-alumina coatings on stainless steel foil, by the spray pyrolysis method, which can be used in three-way catalytic processes.

EXPERIMENTAL

Active porous alumina was prepared by the sol–gel method using aluminum alkoxide as a precursor. To prepare boehmite sols, aluminum isopropoxide was hydrolyzed in excess amount of water (100:1 H_2O:Al(III), mol) at 80 °C, followed by peptization with the appropriate amount of HNO_3 (0.07:1 H^+:Al(III), mol) to form a stable colloidal sol.[14] The sol was kept at about 90 °C for about 72 h under reflux conditions, during which time most of the formed alcohol evaporated. The freshly prepared boehmite sol and polyethylene glycol (PEG, *MW* 5600, molecule radius: 2.3 nm) or variable concentration of lanthanum nitrate solution combined with PEG, were mixed together and then vigorously stirred in order to obtain homogeneous PEG-doped and La(III)-doped boehmite sols. The doped boehmite sols were then gelled at 40 °C. The gels were heated from room temperature at a rate of 2 °C/min and calcined in air at different temperatures (500–1200 °C) for 5 h to obtain activated alumina samples. The experimental parameters and the variables are given in Table I.

TABLE I. Experimental parameters and variables

Experimental parameters	Variables
Calcinations temperature, °C	500, 700, 1000, 1100 and 1200
Concentration organic additive	1g PEG / 100 ml boehmite sol
Amount of lanthanum, mol La(III)/mol Al(III)	1.5, 3, and 4.5

Nitrogen adsorption was performed at –196 °C and a relative pressure interval between 0.05 and 0.98 in a high vacuum volumetric apparatus.[15] Before each measurement, the sample was degassed at 250 °C under vacuum for time sufficient (4 h < t < 10 h) to obtain vacuum stability. The adsorbed amount of nitrogen was measured by volume at standard temperature and pressure. The specific surface areas S_{BET} and C were calculated by the BET method from

the nitrogen adsorption isotherms, using data up to p/p_0 = 0.03; the pore size distribution was computed from the desorption branch of the isotherms.[16-18]

RESULT AND DISCUSSION

Effect of the calcination temperature

The complete N_2 adsorption–desorption isotherms of alumina samples obtained for the pure and PEG-doped boehmite sols at calcinations temperatures 500–1200 °C are shown in Figs 1a–1e.

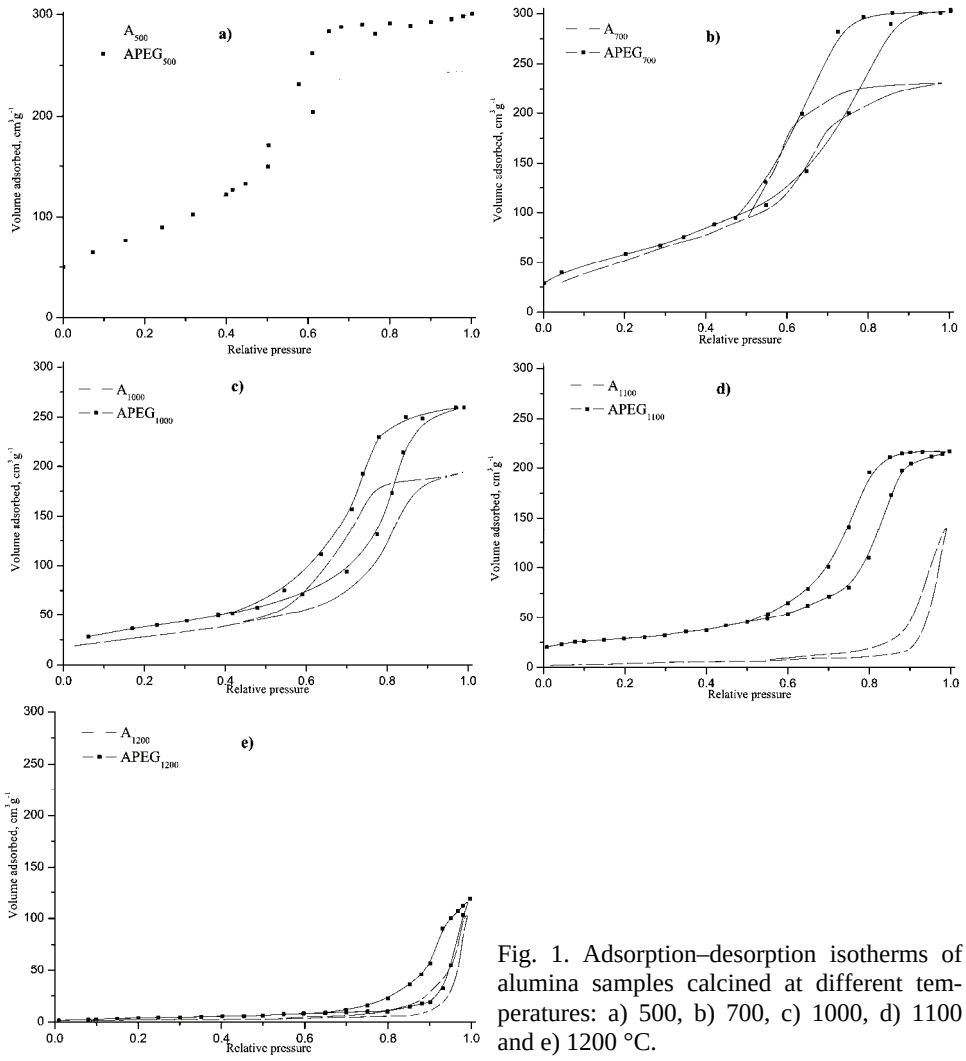

Fig. 1. Adsorption–desorption isotherms of alumina samples calcined at different temperatures: a) 500, b) 700, c) 1000, d) 1100 and e) 1200 °C.

All isotherms at low relative pressures were reversible, but exhibited a hysteresis loop at higher relative pressures. Such a type of adsorption isotherm indicates that the multilayer adsorption of nitrogen onto the sample surface was connected with capillary condensation in the mesopores. The alumina samples calcined at 500 and 700 °C (Figs. 1a and 1b) are characterized by a type IV isotherm with a hysteresis loop of the H2 type.[18] The slope of the desorption branch for the alumina samples obtained from the PEG-doped boehmite sol indicated a broader pore size distribution than in the non-doped alumina sample. However, the adsorption isotherms for the alumina samples calcined at a temperature of 1100 °C (Fig. 1d) are characterized as type II isotherms. A type II isotherm is encountered when adsorption occurs onto a low porosity material or on material with pore diameters mostly mesoporous. They also showed hysteresis on the desorption isotherm curve with a smaller desorption step. The most prominent changes of the adsorption–desorption isotherms were obtained from the non-doped boehmite sol, indicating the biggest changes of its porous structure after sintering at 1100 °C.

The cumulative pore volumes and the pore size distributions were computed from the desorption branch of the isotherms.

The pore size distribution profiles of the alumina samples obtained from pure and PEG-doped boehmite sols at calcination temperatures of 500–1200 °C are present in Fig. 2. With increasing calcination temperature, the mean pore size increased but the total pore volume decreased. The decrease in pore volume can be associated with ≈ 50 % volume shrinkage at 1200 °C, which essentially eliminates all porosity.[19] The larger pore volume in alumina samples obtained from the boehmite sol doped with the large molecular weight PEG (molecule radius: 2.3 nm) was affected by the specific surface action of PEG molecules as alumina gel network modifiers, which after calcinations at 500 °C are burnt out, leaving some micro-cavities in the gel. Increasing the treatment temperature within the range from 500 to 700 °C did not cause any significant cumulative pore volume changes, but it caused a slight increase of the predominant pore diameter.

The specific surface areas, S_{BET}, were calculated by the BET method from nitrogen adsorption isotherms, using data up to p/p_0 = 0.3. The effects of the treatment temperature on the specific surface area for non-doped and PEG-doped alumina samples are given in Table II.

The specific surface area decreased approximately linearly with increasing treatment temperature up to *cca* 1000 °C. Thermal treatment of the non-doped alumina sample at 1100 and 1200 °C caused a considerable decrease of its specific surface area to a value of 20 and 10 $m^2\ g^{-1}$, respectively. The alumina obtained from the PEG-doped boehmite sol retained a surface area of 65 $m^2\ g^{-1}$ after thermal treatment at 1100 °C for 5 h, but treatment at 1200 °C reduced its surface area to 15 $m^2\ g^{-1}$.

The changes in the porous structure were accompanied by phase transformation of the γ-Al_2O_3. At higher temperatures (1100 °C), the formation of larger pores due to the collapse of the pores with shrinkage of the material structure resulted in a large increase in the crystallite size and a decrease of the surface area and pore volume. This means that the rapid collapse of the fine mesoporous structure started as conversion to the stable α-Al_2O_3 phase, which is at a temperature of 1100 °C. The transformation into the α-Al_2O_3 occurred at calcination temperatures higher than 1000 °C.[19,20]

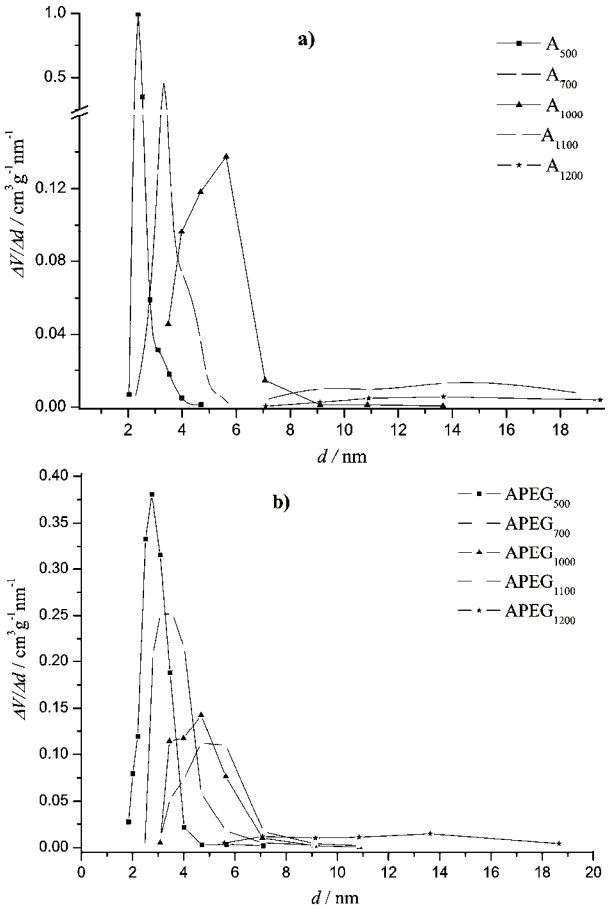

Fig. 2. Pore size distribution of (a) pure alumina and (b) PEG--doped alumina samples calcined at different temperatures.

The surface fractal dimensions, *d*, of the non-doped and PEG-doped alumina samples are also given in Table II. The experimental data fitted the model well with r^2 values greater than 0.99 for each fit, and the *d* values of the alumina samples were calculated from the nitrogen adsorption data, using the Mahnke and Mögel method. It was shown that the *d* values display very similar trends for

both alumina samples. For the non-doped alumina samples, increasing the calcination temperature from 500 to 700 °C resulted in an increase in the surface fractal dimension from 2.082 to 2.122. This is due to the pore formation mechanism in the aluminas, which caused higher surface roughness and more irregular surfaces. However, at 1000 °C, the surface fractal dimension of the non-doped alumina samples decreased to 2.048, which implies that larger pores were formed due to the collapse of the pores, which led to a decrease in the porosity. A similar trend was observed for the PEG doped aluminas.

TABLE II. Specific surface area and surface fractal dimension, *d*, of the non-doped and PEG--doped alumina samples

Sample	Calcinations temperature, °C	Specific surface area $m^2 g^{-1}$	Surface fractal dimension
Alumina	500	290	2.082
	700	230	2.122
	1000	102	2.048
	1100	20	2.387
	1200	10	2.323
PEG-doped alumina	500	295	2.040
	700	241	2.047
	1000	136	2.013
	1100	65	2.116
	1200	15	2.311

The sintering process at 1100 °C for the non-doped alumina and at 1200 °C for the PEG-doped alumina induced a restructuring phenomenon, which resulted in an increase of the mass fractal dimension of the alumina clusters; hence, there was a sharp increase of the surface fractal dimension in the alumina samples. The increasing in pore surface fractal dimension can also be associated with the appearance of new pores due to solubilization of the alumina constituents and to crystallization of the α-Al_2O_3 phase inside the pores, which contributed to the irregularities of the alumina surface. According to the present analysis, the surface fractal dimensions of alumina were rather stable during calcination (until the appearance of the α-alumina phase).

Effect of amount of La(III)-added

The effect of different amounts of La(III) added to the PEG-doped boehmite sol on the surface areas and the pore volumes of the alumina samples calcined at 1000 °C temperature was studied. The complete N_2 adsorption–desorption isotherms of PEG–La(III)-doped alumina samples at calcined at a temperature of 1000 °C are shown in Fig. 3a.

The isotherms of all alumina samples exhibited type IV isotherms with a hysteresis loop of the H2 type. This means that all samples were porous and con-

tained mostly mesopore area. The pore size distributions of the PEG–La(III)-doped aluminas with different amount of doped lanthanum are shown in Fig. 3b. The pore size distribution profiles became narrower, the average pore size gradually decreased and the pore volume slightly increased with increasing amount of lanthanum. These results show that with increasing amount of lanthanum, the homogeneity of the distribution of the pores increased due to surface screening effects. This effect also leads to smoothening of the pore surface of the La(III)-modified aluminas. The value of surface fractal dimensions of PEG-aluminas doped with 0.015, 0.03 and 0.045 mol La(III)/mol Al(III) were 2.170, 2.137 and 2.133, respectively. It can be seen that, the surface fractal dimensions decreased with increasing amount of lanthanum added to the sol. This indicates that the pore surface of alumina became smoother and less irregular as the content of lanthanum particles increased. The smoothening of pore surface roughness was due to the blocking of the alumina pores by lanthanum particles.

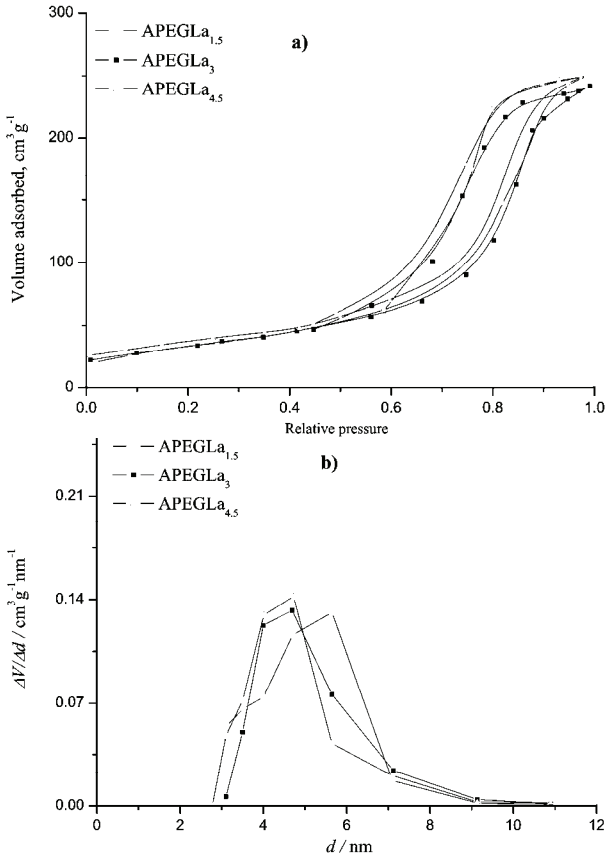

Fig. 3. Adsorption–desorption isotherms (a) and pore size distributions (b) of alumina samples doped with different amounts of lanthanum.

Synergism between poly(ethylene glycol) and La(III)-ion added in the aluminas

The influences of the calcination temperature on the specific surface area and surface fractal dimension for PEG–La(III)-doped aluminas with 0.03 mol La(III)/mol Al(III) are presented in Table III.

TABLE III. Specific surface area and surface fractal dimension for PEG–La(III)-doped aluminas (0.03 mol La(III)/mol Al(III))

Temperature, °C	Specific surface area, $m^2 g^{-1}$	Surface fractal dimension
500	235	2.068
700	207	2.084
1000	155	2.137
1100	115	2.178
1200	65	2.192

Increasing the calcination temperature from 500 to 1200 °C decreased the surface area and the pore volume of the alumina samples. The addition of La(III) to the boehmite sol inhibited the decrease of the surface area of the produced aluminas during its calcination at high temperatures. Increasing the temperature, especially in the range from 1000 to 1200 °C, decreased the surface area of the La(III)-doped aluminas less than the undoped ones (Table III). In accordance with this, the thermal treatment of La(III)-doped alumina samples at temperatures from 500 to 1200 °C caused a considerable increase in their surface fractal dimension form 2.068 to 2.192. These results were consistent with the deductions from the adsorption isotherms and the pore size distribution analysis. The surface fractal dimension as well as the pore connectivity did not change significantly during thermal treatment until the formation of crystalline α-Al_2O_3 commenced.

Hence, the addition of lanthanum to the boehmite sol in an atomic ratio of 0.03 La(III)/Al(III) can raise the temperature of the phase transformation to α-Al_2O_3 to above 1200 °C. If the most likely nucleation and growth mechanism for the phase transformation to α-Al_2O_3 is assumed, the obtained results indicates that the presence of La(III)-ions on the surface of the alumina crystallites reduce the nucleation of α-Al_2O_3, thus raising the phase transformation temperature.

CONCLUSIONS

Porous, high surface area, active alumina samples, pure and doped with PEG or PEG+La(III) ions, were obtained by the sol–gel process. The influence of calcination temperature, organic additive and different amounts of lanthanum on the mesoporous structure and surface fractal dimension was investigated using the Mahnke and Mögel model. The calcination temperature induces a change of pore surface roughness of the porous materials. The surface fractal dimension of pure and PEG-doped alumina samples increased slightly on increasing the calcination temperature from 500 to 700 °C and then decreased at 1000 °C for the pure alu-

mina, *i.e.*, 1100 °C for the PEG-doped alumina. This phenomenon can be explained by the deformation mechanism of the pore size. When the calcinations temperature increases, the average pore size increases and the pore volume decrease due to volume shrinkage, which eliminates some of the smaller pores.

The addition of La(III) to the boehmite sol inhibits the surface area loss of the produced aluminas during its calcination at high temperatures. Thermal treatment of La(III)-doped alumina samples at a temperature from 500 to 1200 °C caused a considerable increase in the surface fractal dimension of the samples from 2.068 to 2.192. The surface fractal dimension as well as the pore connectivity did not change significantly during the thermal treatment until the formation of crystalline α-Al_2O_3.

Acknowledgment. This work was supported by the Ministry of Science and Technological Development of the Republic of Serbia (Project No. ON 142019B).

ИЗВОД

ФРАКТАЛНА АНАЛИЗА ПОВРШИНЕ МЕЗОПОРОЗНОГ АЛУМИНИЈУМ(III)-ОКСИДА СА ДОДАТКОМ PEG И La(III) ДОБИЈЕНОГ СОЛ–ГЕЛ ПОСТУПКОМ

ТАТЈАНА Б. НОВАКОВИЋ[1], ЉИЉАНА С. РОЖИЋ[1], ЗОРИЦА М. ВУКОВИЋ[1], СРЂАН П. ПЕТРОВИЋ[1] и ВЕРА Т. ДОНДУР[2]

[1]*ИХТМ–Центар за катализу и хемијско инжењерство, Универзитет у Београду, Његошева 12, Београд и* [2]*Факултет за физичку хемију, Универзитет у Београду, Студентски трг 12–16, Београд*

Активни порозни алуминијум-оксид добијен сол–гел методом је термички обрађен на повишеним температурама у интервалу од 500 до 1200 °C. Испитиван је утицај температуре термичке обраде и додатка полиетилен гликола (PEG) и La(III) јона на специфичну површину, запремину пора и пречник пора, као и фракталну димензију површине активираног алуминијум-оксида. На основу података из адсорпционо–десорпционих изотерми азота одређен је тип пора и израчунате су вредности основних параметара текстуралних својстава узорака. Пораст температуре термичке обраде проузроковао је смањење специфичне површине са 280 на 65 $m^2\ g^{-1}$, запремине пора са 0,45 на 0,27 $cm^3\ g^{-1}$, пораст преовлађујућег пречника пора од 3 до 6 nm и пораст фракталне димензије површине од 2,068 до 2,192. Добијени бемитни сол са додатком PEG и La(III) јона може се искористити као прекурсорска дисперзија при спреј-пиролитичкој методи синтезе алуминијум оксидних превлака на носачу од нерђајућег челика.

(Примљено 22. септембра, ревидирано 10. децембра 2009)

REFERENCES

1. E. J. A. Pope, J. D. Mackenzie, *J. Non-Cryst. Solids* **87** (1986) 185
2. J. Čejka, *Appl. Catal. A* **254** (2003) 327
3. H. Schaper, E. B. M. Doesburg, L. L. Van Reijen, *Appl. Catal.* **7** (1983) 211
4. H. Arai, M. Machida, *Appl. Catal. A* **138** (1996) 161
5. L. C. Klein, T. A. Gallo, *J. Non-Cryst. Solids* **121** (1990) 119
6. Y. Wang, J. Wang, M. Shen, W. Wang, *Journal of Alloys and Compounds* **467** (2009) 405
7. 7. M. Ozawa, Y. Nishio, *J. Alloys Compd.* **374** (2004) 397
8. J. J. Fripiat, L. Gatineau, H. Van Damme, *Langmuir* **2** (1986) 562

9. P. Pfeifer, D. Avnir, *J. Phys. Chem.* **79** (1983) 3558
10. D. Avnir, D. Farin, *J. Phys. Chem.* **79** (1983) 3566
11. D. Avnir, *The Fractal Approach to Heterogeneous Chemistry*, Wiley, New York, 1990
12. M. Mahne, H. J. Mögel, *Colloids Surf. A* **216** (2003) 215
13. J. A. Nelder, R. Mead, *Comput. J.* **7** (1965) 308
14. B. E. Yoldas, *Am. Ceram. Soc. Bull.* **54** (1975) 289
15. Lj. Rožić, S. Petrović, T. Novaković, Ž. Čupić, Ž. Grbavčić, D. Jovanović, *Chem. Eng. J.* **120** (2006) 55
16. S. H. Gregg, K. S. Sing, *Adsorption, Surface Area and Porosity*, Academic Press, New York, 1967
17. B. C. Lippens, B. G. Linsen, J. H. de Boer, *J. Catal.* **3** (1964) 32
18. K. Sing, D. Everet, R. Haul, L. Moscou, R. Pierotti, J. Rouquerol, T. Siemieniewska, *Pure Appl. Chem.* **57** (1985) 603
19. C. Falamaki, M. S. Afarani, A. Aghaie, *J. Eur. Ceram. Soc*. 24 (2004) 2285
20. A. C. Pierre, *Ceram. Int*. **23** (1997) 229.

Journal of the Serbian Chemical Society
JSCS@tmf.bg.ac.rs • www.shd.org.rs/JSCS
J. Serb. Chem. Soc. 75 (6) 845–853 (2010) UDC 628.3:628.316.12:546.56:66.021.3.081.3
JSCS–4012 *Original scientific paper*

Removal of Cu(II) from wastewater by waste tire rubber ash

HASSAN ZAVVAR MOUSAVI[1]*, ABDORRAHMAN HOSSEINIFAR[2] and VAHDAT JAHED[2]

[1]*Chemistry Department, College of Sciences, Semnan University, Semnan and* [2]*Aja University of Medical Sciences, Tehran, Iran*

(Received 10 April 2009, revised 17 March 2010)

Abstract: The influence of pH, adsorbent dose, initial Cu(II) concentration and contact time on the removal of Cu(II) from aqueous solution by the batch adsorption technique using waste tire rubber ash as a low-cost adsorbent was investigated. The adsorption equilibrium was achieved after 2 h at pH 4–6, the optimum for the adsorption of Cu(II) ions. A dose of 1.5 g/L of adsorbent was sufficient for the optimum removal of copper ions. The experimental data were analyzed by the Langmuir and Freundlich isotherms and the corresponding sorption constants were evaluated. The adsorption kinetics data were fitted by a first-order equation. The cost of removal is expected to be quite low, as the adsorbent is cheap and easily available in large quantities. The present study showed that waste tire rubber ash was capable of removing copper ions from industrial wastewater samples.

Keywords: removal; copper; waste tire rubber ash; wastewater; isotherm.

INTRODUCTION

Today contamination of water by toxic heavy metals resulting from the discharge of industrial wastewater is a worldwide environmental problem. Many industries, particularly in metal processing operations and refineries, represent significant sources of heavy metal emissions. Unlike organic compounds, soluble heavy metals, such as copper, cadmium, lead, and chromium, are non-biodegradable and toxic even at trace levels. Heavy metals can accumulate in living organism and cause various diseases.[1–4]

Copper and its compounds are widely used in many industries and there are many potential sources of copper pollution. The continued intake of copper by humans leads to necrotic changes in the liver and kidney, mucosal irritation; wide spread capillary damage, depression, gastrointestinal irritation, and lung cancer.[5] According to the Safe Drinking Water Act, the permissible limit of copper in

*Corresponding author. E-mail: hzmousavi@semnan.ac.ir
doi: 10.2298/JSC090410044M

drinking water is 1.3 mg/L.[6] Excessive copper concentrations can lead to weakness, lethargy and anorexia, as well as damage to the gastrointestinal tract.[7] Therefore, there is a considerable need to treat industrial effluents containing such heavy metals prior to discharge to protect public health. The metal needs to be removed from industrial effluents before discharge into the environment to mitigate any impact on plant, animal and human receptors.

The most common treatment processes for metal contaminated wastewater include: chemical precipitation, membrane filtration, reverse osmosis and ion exchange. These methods have been found to be limited, since they often involve high capital and operational costs and may also be associated with the generation of secondary wastes which present treatment problems.[8–12]

Adsorption is arguably the most important type of physicochemical processes responsible for the removal of heavy metals from aqueous environments. In recent years, adsorption was shown to be an economically feasible method for the removal of metal ions from water and wastewater. The biggest barrier in the industrial application of this process is the high cost of adsorbents presently available for commercial use. The cost of the application of adsorption technologies can be reduced if the adsorbent is inexpensive; hence, the search for low-cost adsorbents that have metal-binding capacities has intensified. This has led many workers to search for cheaper alternatives among plant wastes or industrial by-products, such as granular red mud,[13] chitosan,[14,15] potato peel,[16] fired coal fly ash,[17] sugar beet pulp,[18,19] palm kernel husk,[20] bagasse fly ash,[21] modified cellulosic materials,[22] spent grain,[23] peanut husks carbon,[24] sawdusts,[25] papaya wood,[26] sugarcane bagasse,[27] rice husk,[28] and pomegranate peel.[29]

Waste tires have been a major management and disposal problem in many countries for decades. Many waste tires are currently stockpiled in various countries around the globe. These stockpiles are dangerous because they pose a potential environmental concern, are fire hazards and provide breeding grounds for mosquitoes. The practice of disposing waste tires in landfills is becoming unacceptable because of the rapid depletion of available landfill sites.

This work is focused on the removal of Cu(II) ions from aqueous solutions using waste tire rubber ash (WTRA) as an adsorbent. The influences of pH, contact time, initial iron concentration, temperature and adsorbent dosage on the removal of Cu(II) from wastewater and water solutions were investigated. Equilibrium isotherm data were analyzed by the Langmuir and Freundlich equations using linear regression analysis. The adsorption efficiency towards copper ion removal was tested using different industrial wastewaters.

EXPERIMENTAL

Material

Analytical grade chemicals were used throughout the investigation. Merck salts and standards used for quantification were of high purity (99.9 % or more) having trace metal

contents far below their detection limits. Aqueous standard solutions of Cu(II) were prepared by dissolving an accurately weighed amount of $Cu(NO_3)_2$ salt in deionized water so as to yield a metal ion concentration of 1000 mg L^{-1}. Appropriate aliquots were taken from these standards for subsequent dilution to the desired concentration level. NaOH and HCl solutions, both 0.10 mol L^{-1}, were used for pH adjustment. A Metrohm (model E-632) pH meter was used for the pH measurements. Polyethylene bottles were selected as containers. The bottles were first cleaned with a metal-free non-ionic detergent and washed with tap water. They were then soaked in 1:1 HNO_3 + H_2O solution for 24 h at 70 °C and subsequently rinsed thrice with de-ionized water. The total copper concentrations in the solution samples were determined using flame atomic absorption spectroscopy (FAAS) equipped with copper hallow cathode lamp (λ = 324.8 nm) and acetylene–air as the fuel-oxidant.

Adsorbent preparation and characterization

The material used in this study was obtained by treatment of waste tire rubber in order to prepare the desired ash. Thus, it was first washed with detergent solution and then with dilute HCl in order to remove soil debris. Then the clean and dry parts were burnt and the residue was taken in a porcelain crucible and burnt completely at 500 °C in a muffle furnace for 4 h. The cooled ash was then washed with a very dilute acidic solution, such as 0.0010 mol L^{-1} HCl to remove salts of metals, such as Na, K and Ca. Subsequently, the mixture was filtered out using a Whatman grade 42 filter paper. Then the adsorbent was washed with 100 mL of double distilled water and dried at 105 °C for 2 h before use.

The adsorbent was characterized by standard methods. The microstructure and surface morphology of the adsorbent samples were characterized by SEM images of WTRA particles obtained using a Phillips PW3710 Field Emission Scanning Electron Microscope (SEM) with an accelerating voltage of 15.0 kV.

Adsorption studies

Adsorption isotherms were determined using the batch equilibrium method. The adsorption of Cu(II) was studied after adding 50 mg of WTRA into an aqueous solution containing the desired Cu(II) concentration (50–500 mg L^{-1}), adjusting the pH of the solution to between 2 and 6, shaking at 150 rpm for 2 h at 25 °C in a reciprocating shaker and then the samples were centrifuged at 5000 rpm for 5 min. The WTRA particles were separated from the suspensions by filtration through a 0.45 μm membrane filter. The residual concentration of copper ions was determined by atomic absorption spectrometry.

In addition to the adsorption tests, a set of blank tests with WTRA was conducted in order to evaluate the removal by metal hydroxide precipitation at various pH values. The amount of Cu(II) adsorbed on the WTRA was calculated from the difference between the initial concentration and the equilibrium concentration of Cu(II). The percent Cu(II) removal, R_e, was calculated using the following equation:

$$R_e = 100\frac{c_i - c_f}{c_i} \quad (1)$$

where c_i and c_f are the initial and equilibrium concentrations of the adsorbate, respectively. The reported value of Cu(II) ions adsorbed by WTRA in each test was the average of at least three measurements.

RESULTS AND DISCUSSION

Adsorbent characteristics

The characteristics of the WTRA were as follows: surface area (BET), 410 m^2/kg, specific gravity, 2.35, average particle size, 9.0 μm, chemical composition: SiO_2 (26.5 %), Al_2O_3 (8.7 %), TiO_2 (1.0 %), Fe_2O_3 (9.3 %), MgO (6.4 %), CaO (12.9 %), Na_2O (1.4 %), K_2O (1.1 %), SO_3 (1.6 %) and Zn (20.2 %).

The SEM images of the WTRA particles are shown in Fig. 1.

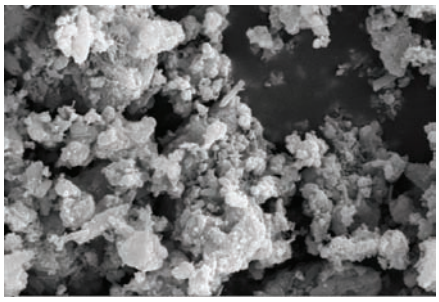

Fig. 1. SEM Images of the WTRA particles.

Adsorption studies

Effect of contact time. The results of the effect of equilibrium time on the sorption of Cu(II) by WTRA are shown in Fig. 2, which clearly shows that the adsorption of Cu(II) ions onto the WTRA was relatively fast and the complete adsorption equilibrium between the two phases was obtained after 2 h. The results show that 120 min was a sufficient time for copper adsorption onto the WTRA. The fast metal uptake by the sorbents may be attributed to their highly porous and mesh structure, which provides ready access and a large surface area for the sorption of the metal ions onto the binding sites. Thus, for subsequent experiments, an equilibration time of 2 h was chosen for the sake of convenience (Fig. 2).

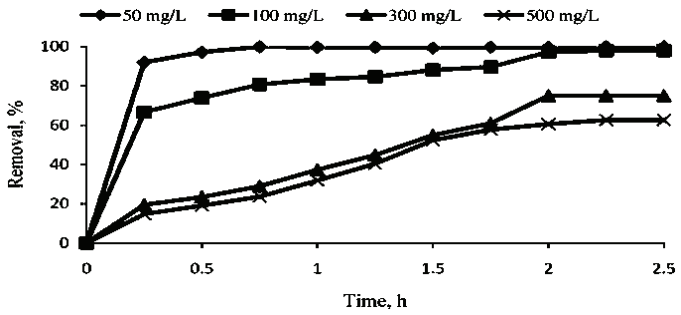

Fig. 2. Effect of contact time on the sorption of copper by WTRA. Conditions: 1.5 g L^{-1} of WTRA, 100 mL of Cu(II) solution, temperature: 25 °C.

Effect of adsorbent dose. The removal of metal ions is a function of adsorbent dosage; hence, the efficiency of the WTRA was evaluated at different doses using the percent removal of copper. The experiments were conducted at a constant initial Cu(II) concentration (100 mg L^{-1}), contact time (2 h), temperature (25±1 °C), stirring speed (150 rpm) with varying adsorbent doses (0.1–2.5 g L^{-1}). The measurement of the percentage Cu(II) removal as a function of time at different doses indicated that the removal of Cu(II) increased with increasing adsorbent dose (Fig. 3). The increase in copper removal with adsorbent dose can be attributed to the increased surface area and the availability of more adsorption sites. The removal efficiency was found to increase proportionally with the amount of WTRA until a certain value was reached; afterwards, the removal efficiency remained constant even if WTRA was added. Therefore, 1.5 g L^{-1} of adsorbent was sufficient for the quantitative removal of copper from wastewater (Fig. 3).

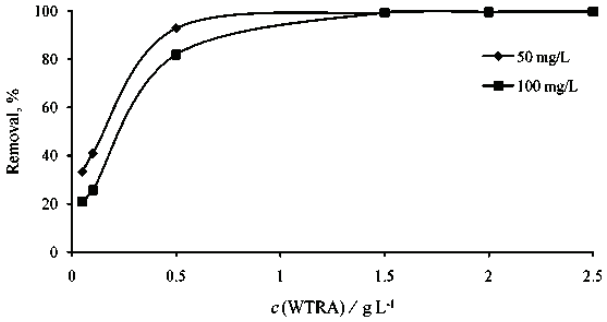

Fig. 3. Effect of WTRA dosage on the removal of Cu(II). Conditions: 100 mL of Cu(II) solution, contact time: 2 h, temperature: 25 °C.

Effect of pH. WTRA is a strong alkali material, which exhibits a pH of 10–13 when added to water, and its surface is negatively charged at high pH values. Hence, it can be expected that metal ions can be removed from aqueous solutions by precipitation or electrostatic adsorption. In fact, a number of studies were conducted to show the effectiveness of fly ash in the removal of heavy metal ions from aqueous solutions.[30]

All experiments were performed in the pH range of 2.0–6.0, at which values chemical precipitation is avoided. Thus the metal removal could be related to the adsorption process. Adsorption of Cu(II) onto the WTRA (1.5 g L^{-1}) was studied at various pH values to optimize the removal of Cu(II) at 25 °C. It is apparent that the uptake was low at lower pH values; however, with increasing pH, a significant enhancement in the adsorption was recorded. The optimum pH for the removal of Cu(II) was found to be in the range 4.5–6.0, with a removal of about 99.8 % Cu(II) from the solution.

The low adsorption capacity at pH values below 4.5 was attributed to hydrogen ions that compete with the metal ions for the sorption sites.[31] In other words, at lower pH values, due to protonation of the binding sites resulting from the high concentration of protons, the negative charge intensity on the sites was reduced, resulting in a reduction or inhibition of the binding of metal ions. At pH value higher than 6, the copper ions precipitated as its hydroxide, which decreased the rate of adsorption and subsequently the percent removal of metal ions.

Effect of temperature. The adsorption mechanism (chemical or physical) is often an important indicator to describe the type and level of interactions between the adsorbate and adsorbent. If the adsorption decreases with increasing temperature, it may be indicative of physical adsorption and the reverse is generally true for chemisorption. However, there are a number of contradictory cases in the literature.[32]

The effect of temperature on the removal of copper by the WTRA was studied at 1, 25 and 52 °C for concentration range 50–200 mg L^{-1} at pH 6.0. The results showed that the adsorption increased with increasing temperature, which means that the removal of Cu(II) was favored at high temperatures. Thus, the removal process was endothermic (Fig. 4).

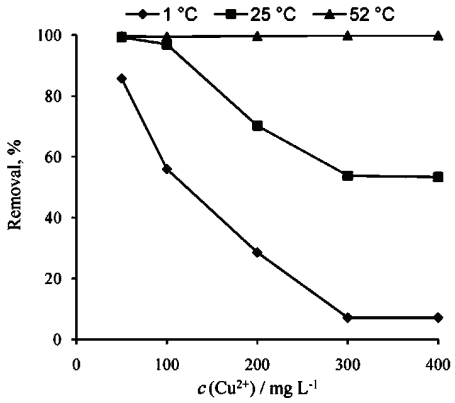

Fig. 4. Effect of temperature on the removal of Cu(II). Conditions: 1.5 g L^{-1} of WTRA, 100 mL of Cu(II) solution, contact time: 2 h; ♦ – 1, ■ – 25 and ▲ – 52 °C.

Adsorption isotherm. Adsorption isotherms play a crucial role in the predictive modeling procedures for the analysis and design of adsorption system. Therefore, in this study, the adsorption data of Cu(II) were tested with the Langmuir and Freundlich isotherm models. The equilibrium studies were performed at 25 °C for the contact time required to reach adsorption equilibrium. A Langmuir isotherm can be represented by the following equation:

$$\frac{c_e}{Q_e} = \frac{1}{Q_{max} b} + \frac{c_e}{Q_{max}} \quad (2)$$

where c_e is the equilibrium concentration, Q_e is the amount of copper adsorbed, and Q_{max} and b are Langmuir constants related to the adsorption capacity and energy, respectively.

The data from this study showed that a straight line was obtained when c_e/Q_e was plotted against c_e. This indicates that the Langmuir isotherm was followed under the present conditions with $R^2 = 0.997$.

The Freundlich isotherm is an empirical equation employed to describe heterogeneous systems. The Freundlich equation is expressed as:

$$Q_e = K_F c_e^{1/n} \quad (3)$$

The linear form of this equation can be written as:

$$\ln Q_e = \ln K_F + (1/n) \ln c_e \quad (4)$$

where K_F and n are the Freundlich constants related to the adsorption capacity and adsorption intensity, respectively. The intercept and the slope of the linear plot of ln Q_e *vs.* ln c_e for given experimental conditions provide the values of K_F and $1/n$, respectively.

In general, the Langmuir model fitted the experimental results slightly better than the Freundlich model. This suggests that the adsorption of Cu(II) ions by WTRA is a monolayer-type and agrees with the observation that the metal ion adsorption from an aqueous solution usually forms a layer on the adsorbent surface (Table I).

TABLE I. Langmuir and Freundlich isotherm constants

Ion	Freundlich isotherm			Langmuir isotherm		
	K_F	n	R^2	Q_{max} / mg g^{-1}	b / mg^{-1} L^{-2}	R^2
Cu(II)	1.42	0.66	0.96	34.3	0.064	0.99

Kinetic modeling

In order to investigate the controlling mechanism of the sorption process, such as mass transfer and chemical reaction, the Lagergren kinetics first-order model was used to test the experimental data of copper sorption by WTRA.

The Lagergren kinetics equations have been most widely used for the adsorption of an adsorbate from an aqueous solution, which is expressed by Eq. (5):

$$\log (q_e - q_t) = \log q_e - k_t/2.303 \quad (5)$$

where q_e and q_t are the amounts of Cu(II) adsorbed at equilibrium and at time t, in, and k_t is the first order rate constant. This equation was applied to the present studies of Cu(II) adsorption. The plots were found to be linear, indicating that the Lagergren Equation is applicable to Cu(II) adsorption on WTRA and the adsorption was first order and the value of first-order rate constant k_t was evaluated to be 0.0012 min^{-1}.

Treatment of metal industry wastewater

Based on the promising results obtained for copper ions removal from aqueous solutions, tests were conducted to evaluate these results using real wastewater. The wastewater used was taken from a local metal plating factory. It had a pH of 4.25 and contained Cu(II) at a concentration of 1.89 mg L^{-1}. Tests were conducted over a range of pH values (2–6) with varying WTRA concentrations. The samples were shaken at 25 °C for 2 h. At the end of this period, the solutions were separated by filtration and the residual metal concentration in the supernatant was determined by atomic absorption spectrophotometry. As observed in the tests with artificial solutions of Cu(II), the removal increased with increasing WTRA concentration, as well as increasing pH value. When the WTRA dosage was increased to 1.5 g L^{-1}, the Cu(II) removal increased to 100 %. Therefore, waste tire rubber ash was effective in removing Cu(II) from wastewater.

CONCLUSIONS

The results obtained in this study demonstrate that waste tire rubber ash can be used as an excellent adsorbent to remove copper from wastewaters with a good efficiency and low cost. Several parameters were studied and maximum adsorption was found to occur in the pH range 4.5–6.0 within 120 min-contact. The adsorption efficiencies increased with increasing contact time and initial metal concentration; the maximum observed capacity of the material was 34.3 mg/g of material. Furthermore, it can be concluded that waste tire rubber ash holds great potential to be an effective adsorbent for the removal of Cu(II) from wastewater samples.

Acknowledgements. The authors thank the Research Council and Office of Gifted Students of Semnan University for their financial support of this work.

ИЗВОД

УКЛАЊАЊЕ Cu(II) ИЗ ОТПАДНИХ ВОДА КОРИШЋЕЊЕМ ПЕПЕЛА ДОБИЈЕНОГ САГОРЕВАЊЕМ ОТПАДНИХ АУТОМОБИЛСКИХ ГУМА

HASSAN ZAVVAR MOUSAVI[1], ABDORRAHMAN HOSSEINIFAR[2] и VAHDAT JAHED[2]

[1]*Chemistry Department, College of Sciences, Semnan University, Semnan и*
[2]*Aja University of Medical Sciences, Tehran, Iran*

Испитан је утицај pH, дозе адсорбента, почетне концентрације Cu(II) и времена контакта на уклањање Cu(II) из воденог раствора техником шаржне адсорпције, коришћењем отпадног пепела од сагоревања аутомобилских гума као јефтиног адсорбента. Адсорпциона равнотежа је постизана након 2 часа при pH 4 до 6, што је оптимум за адсорпцију Cu(II) јона. Доза од 1,5 g/L адсорбента је била довољна за оптимално уклањање бакарних јона. Експериментални резултати су анализирани Лангмировом и Фројндлиховом изотермом, и одређене су одговарајуће константе сорпције. Подаци о кинетици адсорпције апроксимирани су једначином првог реда. Очекује се да трошак уклањања буде низак, с обзиром да је адсорбент јефтин и доступан у великим количинама. Ова студија је показала да пепео добијен са-

горевањем аутомобилских гума може да уклони јоне бакра из узорака индустријске отпадне воде.

(Примљено 10. априла 2009, ревидирано 17. марта 2010)

REFERENCES

1. L. R. B. Sanchez, B. S. V. de la Riva, J. M. C. Fernandez, R. Pereiro, A. S. Medel, *Talanta* **55** (2001) 1071
2. F. Liu, X. Luo, X. Lin, L. Liang, Y. Chen, *J. Hazard. Mater*. **171** (2009) 802
3. V. K. Gupta, C. K. Jain, I. Ali, M. Sharma, V. K. Saini, *Water Res*. **37** (2003) 4038
4. F. Gode, E. Pehlivan, *J. Hazard. Mater*. **100** (2003) 231
5. S. Rengaraj, J. W. Yeon, Y. Kim, Y. Jung, Y. K. Ha, W. H. Kim, *J. Hazard. Mater*. **143** (2007) 469
6. P. D. Johnson, M. A. Watson, J. Brown, I. A. Jefcoat, *Waste Manag*. **22** (2002) 471
7. T. Theophanides, J. Anastassopoulou, *Oncology/Haematology* **42** (2002) 57
8. J. Zeng, H. Ye, Z. Hu, *J. Hazard. Mater*. **161** (2009)1491
9. E. Pehlivan, T. Altun, *J. Hazard. Mater*. **134** (2006) 149
10. S. Rengaraj, J. W. Yeon, Y. Kim, Y. Jung, Y. K. Ha, W. H. Kim, *J. Hazard. Mater*. **143** (2007) 469
11. A. Baraka, P. J. Hall, M. J. Heslop, *J. Hazard. Mater*. **140** (2007) 86
12. J. W. Patterson, *Industrial wastewater treatment technology*, Butterworth-Heinemann, Stoneham, MA, 1985, p. 175
13. C. Zhu, Z. Luan, Y. Wang, X. Shan, *Sep. Purif. Technol*. **57** (2007) 161
14. A. T. Paulino, L. B. Santos, J. Nozaki, *React. Funct. Polym*. **68** (2008) 634
15. M. Radetić, D. Radojević, V. Ilić, D Jocić, D. Povrenović, B. Potkonjak, N. Puac, P. Jovančić, *J. Serb. Chem. Soc*. **72** (2007) 605
16. T. Aman, A. A. Kazi, M. U. Sabri, Q. Bano, *Colloids Surf. B* **63** (2008) 116
17. A. Papandreou, C. J. Stournaras, D. Panias, *J. Hazard. Mater*. **148** (2007) 538
18. E. Pehlivan, B. H. Yanık, G. Ahmetli, M. Pehlivan, *Bioresour. Technol*. **99** (2007) 3520
19. H. S. Altundogan, *Process Biochem*. **40** (2005)1443
20. J. A. Omgbu, V. I. Iweanya, *J. Chem. Ed*. **67** (1990) 800
21. V. K. Gupta, I. Ali, *J. Colloid Interface Sci*. **271** (2004) 321
22. F. E. Okieimen, D. E. Ogbeifun, G. N. Nwala, G. A. Kumsah, *Bull. Environ. Contam. Toxicol*. **34** (1985) 866
23. K. S. Low, C. K. Lee, S. C. Liew, *Process Biochem*. **36** (2000) 59
24. S. Ricordel, S. Taha, I. Cisse, G. Dorange, *Sep. Purif. Technol*. **24** (2001) 389
25. B. Yu, Y. Zhang, A. Shukla, S. S. Shukla, K. L. Dorris, *J. Hazard. Mater*. **80** (2000) 33
26. A. Saeed, M. W. Akhter, M. Iqbal, *Sep. Purif. Technol*. **45** (2005) 25
27. S. C. Ibrahim, M. A. K. M. Hanafiah, M. Z. A. Yahya, *J. Agric. Environ. Sci*. **1** (2006) 179
28. S. Mohan, G. Sreelakshmi, *J. Hazard. Mater*. **153** (2008) 75
29. E.-S. Z. El-Ashtoukhy, N. K. Amin, O. Abdelwahab, *Desalination* **223** (2008) 162
30. H. Cho, D. Oh, K. Kim, *J Hazard Mater*. **127** (2005) 187
31. C. P. Huang, C. P. Huang, A. L. Morehart, *Water Res*. **25** (1991) 1365
32. M. S. Celik, R. H. Yoon, *Langmuir* **7** (1991) 79.

Journal of the Serbian Chemical Society
JSCS@tmf.bg.ac.rs • www.shd.org.rs/JSCS
J. Serb. Chem. Soc. 75 (6) 855–872 (2010)
JSCS–4013
UDC 677.027.48:667.286:66.046.59+544.4
Original scientific paper

Decolorization of a textile vat dye by adsorption on waste ash

MIODRAG ŠMELCEROVIĆ, DRAGAN ĐORĐEVIĆ*, MILE NOVAKOVIĆ and MIRJANA MIZDRAKOVIĆ

University of Niš, Faculty of Technology, Bulevar oslobođenja 124, 16000 Leskovac, Serbia

(Received 24 July 2009, revised 15 February 2010)

Abstract: An adsorption process using cheap adsorbents could be described as a simple, selective and low cost alternative for the treatment of colored waste water compared to conventional physical and chemical processes. In this study the use of a natural waste adsorbent–ash was investigated for the removal of a textile vat dye Ostanthren blue GCD remaining after the dyeing of cotton textile. The ash obtained as a waste material during the burning of brown coal in the heating station of Leskovac (Serbia) was used for the treatment of waste waters from the textile industry, *i.e.*, waste water after the dyeing process. The effect of ash quantity, initial dye concentration, pH and agitation time on adsorption was studied. The Langmuir model was used to describe the adsorption isotherm. Based on the analytical expression of the Langmuir model, the adsorption constants, such as adsorption capacity and adsorption energy, were found. Pseudo first and second order kinetic models were studied to evaluate the kinetic data.

Keywords: textile vat dye; adsorption; ash; Langmuir model; kinetics.

INTRODUCTION

Many industries, such as the textile, leather, paper and plastics industries, are extensive dye users. Among them, the textile industry is the first by quantity and quality of dyes used for the dyeing of various fiber types. Wastewaters from the textile industry contain, in addition to dyes, a number of other polluting matters, such as toxic organic residuals, acids, bases and inorganic matter. Some dyes are carcinogenic and mutagenic being formerly produced from dangerous chemicals, such as benzidine, metals, *etc*. The effluence of colored liquid waste into receptor waters affects not only their esthetic nature but also the transmittance of sun light, thereby reducing photosynthesis and disturbing the natural balance of water life and the food chain.[1–3]

* Corresponding author. E-mail: drdrag64@yahoo.com
doi: 10.2298/JSC090717051K

During the previous several decades, a number of physical, chemical and biological methods for purification–decolorization were published and some of them were accepted by the textile industry. Among many decolorization procedures, the adsorption technique gives good results because it can be used for the removal of various types of colored matter. Commercial systems use mostly activated carbon as the sorbent for decolorization of waste waters because of its excellent absorption ability. Although activated carbon has an advantage as a sorbent, its massive employment is restricted due to its high price. To reduce the treatment costs, cheap alternative adsorbents are being sought.

Various studies[5,6] have confirmed the existence of alternative materials as potential adsorbents for pollutants and colored compounds. The considered possibilities for the adsorptive removal of color[7,8] include synthetic[9] and natural materials[6] and the use of solid natural organic materials is increasing exponentially. Among the organic compounds, many materials have color removal potential but they are not economic. Natural materials and wastes[10–15] build a complete collection of cheap adsorbents and they are environmentally friendly. Many articles have been published about the use of corn cobs,[16] palm fruit parts,[17–19] eucalyptus bark,[20] cotton,[21] sunflower stalks[22] and wheat straw[14] as decolorizing adsorbents. The removal of textile dyes by new adsorbents is usually evaluated by comparing their efficiency with that of activated carbon. Activated carbon is neither economical nor effective due to its non-polar nature in the unactivated state and in the most cases due to the polar nature of dyes. Therefore activation is often performed to introduce polar groups intended for different applications of carbon adsorbents.

As with other substrates, the adsorption of dyes not only depends mainly on the characteristics of the dyes and their structures but also to the same degree on the surface chemistry of adsorbent.

EXPERIMENTAL

As the adsorbent, the ash from the "Heating Station Leskovac" (Serbia), obtained by burning brown coal, was used. After collecting and drying, the ash was sifted up to a particle size of 0.5 mm. To increase the functionality, the ash was demineralized by treatment with 7.5 % H_2SO_4 for 60 min followed by copious rinsing with water, repeated treating with acid and finally adjustment of the pH of the water ash slurry to between 7 and 8.

As the adsorbate, vat dye Ostanthren Blue GCD (C.I. Vat Blue 14) from Synthesia, the Czech Republic was used.

The structure of the dye and its behavior in conventional textile dyeing processes are shown in Fig. 1. It should be noted that the dye samples used in the experimental part of this study were not obtained after the classical dyeing procedure but after heating the dye at 60 °C for 60 min without any additives and without textile material. The aim was to test the adsorption of the dye itself without any of the usual additives in the dyeing process, *i.e.*, reduction agents, hydrolysis agents, wetting agents, leveling agents, *etc.*, that would affect the adsorption process and complicate the interpretation of the results. It should be noted that the

dye is oxidized after dyeing and returns to its original insoluble form and as such exists in waste waters.

Common vat dyes are quinonic dyes and particularly common are the anthraquinones and indigoids. Moreover, vat dyes include the natural dyestuff, indigo, and the artificial dyes called by the trade names, indanthrene, and flavanthrene. These dyes are essentially insoluble in water and incapable of dyeing fibers directly. However, reduction in the alkaline liquor produces the water soluble alkali metal salt of the dye (Fig. 1). In this leuco form, these dyes have an affinity for the textile fibers. Subsequent oxidation reforms the original insoluble dye. Most vat dyes are less suitable than fiber reactive dyes for domestic use as they are difficult to work with; they require a reducing agent to solubilize them.[23]

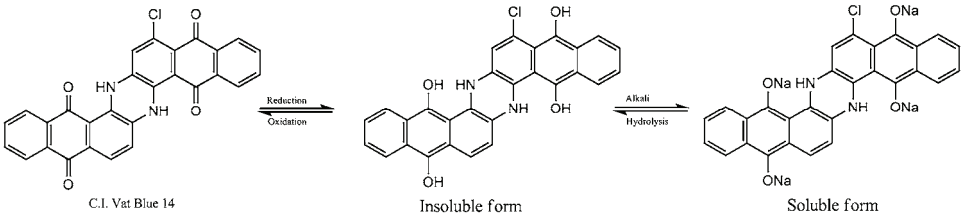

Fig. 1. Vat dye behavior in the process of textile dyeing.

The effect of pH on adsorption by the ash was tested by adjusting the pH of the solution to the required values with 1.0 M NaOH and H_2SO_4 solutions. According to the obtained results, the most effective adsorption was obtained at pH 13 and all subsequent processes were performed at this pH value.

The adsorption experiments were performed at room temperature (20 °C) in glass Erlenmeyer flasks, closed with cork stoppers and placed on a shaker at 150 rpm. The quantity of ash was varied between 1 and 4 g, using a constant volume of solution (100 cm^3) containing dye at concentrations of 50, 100, 150, 200 and 250 mg dm^{-3}. The treatment times were 10, 20, 30, 45 and 60 min with continuous agitation.

The selected dye concentrations were chosen because they mostly correspond to the residual dye quantities in the solution after the dyeing of textile. In the experiments, pure dye was used without the additives usually present in the dyeing process. The equilibrium adsorption time for the adsorption of dye on ash was determined to be 60 min and extension of the treatment time did not change the quantity of adsorbed dye.

The degree of dye removal was determined by spectrophotometrically measuring the quantity of dye in the solution before and after adsorption using a Cary 100 Conc UV–Vis spectrometer (Varian) at a wavelength of 590 nm

The percent dye removal is given by:

$$\text{Dye removal} = 100(c_0 - c)/c_0$$

where c_0 and c are the initial and final dye concentrations in the solution, respectively.

The adsorption of an adsorbate on a material can be described by the Langmuir isotherm, which in its linear form is given by:[24]

$$\frac{c_M}{a} = \frac{1}{a_{max}} c_M + \frac{1}{a_{max} b} \quad (1)$$

where: c_M, mg dm^{-3}, is the equilibrium adsorbate concentration in the solution after adsorption; a, mg g^{-1}, is the quantity of adsorbate adsorbed per mass unit of adsorbent; a_{max}, mg kg^{-1}, is the maximum quantity of adsorbate that could be bound to the adsorbent; b, dm^3 kg^{-1}, is the ratio of the adsorption rate constant and the desorption rate constant of the adsorbate.

The quantity of adsorbed dye (adsorbate) per mass unit of ash (adsorbent) was determined from the expression:

$$a = \frac{\left(c_M^0 - c_M\right)V}{w} \tag{2}$$

where: c_M^0, mg dm^{-3}, is the initial adsorbate concentration in the solution; w, g, is the mass of adsorbate and V, dm^3 is the volume of the solution used for the adsorption.

Equation (1) predicts that a plot of c_M/a *vs.* c_M should give a straight line, which is used for the determination of the values of the constants a_{max} and b as follows:

$$a_{max} = \frac{1}{\text{slope}} \text{ and } b = \frac{1}{a_{max}\left(\text{ordinate intercept}\right)_{c_M=0}}$$

In order to define the kinetics of the adsorption, pseudo first and pseudo second order models were considered. The linear form of the equation of pseudo first order kinetics is:

$$\log\left(a_{max} - a_t\right) = \log a - \frac{k_1}{2.303}t \tag{3}$$

and the equation of the linear form of pseudo second order kinetics is:

$$\frac{t}{a_t} = \frac{1}{k_2 a_{max}^2} + \frac{1}{a_{max}}t \tag{4}$$

where: a_{max}, mg g^{-1}, is the maximum (equilibrium) adsorbed quantity of adsorbate per unit mass of adsorbent; a_t, mg g^{-1}, is the adsorbed quantity of adsorbate per unit mass of adsorbent after time t; t, min, is the time of adsorption; k_1, min^{-1}, is the equilibrium rate constant for pseudo first order kinetics and k_2, g min^{-1} mg^{-1}, is the equilibrium rate constant for pseudo second order kinetics.

RESULTS AND DISCUSSION

Prior to commencing the presentation and analyses of the results of the present investigation of textile vat dye decolorization using waste fly ash, several facts regarding the justification of the use of this waste material from heating stations and power stations should be noted. Namely, it is known that one power station of 1000 MW produces about half a million tons of fly ash annually.[25]

Moreover, there are objectives to use this free material, available in huge amounts, for useful purposes or to dispose of it properly and hence prevent its dissemination because it contains potentially hazardous materials. Ash is an especially problematic residue as it contains high concentrations of heavy metals[26] and trace amounts of polychlordibenzodioxins and furans.[27,28]

Heavy metals are nowadays among the most important pollutants in source and treated water, and are becoming a severe public health problem. They can be toxic to aquatic life and cause natural waters to be unsuitable as potable water

sources.[29] Heavy metal removal from aqueous solutions has commonly been realized by several processes: chemical precipitation, solvent extraction, ion-exchange, reverse osmosis or adsorption.[29,30] Among these processes, adsorption using a suitable adsorbent can be an effective technique for the removal of heavy metals from wastewater.[31–33] As adsorbents activated carbon, alumina, silica and ferric oxide have been proposed. Although they generally have high metal adsorption capacities, they are expensive and difficult to separate from the wastewater after use. This has prompted over recent years growing research interest into the production of low cost alternatives to these adsorbents from a range of carbonaceous and mineral precursors. Ash, one of the most abundant waste materials from the combustion of powdered coal, and its major components make it a potential agent for the adsorption of heavy metal contaminants in water and wastewaters.[30]

Thus, fly ash is potentially a source of heavy metals that could be released into the environment, but it also can be used as an adsorbent for the removal of some heavy metals from their aqueous solutions.

Ash has potential application in wastewater treatment because of its major chemical components, which are alumina, silica, ferric oxide, calcium oxide, magnesium oxide and carbon, and its physical properties, such as porosity, particle size distribution and surface area. Moreover, the alkaline nature of ash makes it a good neutralizing agent. Generally, in order to maximize metal adsorption by hydrous oxides, it is necessary to adjust the pH of the wastewater using lime and sodium hydroxide.[32,33]

Several new technologies, such as immobilization of the ash with cement,[34] acid neutralization,[35] wet chemical treatment[36] and thermal treatment, have been proposed for the removal of heavy metals. The goal is to decontaminate toxic residues and render them inert so that they can be reused or deposited without risk. The major components in the ash which includes cyclone ash and scrubber ash (referred to as fly ash herein) are silica, aluminum, and calcium.[37] One of the ways is the waste melting process, in which the most hazardous materials, such as heavy metals, are tightly fixed in a solid phase, and the slag generated by this process can be used as a construction material.[38] Glassy slag can be generated by melting waste at temperatures exceeding 1300 °C, after which the molten ash is water-quenched or air-cooled. The volume of the resulting slag can be reduced and the slag stabilized such that heavy metals become immobilized in a glassy Si–O matrix; thus, the leaching behavior is improved.[39] The most common processes include the use of the ash as a raw material in the manufacture of brick and as a pozzolan in concrete.[29]

Hence, waste fly ash used in dye adsorption and the heavy metals washed off the ash and solidified (by evaporation and filtration) can be disposed as described above.

Considering an adsorption process, it is known that adsorption from a solution towards a solid surface begins with the interaction of dipoles or charged species of adsorbent and adsorbate. In addition, anion and cation interchange also occurs when neutral molecules come sufficiently close to each other, when an interaction between dissolved organic components, dyes, solvent molecules, water, and the surface of the adsorbent, ash, begins.[4–6]

It could be stated that the adsorption of dissolved matter (adsorbate) from a solution or suspension onto solid matter (adsorbent) occurs according to one of the following mechanisms: interchange of molecules from the solution with those on the adsorbent, physical adsorption induced by van der Waals forces and chemisorption.[7–10]

Adsorption efficiency depends on a number of parameters, such as medium temperature, pH, mechanical agitation, dye diffusion rate, *etc*. As a rule, by increasing the solution temperature, the dyeing rate or rate of diffusion is increased, but likewise, increased temperature reduces the equilibrium dye exhaustion. On this basis, fast adsorbing dyes have an optimal dyeing temperature of, for instance, 40 °C, while with dyes that slowly bind to a fiber, the optimal dyeing temperature is 100 °C. The same analogy can be applied for "binding", *i.e.*, adsorption of a dye onto the adsorbent (ash).[4–6]

It is known that the surface of ash acquires a positive charge by absorbing hydrogen ion (H^+) after immersion in water. In the case of low pH and increased H^+ concentration in a system, the ash surface acquires a strong positive charge. The opposite is true in an alkaline medium.[7,8]

It was found that the highest percentage of vat dye removal occurred in a strong alkaline medium, meaning that under these conditions, a high physical interaction appeared, which was based on the attraction of opposite charges, (+) dye charge and (–) ash charge, Fig. 2. Therefore, an increasing or decreasing percentage dye removed depending on pH should be considered in the light of structural changes of the dye and the condition of the surface layer of the ash.

It was expected that in acidic medium, considering the positively charged dye form, the highest dye adsorption would occur if the ash were negatively charged. This was not the case with the maximum adsorption found when the pH of the solution was 12 and 13, *i.e.*, in a strong alkaline medium. However, it should be noted that the difference in adsorption in strong acid and in strong alkaline medium was very low, about 0.1 %.

The explanation should be looked for in the fact that the reaction in alkaline medium is more risky than in an acidic one because of possible deformations and structural changes of the dye molecule, which could be the for the somewhat higher adsorption observed under very strong alkaline conditions.[40]

On the other hand, it is well known that substances adsorb poorly when they are ionized. Usually, when the pH is such that an adsorbable compound exists in

an ionized form, adjacent molecules of the adsorbed species on the adsorbate surface will repel each other to a significant degree, because they carry the same electrical charge (forces of repulsion/attraction between the actual ions are strong, compared with weak forces, such as Van der Waals forces). Thus, the adsorbing species cannot pack together very densely on the surface, and the equilibrium amount of adsorbed solute is only modest.[41] In contrast, when the adsorbing species is in the non-ionized form, no electrical repulsion exists, and thus the packing density on the surface can be much higher, as in the present case.

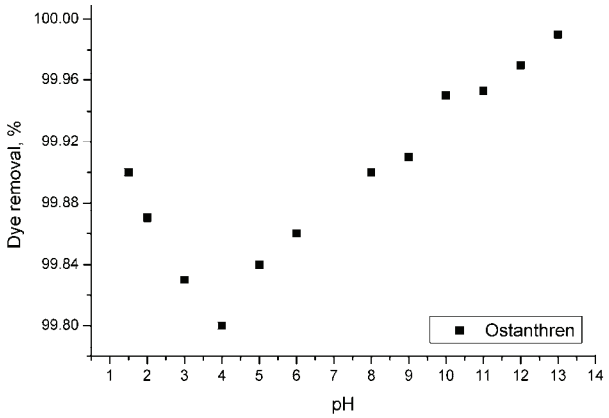

Fig. 2. Percentage of removed vat dye adsorbed on ash in acid and alkaline medium.

On reaction of a dye with an acid (*e.g.*, H_2SO_4), a salt is obtained – hydrogen sulfate and/or sulfate. Hydrogen ions from the acid binds to one and/or both nitrogen atoms of the dye and the produced cations are balanced by hydrogen sulfate or sulfate anions, Fig. 3.

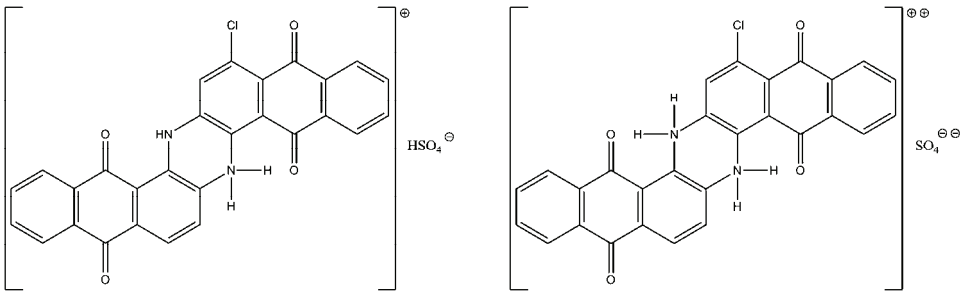

(a) (b)

Fig. 3. Dye structure after reaction with sulfuric acid.
a) hydrogen sulfate dye form; b) sulfate dye form.

In basic medium, reactions occur on the carbonyl groups and by reduction, two to four identical phenol –OH groups are obtained, with later replacement of the hydrogen atom by a sodium atom, Fig. 4.

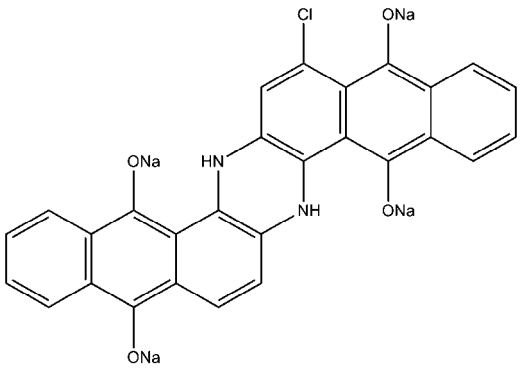

Fig. 4. Dye structure after reaction with sodium hydroxide.

The removal yields of vat dye as a function of the initial and equilibrium dye concentration for the minimum quantity of ash (1 g) are shown in Fig. 5. At lower concentrations, it is obvious that a higher percentage of dye was removed dye is obvious, irrespective of whether the initial or equilibrium dye concentration was considered. On the other hand, generally, the maximum dye concentration (250 mg dm^{-3}) was considerably higher than the previously used concentrations (200, 150, 100 and 50 mg dm^{-3}) but the percentage dye removed was only slightly lower than the values obtained with the other initial concentrations. This means, effectively, that a higher amount of dye was adsorbed with the highest initial concentration. Therefore, the percentage removed dye and the adsorption percentage decreased with increasing dye concentration in solution but the actual quantity of dye adsorbed increased with increasing dye concentration.

Based on this behavior of the dye in a solution containing ash, it could be concluded that the faster removal indicates that the sorption process could be ionic in nature when the dye molecules bind to oppositely charged groups on the adsorbent surface.

Moreover, from the plot in Fig. 5, it is obvious that the adsorption time plays a key role, *i.e.*, with increasing time, the quantity of dye removed from solution by the ash increased. The same effect was found with all the employed quantities of ash.

Plots of % removed dye at equilibrium time *vs.* the quantity of ash for different concentrations of vat dye are shown in Fig. 6, from which a constant increase in the % removed dye with increasing adsorbent mass is obvious and that the lowest dye concentration showed the highest % removed dye, whereas the highest dye concentration gives the lowest % removed dye. Nevertheless, the actual quantity of adsorbed dye increased with increasing dye concentration.

The results of the amount of dye adsorbed on the ash adsorbent with time for different initial concentrations of vat dye and different ash quantities are shown in Fig. 7.

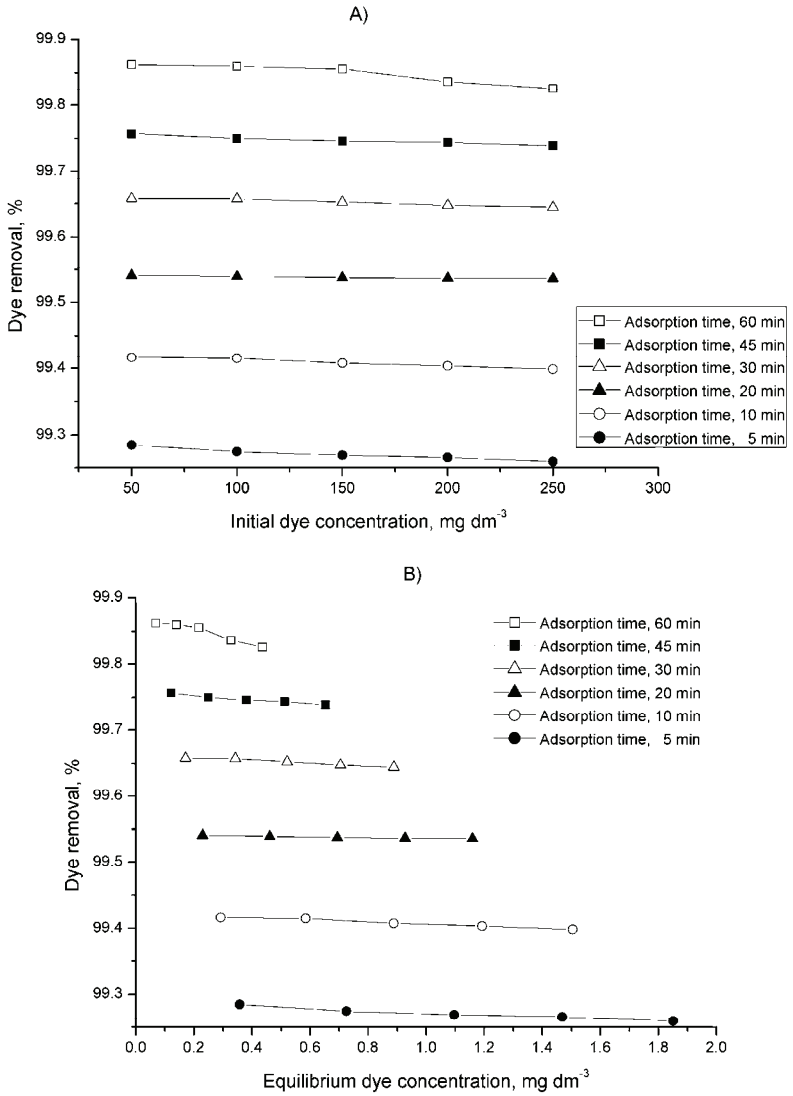

Fig. 5. Percentage of removed vat dye adsorbed on ash as a function of A) the initial and B) the equilibrium dye concentration (adsorption on 1.0 g of ash).

In the main diagrams, Figs. 7A and 7B, are only shown the dependencies for dye concentrations of 50 and 250 mg dm^{-3} and for adsorbent quantities of 1.0 and 4.0 g, respectively. The changes for other dye concentrations were similar but for sake of clarity, they were not given in the main diagrams. In the lower right hand side of the main diagrams, auxiliary diagrams showing the dependencies for all dye concentrations are inserted. Practically, one curve each was chosen from the auxiliary diagrams to give the main diagrams marked as A and

B. Such a presentation gives a more prominent picture of the dependency of the change of amount of dye adsorbed on the adsorbent with time compared to the same presentation in the auxiliary diagrams.

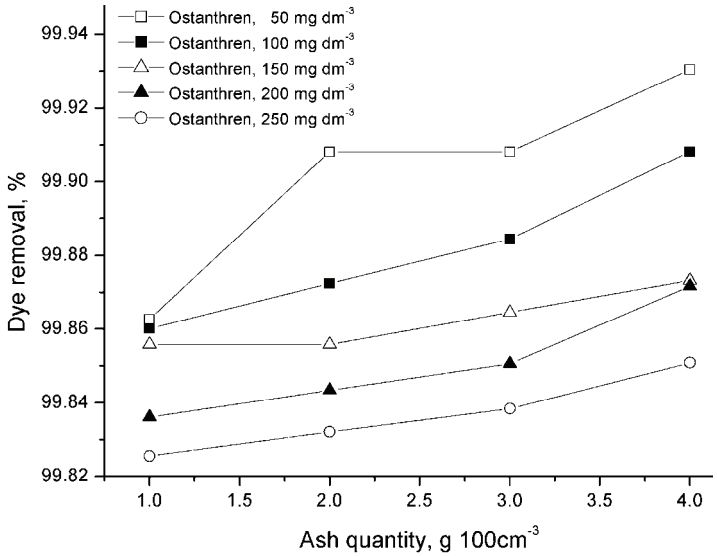

Fig. 6. The percentage of vat dye removed by adsorption as a function of ash quantity for different initial dye concentrations.

The continuity of changes with time are obvious, *i.e.*, the amounts of dye adsorbed per unit mass of adsorbent increased with increasing time. Moreover, the highest adsorption occurred with the highest dye concentration, which was expected.

The Langmuir adsorption isotherm in two forms is shown in Fig. 8, *i.e.*, Fig. 8A represents the relation between adsorbed dye per unit of the minimal used ash mass and equilibrium dye concentration and Fig. 8B shows the relation of c_m/a to the equilibrium concentration of the dye.

It is obvious that adsorption curves are smooth and continuous, indicating that the process proceeds to saturation with different concentrations of dye on the outer interface of the adsorbent. This implies the possibility of the formation of a mono-layer coverage of the adsorbent, which is described by the Langmuir Equation. From the slope and intercept of the right hand plot in Fig. 8, according to Eq. (1), the Langmuir constants a_{max} and b, representing the maximum quantity of adsorbate bound to the adsorbent and the adsorption energy, respectively, were determined.

Under ideal conditions of medium pH and maximum interactions of the dye molecules with the adsorbent, the plots in Fig. 8 represent the essential functionality of the variables, *i.e.*, a high correlation was achieved. The essence of the

adsorption process in this case, covered by the Langmuir isotherm, is based firstly on the initial dye concentration, being an important driving force to overcome all the resistance to mass transfer between the aqueous and solid phase. Generally, a higher initial concentration of vat dye enhances the adsorption process. The case was similar for adsorption onto the maximum amount of ash employed, Fig. 9.

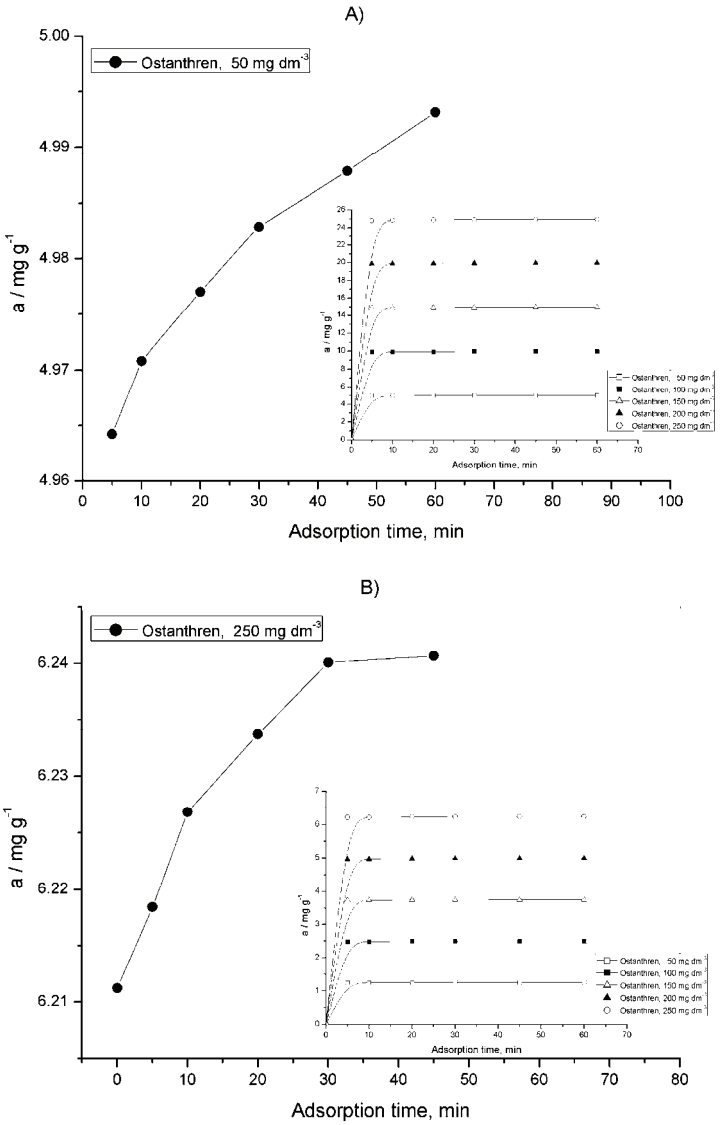

Fig. 7. Adsorbed quantity of adsorbate on adsorbent in time for different dye concentrations. A) 1g of ash; B) 4 g of ash.

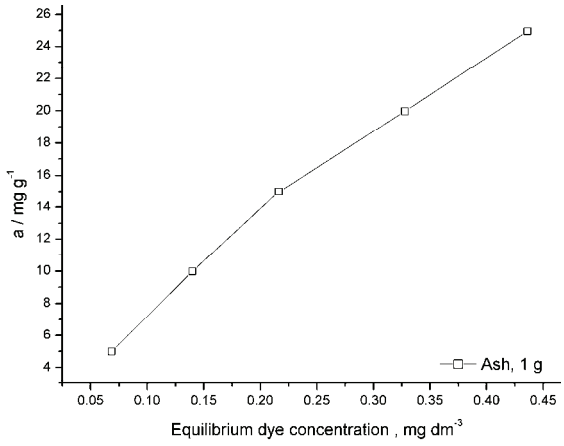

(A)

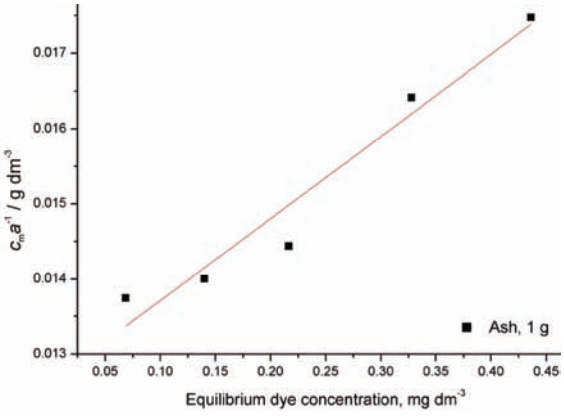

(B)

Fig. 8. Langmuir adsorption isotherms for the minimum studied amount of adsorbate.

The various methods of dye adsorption on ash, as well as the analytical expressions of Langmuir isotherm and Langmuir parameters a_{max} and b, together with the values for the coefficient of determination R^2 for the Langmuir plot c_M/a *vs.* c_M are listed in Table I. The coefficient of determination is a relative measure of the typicality of the regression line or, in this case, a measure of the usefulness of the Langmuir model. The fact that all R^2 values were greater than 0.9 showed that the Langmuir Equation fitted the experimental data very well. The maximum quantity of adsorbate that can be bound to the adsorbent, a_{max}, or the monolayer adsorption capacity, decreased with increasing quantity of the adsorbent, while the ratio of the adsorption and desorption rate constants of the adsorbate, b, which is a constant related to the adsorption free energy, increased.

The results for the kinetics of dye sorption on ash with the minimum and maximum amounts of adsorbent and different initial dye concentrations are shown in Figs. 10 and 11. According to the linear forms of pseudo-first and pseu-

do-second order models and the obtained results, it can be concluded that adsorption rate, under the given experimental conditions, was completely described by the second order model. This was also the case with other used ash quantities (2 and 3 g).

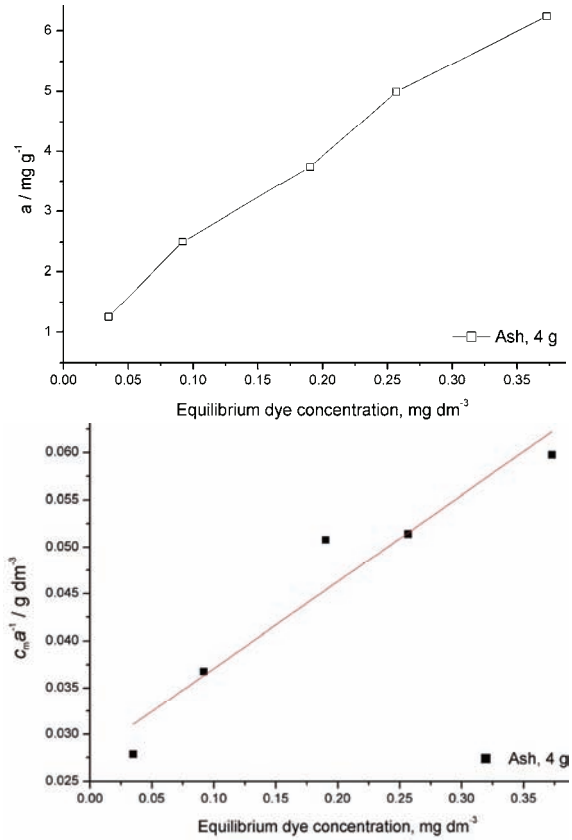

Fig. 9. Langmuir adsorption isotherms for the maximum studied amount of adsorbent.

TABLE I. Analytical expression of the Langmuir isotherm with coefficients

Mass of adsorbant, g	Analytical expression of curve (Langmuir expression)	Langmuir parameters		R^2
		a_{max} / mg g^{-1}	b / dm^3 mg^{-1}	
1	$c_M/a = 0.0126 + 0.0109c_M$	91.6	0.865	0.952
2	$c_M/a = 0.0190 + 0.0383c_M$	26.1	2.02	0.907
3	$c_M/a = 0.0271 + 0.0570c_M$	17.5	2.10	0.954
4	$c_M/a = 0.0279 + 0.0921c_M$	10.8	3.31	0.930

The results of the determination of the kinetic parameters for the adsorption process of vat dye on ash (equilibrium rate constant of pseudo-first and pseudo--second order kinetics) for all the studied adsorbent quantities and all the initial dye concentrations together with values of the parameter a_{max} (calculated, $a_{max,cal}$, and experimental, $a_{max,exp}$) are listed in Table II.

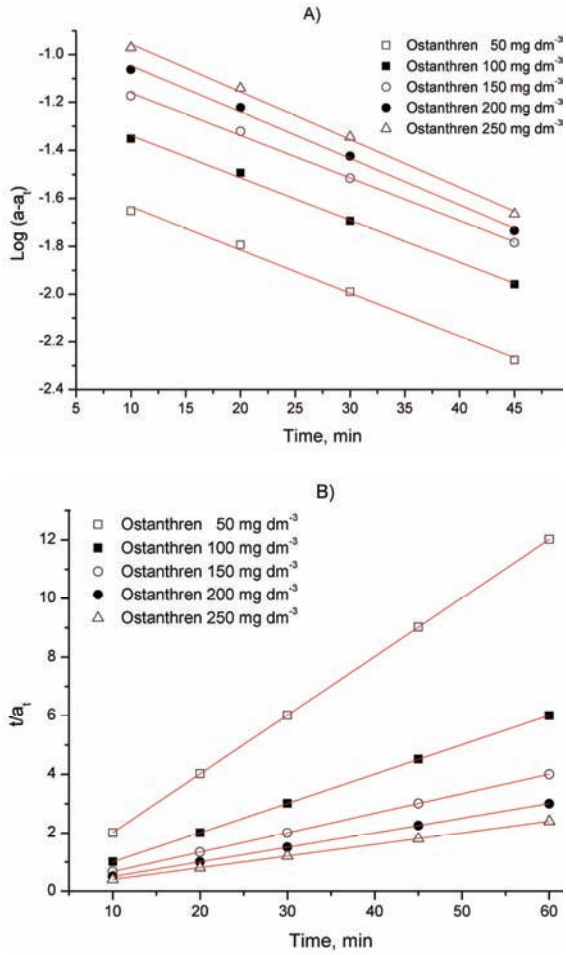

Fig. 10. Sorption kinetics of vat dye with the minimum studied adsorbent quantity; A) pseudo-first order; B) pseudo-second order.

The pseudo first and pseudo second order models were used to check the experimental data, whereby an attempt was made to explain the kinetics of the adsorption process under the given experimental condition.

Although coefficients of determination for the pseudo first order kinetics model were generally higher than 0.9 for all amounts of adsorbent and all the initial dye concentrations, much lower values of the calculated parameter a_{max} ($a_{max,cal}$) were obtained compared to those of the experimental parameter a ($a_{max,exp}$). Therefore, the adsorption cannot be best described by the pseudo first order kinetics model because in most cases first order equation does not cover adequately the whole range of contact times.

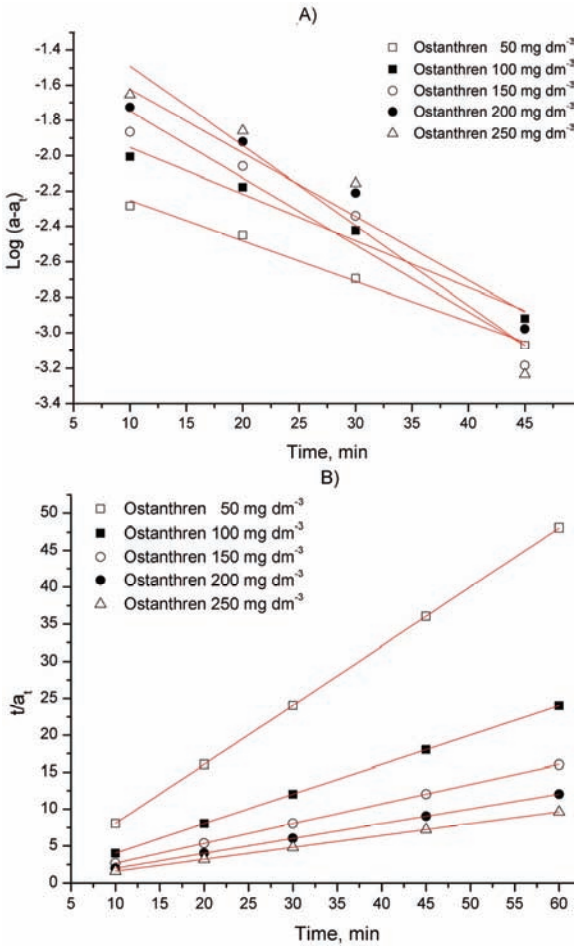

Fig. 11. Sorption kinetics of vat dye with the maximum studied adsorbent quantity; A) pseudo-first order; B) pseudo-second order.

TABLE II. Kinetic parameters of vat dye adsorption on ash (R^2 = 1, for pseudo-second order)

Absorbent quantity, g/100 cm^{-3}	Initial dye concentration, mg dm^{-3}	$a_{max,exp}$ mg g^{-1}	Pseudo-first order			Pseudo-second order	
			k_1 / min^{-1}	$a_{max,cal}$ mg g^{-1}	R^2	k_2 g mg^{-1} min^{-1}	$a_{max,cal}$ mg g^{-1}
1	50	4.99	0.042	0.035	0.997	3.59	5.00
	100	9.99	0.041	0.070	0.997	1.80	9.99
	150	15.0	0.041	0.11	0.998	1.20	15.0
	200	20.0	0.045	0.14	0.997	0.935	20.0
	250	25.0	0.046	0.18	0.998	0.764	25.0
2	50	2.50	0.040	0.018	0.998	7.15	2.50
	100	4.99	0.047	0.036	0.996	3.82	5.00
	150	7.49	0.051	0.055	0.994	2.60	7.49
	200	9.98	0.055	0.076	0.990	2.00	9.99
	250	12.5	0.056	0.095	0.989	1.63	12.5

TABLE II. Continued

Absorbent quantity, g/100 cm^{-3}	Initial dye concentration, mg dm^{-3}	$a_{max,exp}$ mg g^{-1}	Pseudo-first order			Pseudo-second order	
			k_1 / min^{-1}	$a_{max,cal}$ mg g^{-1}	R^2	k_2 g mg^{-1} min^{-1}	$a_{max,cal}$ mg g^{-1}
3	50	1.66	0.050	0.012	0.982	11.6	1.67
	100	3.33	0.057	0.025	0.971	6.05	3.33
	150	4.99	0.067	0.041	0.952	4.22	4.50
	200	6.66	0.075	0.060	0.936	3.20	6.66
	250	8.32	0.087	0.085	0.908	2.64	8.33
4	50	1.25	0.051	0.0090	0.992	15.9	1.25
	100	2.50	0.058	0.019	0.981	8.35	2.50
	150	3.74	0.080	0.034	0.944	6.10	3.75
	200	4.99	0.077	0.044	0.953	4.49	5.00
	250	6.24	0.094	0.065	0.917	3.81	6.24

As opposed to this, the pseudo-second order kinetics model had in all cases $R^2 = 1$, whereby full functionality was achieved and the model can be fully used to describe the adsorption process of vat dye on ash. Moreover, the differences between the calculated $a_{max,cal}$ and the experimental $a_{max,exp}$ were insignificant for this model.

CONCLUSIONS

Dye adsorption as a purification method has some advantages, because other processes, which include alteration or destruction of the chromophore dyes to decolorize the solution, do not remove residuals from waste waters that, as such, can still be detrimental for the environment. As opposed to this, adsorption removes the complete molecule without leaving any parts in the water. This is especially important with dyes containing metals, where bound metal (*e.g.*, Cr, Co, Cu) would remain in the waste water in cases of treatment methods other than adsorption, perhaps even in more harmful forms.

Removal of a vat dye with waste ash obtained from the "Heating Station – Leskovac" was studied under various conditions. The adsorption depended on the contact time, initial dye concentration and solution pH. The equilibrium state was achieved after a contact time of 60 min, while the % adsorption on ash was reduced on increasing the initial dye concentration in the solution, although the actual quantity of adsorbed dye was increased. A Langmuir isotherm describes the adsorption characteristics of the adsorbent in a satisfactorily manner.

The pseudo second order kinetics model fitted very well with the dynamic behavior of vat dye adsorption on natural waste ash under various conditions, with the remark that the adsorption is a very complex process.

Based on the obtained results, it can be concluded that brown coal ash is an efficient adsorbent for the removal of vat dyes from water solutions with a reasonable possibility of application on an industrial scale.

Acknowledgment. The financial support of the Serbian Ministry of Science and Technological Development (Project No. TP-19040A) is gratefully acknowledged.

И З В О Д

ДЕКОЛОРИЗАЦИЈА ТЕКСТИЛНЕ РЕДУКЦИОНЕ БОЈЕ АДСОРПЦИЈОМ НА ОТПАДНОМ ПЕПЕЛУ

МИОДРАГ ШМЕЛЦЕРОВИЋ, ДРАГАН ЂОРЂЕВИЋ, МИЛЕ НОВАКОВИЋ и МИРЈАНА МИЗДРАКОВИЋ

Универзитет у Нишу, Технолошки факултет, Булевар ослобођења 124, 16000 Лесковац

Адсорпциони процес уз помоћ јефтиних адсорбената могао би се декларисати као једноставна, селективна и јефтина алтернатива за пречишћавање обојених отпадних вода у односу на конвенционалне физичко–хемијске поступке. У раду је истраживана примена природног отпадног адсорбента – пепела за одстрањивање редукционе текстилне боје Ostanthren blue GCD заостале после бојења памучног текстила. Пепео добијен сагоревањем мрког угља у топлани у Лесковцу као отпадни материјал, коришћен је за пречишћавање отпадне воде текстилне индустрије, тј. отпадне воде настале после процеса бојење. Истраживан је утицај количине пепела, почетне концентрације боје, pH и времена мешања на адсорпцију. За описивање адсорпционе изотерме примењен је Ленгмиров модел. На основу аналитичког израза Ленгмировог модела нађене су константе, адсорпциони капацитет и енергија адсорпције. Кинетички модели псеудо првог и другог реда су испитивани ради оцене кинетичких података.

(Примљено 24. јула 2009, ревидирано 15. фебруара 2010)

REFERENCES

1. E. Demirbas, M. Koboya, M.T. Sulak, *Bioresour. Technol*. **99** (2008) 5368
2. X. F. Sun, S. G. Wang, X. W. Liu, W. X. Gong, B. Y. Gao, H. Y. Zhang, *Bioresour. Technol*. **99** (2008) 3475
3. N. Emanuel, G. Kumar, *Environ. Chem. Lett*., DOI 10.1007/s10311-0080182-x
4. M. M. Davila-Jimenez, M. P. Elizalde-Gonzalez, A. A. Pelaez-Cid, *Colloids Surf. A* **254** (2005) 107
5. M. M. Nassar, M. S. El-Geundi, *J. Chem. Technol. Biotechnol.* **50** (1991) 257
6. K. R. Ramakrishna, T. Viraraghavan, *Water Sci. Technol.* **36** (1997) 189
7. O. J. Hao, H. Kim, P.-C. Chiang, *Crit. Rev. Environ. Sci. Technol.* **30** (2000) 449
8. T. Robinson, G. McMullan, R. Marchant, P. Nigam, *Bioresour. Technol.* **77** (2001) 247
9. A. Krysztafkiewtcz, S. Binkowski, T. Jesiouowski, *Appl. Surf. Sci.* **199** (2002) 31
10. R. M. Liversidge, G. J. Lloyd, D. A. J. Wase. C. F. Forster, *Process Biochem.* **32** (1997) 473
11. T. Robinson, B. Chandran, P. Nigam, *Environ. Int.* **28** (2002) 29
12. G. Annadurai, R.-S. Juang, D.-J. Lee, *J. Hazard. Mater. B* **92** (2002) 263
13. R. Sivaraj, C. Namasivayam, K. Kadirvelu, Waste Manage. (Oxford) **21** (2001) 105
14. T. Robinson, B. Chandrai, P. Nigam, *Water Res.* **36** (2002) 2824
15. V. K. Gupta, D. Mohan, S. Sharma, M Sharma, *Sep. Sci. Technol*. **35** (2000) 2097
16. M. S. El-Geundi, *Water Res*. **25** (1991) 271
17. M. M. Nassar, M. F. Hamoda, G. H. Radwan, *Water Sci. Technol.* **32** (1995) 27
18. M. M. Nassar, Y. H. Magdy, *Chem. Eng. J*. **66** (1997) 223
19. M. M. Nassar, *Water Sci. Technol*. **40** (1999) 133
20. L. C. Morais, O. M. Freitas, E. P. Goncalves, L. T. Vasconcelos, C. G. Gonzalez, *Water Res*. **33** (1999) 979

21. I. Bouzaida, M. B. Rammah, *Mater. Sci. Eng. C* **21** (2002) 151
22. G. Sun, X. Xu, *Ind. Eng. Chem. Res.* **36** (1997) 808
23. J. Shore, *Colorants and auxiliaries: organic chemistry and application properties*, *Society of Dyers and Colourists*, Bradford, 2002, p. 45
24. Lj. Vračar, A. Despić, V. Dražić, K. Đorđević, D. Jovanović, S. Jovanović, M. Maksimović, B. Nikolić, D. Ovcin, D. Šepa, *Experimental Physical Chemistry*, Faculty of Technology and Metallurgy, Belgrade, 1987, p. 237 (in Serbian)
25. http://www.eps.rs/publikacije/Zastita zivotne sredine/EPS Zastita zivotne sredine.pdf
26. A. Jakob, S. Stucki, P. Kuhn, *Environ. Sci. Technol*. **29** (1995) 2429
27. M. S. Wang, L. C. Wang, C. C. Wang, *J. Hazard. Mater*. 133 (2006) 177
28. S.I. Shih, Y.F. Wang, J.E. Chang, J.S. Jang, F.L. Kuo, L.C. Wang, G.P. Chang-Chien, *J. Hazard. Mater*. **137** (2006) 1817
29. B. Bayat, *Water Air Soil Pollut*. **136** (2002) 69
30. G. Gupta, N. Torres, *J. Hazard. Mater*. **57** (1998) 243
31. J. Ayala, F. Blanco, P. Garcia, P. Rodriguez, J. Sancho, *Fuel* 77 (1998) 1147
32. B. Bayat, *J. Hazard. Mater*. **3** (2002) 251
33. B. Bayat, *J. Hazard. Mater*. **3** (2002) 275
34. Y. M. Kuo, T. C. Lin, P. J. Tsai, *J. Hazard. Mater*. **133** (2006) 75
35. C. A. Johnson, S. Brandenberger, P. Baccin, *Environ. Sci. Technol*. **29** (1995) 142
36. S. Aricke, T. Van Gerven, C. Vandecasteele, *J. Hazard. Mater*. **137** (2006) 235
37. J. Iori, J. Balg, *Residue Treat*. **6** (1995) 9
38. S. Sakai, M. Hiraoka, N. Takeda, T. Tsunemi, *Water Sci. Technol*. **22** (1990) 329
39. J. P. Young, H. Jong, *J. Hazard. Mater*. *B* **9** (2002) 89
40. V. Gundula, *Color Technol*. **122** (2006) 317
41. A. Mishra, M. Bajpai, *Bioresour. Technol*. **97** (2006) 1055.

Journal of the Serbian Chemical Society
JSCS@tmf.bg.ac.rs • www.shd.org.rs/JSCS

J. Serb. Chem. Soc. 75 (6) 873 (2010)

Errata (printed version only)

Issue No. 5 (2010), Vol. 75:

– The paper *JSCS-3993* by Gajendra Kumar *et al*. on pages 629–637 has been corrected in the electronic version, which should be referred to.

– The paper *JSCS-3996* by Ankica Antić-Jovanović *et al*. on pages 659–667 has been corrected in the electronic version, which should be referred to.